UNIVERSITY OF SOUTHAMPTON

Faculty of Social, Human and Mathematical Sciences
School of Mathematical Sciences

Some Topics in the Theory of Ultracold Atomic Gases

by

Donato Romito

ORCiD: 0000-0001-6368-9675

A thesis for the degree of
Doctor of Philosophy

31 August 2021

University of Southampton

Abstract

Faculty of Social, Human and Mathematical Sciences
School of Mathematical Sciences

Doctor of Philosophy

Some Topics in the Theory of Ultracold Atomic Gases

by Donato Romito

This thesis deals with a variety of topics that are relevant for the theory of ultracold atoms, with a focus on the many interaction regimes that can be obtained in these systems. The topics are presented in increasing order of complexity with regards to these interaction regimes. In the first chapter we are prompted by an experiment on a realization of an interacting Aubry-André Hamiltonian driven by a periodic modulation, where a localisation-delocalisation transition is observed. We will model an analogue non interacting system and show that it reproduces an equivalent phase diagram. Moreover we are able to provide a physical explanation for the critical amplitude and the critical frequency for the delocalisation transition. Next, we will consider a model of N atoms which are non interacting with the addition of a single light impurity that interacts with them. We will propose a simplified model based on the Born-Oppenheimer approximation and a polaron-like picture through which we are able to estimate the energy of the system and to address the question of the existence of stable clusters bound by an impurity in the large N limit. In the rest of the thesis the pivot will be on the Andreev-Bashkin effect which describes the drag that each component of a mixture of two superfluids exerts on the other, as a result of their mutual interactions. We will first propose a microscopic theory based on linear response theory that describes the drag, and derive its implications on the nature of the excited states in a superfluid mixture. Then we will compute the effect of the drag on the spin speed of sound and the spin dipole mode which can in principle observed in experiments. Analytical results for the case of a weakly interacting mixture are presented as a benchmark for our methods. Finally we will focus on the Andreev-Bashkin effect in a Bose-Hubbard Hamiltonian in a one dimensional ring lattice. We will show that the effect is enhanced for attractive intraspecies interactions, more so close to the transition to paired superfluidity. A discussion on the correction brought by the drag in the low energy Luttinger theory for the model is also presented.

Declaration of Authorship

I declare that this thesis and the work presented in it is my own and has been generated by me as the result of my own original research.

I confirm that:

1. This work was done wholly or mainly while in candidature for a research degree at this University;
2. Where any part of this thesis has previously been submitted for a degree or any other qualification at this University or any other institution, this has been clearly stated;
3. Where I have consulted the published work of others, this is always clearly attributed;
4. Where I have quoted from the work of others, the source is always given. With the exception of such quotations, this thesis is entirely my own work;
5. I have acknowledged all main sources of help;
6. Where the thesis is based on work done by myself jointly with others, I have made clear exactly what was done by others and what I have contributed myself;
7. Parts of this work have been published as:
   Donato Romito, Carlos Lobo, and Alessio Recati. Localisation transition in the driven aubry-andré model. *The European Physical Journal D*, 72(8):135, Aug 2018. ISSN 1434-6079. . URL https://doi.org/10.1140/epjd/e2018-90081-3
   Donato Romito, Carlos Lobo, and Alessio Recati. Linear response study of collisionless spin drag. *Phys. Rev. Research*, 3:023196, Jun 2021. . URL https://link.aps.org/doi/10.1103/PhysRevResearch.3.023196newlineDaniele Contessi, Donato Romito, Matteo Rizzi, and Alessio Recati. Collisionless drag for a one-dimensional two-component bose-hubbard model. *Phys. Rev. Research*, 3:L022017, May 2021. . URL https://link.aps.org/doi/10.1103/PhysRevResearch.3.L022017

Signed:..... Date:.....

All men are ready to invest their money

But most expect dividends.

I say to you: Make perfect your will.

I say: take no thought of the harvest,

But only of proper sowing.

– T. S. Eliot, *Choruses from "The Rock"*

Contents

Declaration of Authorship **v**

List of Figures **xiii**

1 Introduction **1**
1.1 Outline of the thesis . . . 2

2 Localisation of a quasicrystal under periodic driving **5**
2.1 Introduction: localisation and non-ergodicity in isolated quantum systems 5
2.1.1 Outline . . . 6
2.2 Quasicrystals and Anderson localisation . . . 7
2.2.1 What are quasicrystals? . . . 7
2.2.2 Anderson localisation . . . 8
2.2.2.1 Truly disordered Hamiltonian . . . 9
2.2.2.2 The Aubry-André model and its localisation transition . 10
2.3 Time periodic systems . . . 11
2.3.1 Floquet theorem: elementary concepts . . . 12
2.3.2 Time evolution . . . 13
2.4 Periodically driven Quasicrystal . . . 14
2.4.1 The model . . . 14
2.4.2 Setup . . . 15
2.4.2.1 Imbalance . . . 15
2.4.2.2 Inverse Participation Ratio . . . 17
2.4.3 Results . . . 18
2.4.3.1 Critical frequency . . . 21
2.4.3.2 Critical amplitude . . . 22
2.4.3.3 Role of the interactions . . . 24
2.5 Conclusions . . . 24

3 The N+1 bound problem **25**
3.1 Introduction: the N+1 bound problem . . . 25
3.1.1 Outline . . . 26
3.2 The bosonic case . . . 27
3.3 The fermionic case . . . 28
3.4 Chemical potential and kinetic energy of the impurity in the Born-Oppenheimer approximation . . . 30
3.5 Energetic analysis of the N+1 bound problem . . . 34
3.5.1 Local density approach . . . 34

3.5.2 Positive scattering length near unitarity . . . 36
3.5.3 Negative scattering length . . . 39
3.6 Conclusions . . . 40

4 Linear response study of the collisionless drag 43
4.1 Introduction . . . 43
4.1.1 Outline . . . 44
4.2 The Andreev-Bashkin effect: three fluid hydrodynamics . . . 45
4.3 Microscopic description of the collisionless drag from linear response theory . . . 47
4.3.1 Superfluid densities as current-current response functions . . . 48
4.3.2 Current response and sum rules . . . 51
4.4 Weakly interacting Bose-Bose mixture: drag and excitations . . . 57
4.4.1 Drag in a uniform mixture . . . 58
4.5 Effect of the drag on the excitations of a two component BEC . . . 61
4.5.1 Beyond mean field correction to the spin speed of sound in a homogeneous gas . . . 62
4.5.2 Spin dipole modes in a trap . . . 64
4.6 Measuring the drag via a quick perturbation . . . 67
4.7 Conclusions . . . 69

5 Collisionless drag in a 1D ring lattice 71
5.1 Introduction: why a 1D ring lattice? . . . 71
5.1.1 Outline . . . 72
5.2 Model and setup . . . 73
5.2.1 Model: Bose-Hubbard Hamiltonian on a ring . . . 73
5.2.2 Setup: computing the superfluid densities . . . 74
5.2.3 Superfluid drag at half-filling . . . 75
5.2.4 Superfluid drag approaching the paired superfluid phase . . . 76
5.3 Collisionless Drag and Luttinger liquid parameters . . . 78
5.4 Conclusions . . . 82

6 Conclusions 85

Appendix A Scattering length and zero range approximation 87
Appendix A.1 The dilute limit and the low energy limit for short range interactions . . . 87
Appendix A.2 Low energy scattering and effective range expansion . . . 88
Appendix A.2.1 The zero range approximation . . . 90

Appendix B Experimental realization of the periodically modulated quasicrystal 91
Appendix B.1 Realization of the optical lattice . . . 91
Appendix B.2 Experimental Sequence . . . 93

Appendix C 2-component Bose-Hubbard model 95
Appendix C.1 Linear response on a lattice . . . 95
Appendix C.2 Alternative derivation: drag coefficient as a derivative of the energy . . . 97

Appendix D Thermodynamics of Bose-Bose mixture **101**

References **103**

List of Figures

2.1 Spectrum of the Aubry-André model 11
2.2 Imbalance of the undriven Aubry-André model 16
2.3 Imbalance vs frequency for strong driving, comparison with experiment 19
2.4 Imbalance vs frequency vs disorder strength (logscale), comparison with experiment 19
2.5 Inverse Participation Ratio vs frequency vs disorder strength 20
2.6 Inverse Participation Ratio vs frequency vs disorder strength 20
2.7 Imbalance vs amplitude vs disorder strength 23
2.8 Inverse Participation Ratio vs amplitude vs disorder strength 23

3.1 Few-body fermionic clusters 29
3.2 Inverse effective mass m/m^* vs $1/k_F a$ 33
3.3 Energy vs $1/k_F a$ 36
3.4 Energy at minimum vs N 38
3.5 Energy vs $1/k_F|a|$ for $a < 0$ 40
3.6 Energy at minimum vs N 40

4.1 Density and spin excitations in a superfluid mixtures 52
4.2 Superfluid drag vs η for a weakly interacting mixture 60
4.3 Beyond mean field correction to the spin speed of sound 63
4.4 Excitation of a spin dipole mode 65
4.5 Beyond mean field correction to the spin dipole frequency 67

5.1 Sketch of the two component Bose-Hubbard ring 73
5.2 Superfluid currents vs piercing flux 74
5.3 Superfluid drag vs U_{AB} (away from pair superfluidity) 76
5.4 Superfluid drag vs U_{AB} (crossing the pair superfluidity transition) 78
5.5 Correlation functions in the two superfluid phase and in the paired superfluid phase 79
5.6 Luttinger parameter and spin susceptibility across the paired superfluidity transition 82

Appendix B.1 Experimental sequence for the measurement of the imbalance in the driven Aubry-Andrè model 94

Appendix C.1 Sketch of the two component Bose-Hubbard ring 97

1

Introduction

Ultracold atoms provide a privileged platform to experimentally realize a variety of quantum systems. Indeed, when atoms are trapped and cooled, for example via laser cooling or evaporative cooling, to very low temperatures the quantum mechanical nature of the system takes over. In essence, the *quantumness* in such systems is reached when the thermal de Broglie wavelength $\lambda_T = \sqrt{2\pi\hbar^2/mk_BT}$ is comparable or greater than the average interparticle distance. In this regime, called the degenerate regime, the average de Broglie wavelength of the atoms is big enough that the wavefunctions of the atoms are overlapping and their collective behaviour cannot be accounted for by classical physics. The degenerate regime is thus reached at very low temperatures, as in ultracold atoms experiments, or at very high densities, as for example in neutron stars.

Once the degenerate regime is reached ultracold atoms can be manipulated in many different ways. We can think of a cold atom experiment as a quantum toy that has many knobs. Some knobs can be used to control the geometry of the system, for example restricting its dynamics to occur on a plane or on a single line, or breaking translational invariance by trapping atoms on a lattice. Some other knobs can be used instead to decide which species of atoms (e.g., different elements or different isotopes of the same element) take part in the physics of the system. When a gas of ultracold atoms consists of more than one species it is said to be a *quantum mixture*.

Another possibility, which is unique to ultracold atoms, is to tune the strength of the interaction between atoms by means of Feshbach resonances. This feature allows to go from regimes where the atoms are not interacting at all to regimes where the interactions reach their maximum value. The manifold experimental situations that are offered by ultracold atoms corresponds to a variety of techniques that must be adopted when approaching their description theoretically. While a system of particles that are not interacting can be essentially treated as an ensemble of single particles, a quantum gas where interactions are strong requires to take into account the collective

properties of the many-body system. Between these two extremes, weakly interacting gases have interactions that can be treated as a small perturbation on top of a non interacting gas. Adding to the variety is the possibility in a quantum mixture to switch off the interactions among different species (interspecies) while keeping interactions among atoms of the same species (intraspecies), or vice versa.

In this thesis I explore some of the variety I listed above, the topics being presented in an order that, broadly speaking, reflects the increasing complexity brought by interactions. I start from an ensemble of non interacting atoms in the first chapter, then in successive chapters I will consider a quantum mixture where only interspecies interactions are present, then a mixture where both intra- and interspecies interactions are present and finally I will study a strongly interacting mixture.

1.1 Outline of the thesis

The chapter 2 of this thesis will describe the work that begun during the writing of my master thesis Romito (2017) and was continued and completed in Southampton. This work was prompted by an experiment reported in Bordia et al. (2017) that studies the localisation-delocalisation transition of atoms in a quasiperiodic lattice, described by the Aubry-André many body Hamiltonian, under a time-periodic driving. A brief appendix is included to illustrate the procedure of the original experiment. Our goal is to model the non interacting counterpart of this experiment in order to gain insight on the relationship between the observed localisation phase diagrams and the features of the single particle model. I will show that the non interacting model we consider is able to capture the essential features of the many body experiment. This work lead to the publication of the paper Romito et al. (2018).

Chapter 3 is the study of a mass-imbalanced Fermi system consisting of N fermions and a single particle, or impurity, with mass much smaller than the mass of the majority fermions. The heavy atoms do not interact among themselves but they interact with the single particle. The question that sets out the problem is whether there is a limit to the number of particles that can be bound by the impurity. This question is motivated by theoretical results for few-body systems where it has been shown that a single light particle can bind together up to five fermions.

Last, in chapters 4 and 5, we will be concerned with the study of the Andreev-Bashkin effect or collisionless drag Andreev and Bashkin (1975). The Andreev-Bashkin effect takes place in a binary superfluid mixture and describes the entrainment between the currents of the two superfluids. Since this effect has proven to be quite elusive and has yet to be clearly observed in a controlled experiment, our work is devoted to expand its theoretical understanding in order to make the effect observable in an ultracold atoms setting.

Chapter 4 focuses on the theoretical study of the effect by means of a linear response theory formalism which generalizes other approaches used up to now to make predictions on the effect (see Fil and Shevchenko (2005) for example). This formalism has the advantage of having a clear physical interpretation and a strong connection with experiments, especially for its connection with sum rules (Pitaevskii and Stringari (2016), Nozieres and Pines (1999)). I will propose three different ways to measure the effect in experiments. I will also discuss the limitations of weakly interacting systems in producing a sizeable drag. This work lead to the publication of the paper Romito et al. (2021).

In chapter 5 I will report on the study of the Andreev-Bashkin effect in a one dimensional ring lattice, which is a promising system where to observe the drag. In particular, I will focus on the effect for attractive intraspecies interactions, where we should expect that the drag is enhanced. This work lead to the publication of the paper Contessi et al. (2021).

In appendix A I give a brief overview of scattering theory for typical ultracold atoms experiment, based on well known literature. In appendix B I illustrate the experiment that prompted the work in chapter 2. Appendix C generalizes some result of chapter 4 to the case of a lattice Hamiltonian. The expression of the drag as a derivative of the energy was used in chapter 5 to numerically compute its value. In appendix D I derive some thermodynamics quantities for homogeneous and trapped Bose-Bose mixtures that are necessary for computing the spin speed of sound and spin dipole frequency in chapter 4.

2

Localisation Transition in the Aubry-André model under periodic driving

The work contained in this chapter lead to the publication of the paper Romito et al. (2018).

2.1 Introduction: localisation and non-ergodicity in isolated quantum systems

Statistical mechanics (or, better, equilibrium statistical mechanics) is based on the assumption that systems tend to thermal equilibrium. Most physical systems reach thermal equilibrium by the interaction with their environment, which acts as a bath, draining or pumping energy to the system in an irreversible manner. When this is the case, the system will thermalize and in the process lose memory of all the initial conditions. Then the dynamics of the system is said to be *ergodic*, meaning that its parts will uniformly visit all the available phase space.

A natural question to ask is whether this holds true for isolated systems. It is tempting to think that in absence of an external bath the system would have no way to thermalize. However, in a generic quantum system only local observables are accessible, i.e. observables that probe a finite portion of it. What happens in most cases is that the system as a whole acts as a reservoir for any of its subpart that is sufficiently small, and the information on the initial state is erased from any local observable Deutsch (1991).

It is then interesting to find systems which avoid thermalization and retain the information on the initial state. Such systems are said to be **localised**. It is clear that localised systems must necessarily be isolated. Moreover, a natural way to break ergodicity is to insulating phases, as otherwise transport and exchange of energy will eventually lead to thermalization. Philip W. Anderson has shown in 1958 that these conditions can be met by **introducing randomness in a system** Anderson (1958). The model proposed by Anderson, in presence of a sufficiently strong *randomness*, displays a suppression of transport as a consequence of its egeinstates being localised. The Anderson localisation transition has been observed in an experiment with cold atoms in an optical lattice and reported in Roati et al. (2008).

Of course, the necessity of an isolated system is in itself a technological challenge. One can at best realize an experiment with an almost isolated system, meaning that it can be assumed to be isolated up to a certain time scale. Practically, if some parameter describing the coupling between the system and the environment Γ is small enough, we can consider the system to be isolated when its dynamics occurs with a typical timescale τ such that $\tau \ll \Gamma^{-1}$. Ultracold atoms provide a platform where isolated quantum systems have been realized and their parameters were tuned to reach regimes where localisation occurs Schreiber et al. (2015).

Another point of interest is what happens when an initally localised system is acted upon by a periodic modulation. It is natural to expect that a periodic modulation will favor a delocalised phase, as it will eventually pump enough energy into the system to thermalize it. This can happen provided the parameters of the driving, such as its frequency, are chosen in a way that it can efficiently couple with the dynamics of the system. In this chapter, prompted by an experiment reported in Bordia et al. (2017), we study the physics of such a system: an initially localised system that is driven by a time periodic perturbation. In the original experiment in Bordia et al. (2017) the localised system is a gas of interacting fermions in an optical lattice that has a quasirandom on-site energies. We will focus the non interacting counterpart of this problem in order to see if reproduces the qualitative features of the interacting system.

2.1.1 Outline

An experiment by P. Bordia et al. at LMU in Munich Bordia et al. (2017) has demonstrated that periodically modulating the potential of a localised many-body quantum system described by the Aubry-André Hamiltonian with on-site interactions can lead to a many-body localisation-delocalisation transition. It is emphasized in Bordia et al. (2017) that the amplitude of the modulation is required to exceed a certain threshold in order to drive the system to a delocalised phase. Moreover, while generally a modulation with small frequency is more efficient in bringing the system to a delocalised phase, some non-trivial dependences on the frequency are observed in

the experiment. Our goal is to consider the non interacting counterpart of the many body Aubry-André model in order to explore its phase diagram as a function of the strength of the disordered potential, the driving frequency and its amplitude. The aim is to understand if the results of the experiment can be explained already at the single particle level and if we can give a physical explanation for the observed threshold in the amplitude and for the frequency dependence of the phase diagram. We will first of all mimic the experimental procedure of Bordia et al. (2017) and use the even-odd sites Imbalance as a parameter in order to discern between different phases. Then we compute the Floquet eigenstates and relate the localisation-delocalisation transition to their Inverse Participation Ratio.

The chapter is divided into two main parts. In the first two sections, secs. 2.2 and 2.3 the two main ingredients of the work on periodically driven quasicrystal are introduced. Sec. 2.2 is devoted to explain what is meant by a quasiperiodic crystal and how the Anderson localisation transition occurs in these type of systems. In sec. 2.3 we focus instead on the theory of time periodic systems. Finally in sec. 2.4 we will show the main results of the work on the driven Aubry-André model and how they compare with the experiment in Bordia et al. (2017).

2.2 Quasicrystals and Anderson localisation

2.2.1 What are quasicrystals?

Solid matter have been for a long time divided in a dichotomistic way in two categories: *ordered* (or crystalline) and *disordered* (or amophous) matter. In this sense ordered matter is identified with spatially periodic arrangements of atoms and amorphous matter with a random distribution of its constituents. In this frame quasicrystals were regarded as a somewhat intermediate structure between an ordered and a disordered system Shechtman et al. (1984). This notion however was later challenged in light of the fact that the so-called quasicrystals exhibit long range order, orientational symmetries and a discrete diffraction patterns Levine and Steinhardt (1984), all properties that are shared with ordered matter. This suggests that quasicrystals should be interpreted as an extension of the notion of crystals.

The modern view on this matter is to introduce a **hierarchy of order**, instead of the strict dychotomy between ordered and disordered matter. The new definition of terms reflects the modern stance that spatial periodicity is not a necessary condition for cristallinity, and this role should be taken by long range order. While the latter implies the former, the converse is not true, as the mere existence of quasicrystals proves.

Following Maciá (2014), we illustrate the concept by defining a function $f(\mathbf{x})$ which describes the spatial distribution of atoms in a lattice. This function can be expressed

in terms of its Fourier coefficients, namely:

$$f(\mathbf{x}) = \sum_{\mathbf{k}} a_{\mathbf{k}} e^{i\mathbf{k}\cdot\mathbf{x}}, \tag{2.1}$$

where k are the reciprocal lattice vectors Ashcroft et al. (1976).

The aforementioned *hierarchy of order*, with increasing order, is then expressed in terms of the number of lattice vectors k that are required to generate the spatial arrangement of atoms, namely:

1. An almost periodic crystal is a crystal whose atomic distribution can be described by an aperiodic function, i.e. a function whose Fourier transform contains a countable infinity of incommensurate lattice vectors.
2. A quasiperiodic crystal is an almost periodic crystal whose lattice vectors can be generated from a finite dimensional basis.
3. A periodic crystal is a quasiperiodic crystal whose lattice vectors can be generated from a basis whose dimensionality equals that of the real space considered.

A non periodic arrangement of atoms, such as in a liquid or in a gas requires instead an uncountable number of Fourier basis vectors, i.e. a Fourier transform.

The simplest example of a quasiperiodic structure in one dimension is represented by the function:

$$f(x) = A\cos(x) + B\cos(\alpha x) \tag{2.2}$$

where α is an irrational number. This corresponds to the superposition of two lattices whose length are *incommensurate*, i.e. such that their ratio is an irrational number. It's interesting to mention that the distribution function in (2.2) can be viewed as the projection on a one dimensional space of a function which is periodic in two dimensions:

$$f(x,y) = A\cos(x) + B\cos(y) \tag{2.3}$$

The one dimensional quasiperiodic function is obtained by restricting $y = \alpha x$. This simple intuition is at the basis of the so-called cut and project method, which in its essentials consists in applying the notions of classical cristallography to quasicrystals by considering an appropriate hyperspace.

2.2.2 Anderson localisation

This section will describe two different localisation transitions: one is the textbook example of Anderson Localisation in a truly disordered Hamiltonian, the other is

localisation in the Aubry-André model, which is the most simple example of a quasiperiodic Hamiltonian, and the focus of our work.

2.2.2.1 Truly disordered Hamiltonian

It is known after the seminal paper by Anderson Anderson (1958) that *disorder (or randomness)* can produce localised dynamics for a quantum particle. For a given disorder strength the eigenstates of a disordered Hamiltonian are either localised or delocalised. The model Anderson proposed in Anderson (1958) describes a single particle subject to the tight binding Hamiltonian in one dimension:

$$\hat{H} = J \sum_i \left(|i\rangle \langle i+1| + |i+1\rangle \langle i| \right) + \lambda \sum_i \epsilon_i |i\rangle \langle i| \ , \tag{2.4}$$

where $|i\rangle$ is the Wannier state localised at site i in Dirac notation and J is the tunneling coefficient, which represents the probability amplitude to tunnel from a site to a neighbouring one. Randomness is introduced by means of the on site energies $\lambda\epsilon_i$ which are drawn from a chosen probability distribution, the standard choice being a uniform distribution with support $\left[-1/2, 1/2\right]$. Thus the coefficient λ (which has units of energy) quantifies the amount of randomness of the lattice and is called *disorder strength*.

The Anderson model undergoes a phase transition: namely for $\lambda > \lambda_c$ the eigenstates of the Hamiltonian become exponentially localised, with a localisation length ξ, namely, for any eigeinstate ψ:

$$|\psi(\mathbf{r})|^2 \propto \exp\left(-|\mathbf{r} - \mathbf{r_0}|/\xi\right) \tag{2.5}$$

In his paper Anderson proved that for a one or two dimensional system an arbitrarily small disorder strength is sufficient to localise the eigenstates, i.e. $\lambda_c = 0$. For finite disorder strength **all** the eigenstates of the Anderson Hamiltonian are localised. The localisation length of the wavefunctions depends on the disorder strength, and it increases monotonically with decreasing disorder strength, approaching the limit $\xi \to \infty$ for vanishing disorder strength. Thus, in a system with finite size the localisation length can be larger than the system's size, so the actual localised phase is defined only in the thermodynamic limit.

For the Anderson model in three dimensions the picture is similar, but the transition occurs for a finite value of the disorder strength, i.e. $\lambda_c \neq 0$. Moreover the localisation transition in three dimensions doesn't occur for all the eigenstates at once: below the critical strength the eigenstates at the center of the energy band are extended, while eigenstates above a certain energy E_c (and below $-E_c$), called mobility edge, are

localised. For a complete review on the main results regarding single-particle Anderson localisation see Evers and Mirlin (2008).

2.2.2.2 The Aubry-André model and its localisation transition

The model we will consider in the remainder of the chapter is the most simple description of a one dimensional quasicrystal which is the **Aubry-André Model**, whose Hamiltonian in the tight binding approximation reads:

$$\hat{H} = J\sum_i \left(|i\rangle\langle i+1| + |i+1\rangle\langle i|\right) + \lambda\sum_i \cos\left(2\pi\beta i + \phi\right)|i\rangle\langle i| \tag{2.6}$$

Where β is an irrational number and $\phi \in [0, 2\pi]$ is a phase. The Hamiltonian in Eq. (2.6) describes a particle moving with tunneling rate J in a one dimensional lattice realized by superimposing two lattice lengths L_1 and L_2 which are incommensurate, and $\beta = L_1/L_2$. The form of this Hamiltonian is very similar to the Anderson Hamiltonian, the only difference being that the on site energies are not drawn from a random distribution but rather are generated by the quasiperiodic potential $\cos\left(2\pi\beta i + \phi\right)$.

The model has gained in the years increasing interest both in physics and in mathematics. In relation to the latter, the spectrum was conjectured to be a Cantor set for any $\lambda \neq 0$, namely a closed, nowhere dense set with no isolated points. This conjecture was called "Ten Martini Problem" and was proved in Avila and Jitomirskaya (2009). In Fig. (2.1) we show the energy spectrum of the Aubry-André model as a function of the potential depth λ/J, for $N = 50$. The spectrum of the Aubry-André model has Lebesgue measure $|4 - 2\lambda|$, which means that at the transition its measure is 0.

In 1980 Aubry and André predicted that the namesake model undergoes a **metal to insulator transition** for a critical strength of the quasiperiodic potential $\lambda = \lambda_c$ Aubry and André (1980), as the Anderson model in more than two dimensions. This analogy is one of the reasons behind the interest for this model: it displays a phase transition (analogously to the Anderson model in more than two dimensions) while already in one-dimension, making it easier to study. However for the Aubry-André model, much like in the one dimensional Anderson model, there are no *mobility edges*, which means that for $\lambda < \lambda_c$ all the states are extended, while for $\lambda > \lambda_c$ all the states are localised. At the critical point the nature of the eigenstates of the Hamiltonian is self-similar, or fractal. The wavefunction amplitude ψ_n displays a main maximum with decaying tails which however cannot be fitted by an exponential. Then, further away from the main maximum there are subsidiary smaller peaks which reproduce the main maximum, and so on.

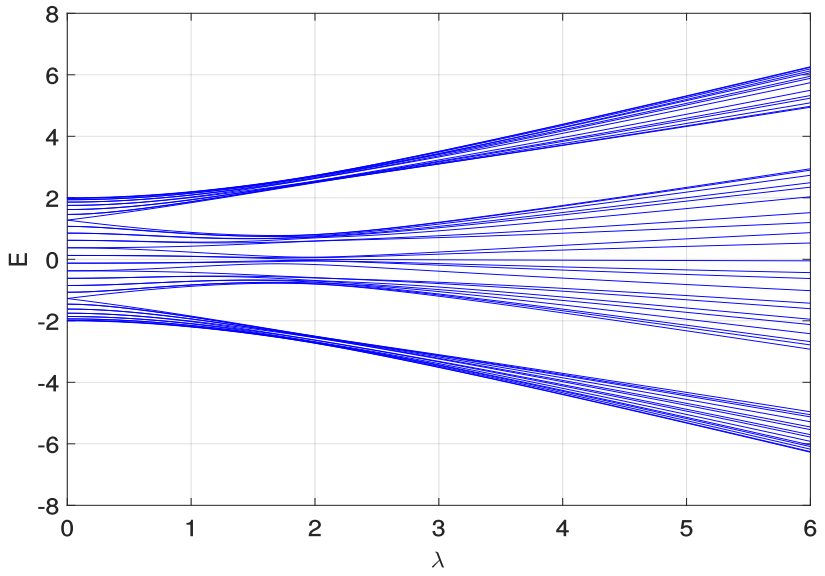

FIGURE 2.1: Spectrum of the Aubry-André model as a function of λ for $N = 50$ lattice sites.

The rigorous proof of the occurence of the Metal to Insulator Transition for the Aubry-André model was given in Jitomirskaya (1999), after the conjecture made by Aubry and André based on numerical simulations. We mention that at the transition the spectrum of the Aubry-André model for different values of β has a fractal structure and takes the name of Hofstadter Butterfly Hofstadter (1976).

2.3 Time periodic systems

The study of time periodic systems has gained rising interest in the last years in the context of closed quantum systems. The most important tool to study their properties is the Floquet theorem, which allows to write the evolution over multiples of the driving period in terms of a time independent effective Hamiltonian Shirley (1965), Sambe (1973). The existence of such an effective Hamiltonian can open the way to the so called Floquet engineering, that is, the possibility to realise non trivial time independent models by periodically modulating a quantum system with a suitable protocol. This concept has been employed very successfully in various experiments with ultracold atoms in driven optical lattices. This includes dynamic localisation (Dunlap and Kenkre (1986), Holthaus (1992), Grifoni and Hänggi (1998), Lignier et al. (2007)), "photon"-assisted tunneling (Zak (1993), Eckardt and Holthaus (2007)), control of the bosonic superfluid-to-Mott-insulator transition (Eckardt et al. (2005), Zenesini et al. (2009)) and the realisation of artificial magnetic fields (Jotzu et al. (2014), Aidelsburger et al. (2011), Struck et al. (2012), Goldman and Dalibard (2014)). The interplay between localisation and a time periodic driving is also of great interest and

raises the question of whether and when a modulating force pumping energy into the system can bring it to an ergodic phase (see e.g. Abanin et al. (2016), Gopalakrishnan et al. (2016), Rehn et al. (2016)). In this chapter we briefly overview the main ideas that are useful to study time-periodic quantum systems and that we will use in order to investigate this interplay.

2.3.1 Floquet theorem: elementary concepts

Consider a model whose Hamiltonian is periodic in time, with period $T = 2\pi/\omega$, namely:

$$\hat{H}(t+T) = \hat{H}(t)\,. \tag{2.7}$$

Under this condition the Schrödinger equation falls under the hypothesis of *Floquet theorem* Shirley (1965). According to the Floquet theorem the solutions of the corresponding time-dependent Schrödinger equation can be written in the form:

$$\psi_n(x,t) = e^{-i\epsilon_n t/\hbar} u_n(x,t)\,, \tag{2.8}$$

where $u_n(x,t) = u_n(x,t+T)$ is a periodic function and is referred to as *Floquet mode* or *Floquet eigenmode*. The state $\psi_n(x,t)$ is called **Floquet state** or *Floquet eigenstate*. We will drop in what follows the dependence on x.

The ϵ_n are the so-called quasienergies and can be readily found noting that the Floquet modes are solutions of the eigenfunction equation:

$$\hat{Q}\,|u_n(t)\rangle = \epsilon_n\,|u_n(t)\rangle \tag{2.9}$$

where we defined the *quasienergy operator* $\hat{Q}$ as:

$$\hat{Q} = \hat{H} - i\hbar\frac{d}{dt}\,, \tag{2.10}$$

If we define $\epsilon_{nm} = \epsilon_n + m\hbar\omega$ and

$$u_{nm}(t) = e^{im\omega t} u_n(t)\,, \tag{2.11}$$

u_{nm} is still periodic and the solution $\psi_n(t)$ can be written in the form:

$$\psi_n(t) = e^{-i\epsilon_n t/\hbar} u_n(t) = e^{-i\epsilon_n t/\hbar} e^{-im\omega t} u_{nm}(t) = e^{-i\epsilon_{nm}\,.\,t/\hbar} u_{nm}(t) \tag{2.12}$$

That is, we have the same physical solution, but the corresponding Floquet mode is a solution of the quasienergy eigenvalue problem with eigenvalue $\epsilon_{nm} = \epsilon_n + m\hbar\omega$.

This means that quasienergies are defined modulo $\hbar\omega$, thus explaining the prefix quasi-, in analogy with Bloch theorem, where solutions are labelled by quasimomenta

defined up to a reciprocal lattice vector. Fixing each quasienergy within this choice fixes the Floquet modes. In particular one can choose the quasienergies to lie in an interval of width $\hbar\omega$. It comes as no surprise that this interval is called *Brillouin zone* or *Floquet Brilloun zone*.

2.3.2 Time evolution

Consider the standard time evolution operator in quantum mechanics:

$$U(t,t') \equiv \mathcal{T} \exp\left(-\frac{i}{\hbar}\int_{t'}^{t} H(\tau)d\tau\right). \tag{2.13}$$

It can be easily proven from their factorization that the Floquet states are eigenstates of the time evolution operator over one period T, namely:

$$\hat{U}(t_0+T,t_0)\,|\psi_n(t_0)\rangle = \exp\left(-i\frac{\epsilon_n T}{\hbar}\right)|\psi_n(t_0)\rangle \tag{2.14}$$

This allows us to compute the Floquet states from the propagator over one period.

The time evolution operator for arbitrary times admits a spectral representation in terms of Floquet eigenmodes, we start from:

$$U(t,t_0)\,|\psi(t_0)\rangle = |\psi(t)\rangle\ . \tag{2.15}$$

Multiplying for $|\psi(t)\rangle$ on both sides and using the expression of the Floquet states in terms of the Floquet modes one finds that:

$$U(t,t_0) = \sum_n e^{-i\epsilon_n(t-t_0)/\hbar}\,|u_n(t)\rangle\,\langle u_n(t_0)| \tag{2.16}$$

Thus one can in general express the evolution of an arbitrary state as

$$|\psi(t)\rangle = \sum_n c_n e^{-i\epsilon_n(t-t_0)/\hbar}\,|u_n(t)\rangle \tag{2.17}$$

with $c_n = \langle u_n(t_0)|\psi(t_0)\rangle$. This expression allows us to identify two distinct contributions to the time evolution of a generic initial state.

- The first is a periodic contribution given by the periodic evolution of the Floquet modes $|u_n(t)\rangle$, called **micromotion**.
- The second contribution is given by the "interference" of the different phases $\epsilon_n t/\hbar$, which is present if the initial state is not a Floquet mode with definite quasienergy.

We stress the important fact that c_n is independent of time. Thanks to this, if we ignore the micromotion and are interested only in the evolution at times which are integer multiples of the period we can view the quasienergy as if they were the energies of a time independent system. Such dynamics which takes into account only integer multiples of the period is often referred to in literature as **stroboscopic evolution**. From this intuition stem the concepts of **Floquet Hamiltonian** and **Effective Hamiltonian** that give the possibility to study a periodically driven quantum systems using intuitions, theorems and concepts which are used for time independent systems.

If one is interested only in the stroboscopic evolution, the picture is not dissimilar from the case of a time independent Hamiltonian. Here the Floquet states take the role of the usual eigenstates of the Hamiltonian. In the following section we will make use of this intuition and Eq. (2.17) will be relevant for characterizing the long time dynamics of the system by looking at the properties of the Floquet states, which will be computed using Eq. (2.14).

2.4 Periodically driven Quasicrystal

2.4.1 The model

We consider the Aubry-André Hamiltonian H_0, with periodically modulated potential $V(t)$:

$$H(t) = H_0 + V(t) \tag{2.18}$$

where H_0 is the Hamiltonian of the time independent model with tunneling coefficient J and disorder strength λ:

$$H_0 = J\sum_{i}^{N}\left(|i\rangle\langle i+1| + |i+1\rangle\langle i|\right) + \lambda\sum_{i}\cos(2\pi\beta i+\phi)\,|i\rangle\langle i| \tag{2.19}$$

and $V(t) = V(t+T)$ is a time periodic potential with period $T = 2\pi/\omega$ which modulates the onsite energies:

$$V(t) = A\cos(\omega t)\sum_{i}\cos(2\pi\beta i+\phi)\,|i\rangle\langle i| \tag{2.20}$$

As in the time independent case, β is an irrational number, $|i\rangle$ is the Wannier state localised at site i in Dirac notation, J is the tunneling coefficient and λ is the disorder strength. We choose periodic boundary conditions for the lattice.

The qualitative features of the undriven system in the many-body and the single particle (non interacting) cases are quite similar Schreiber et al. (2015). We illustrated the properties of the non interacting model in the previous sections. In the many-body

case the transition is controlled by the parameters J, λ and the additional parameter U, which is the intensity of the repulsive on-site interactions. There is a critical disorder strength which depends on J and U above which the system becomes localised Schreiber et al. (2015). More precisely, until $U_c \approx 2\lambda$ the interaction decreases the degree of localisation, while for large $|U|$, increasing U helps to make the system more localised. This is understood as a consequence of the formation of repulsive stable bound atom pairs in optical lattices described by a Hubbard Hamiltonian (Mattis (1986)) (for the first realization of this effect with cold atoms see Winkler et al. (2006)). These pairs have a reduced effective tunneling rate of $J_{eff} \approx J^2/|U|$ which thus increases the degree of localisation . Both above and below U_c for each value of U there is a definite value of λ for which the transition occurs. It is interesting to see whether the analogies between the non interacting and the interacting model are retained in presence of the time periodic modulation.

2.4.2 Setup

2.4.2.1 Imbalance

As a first step to explore the phase diagram of the model we mimic as closely as possible the procedure described in Bordia et al. (2017) but in a single particle context. The initial state there is chosen as a density-wave pattern in which fermions occupy the even sites of the lattice. The parameter which discerns between a localised and a non-localised phase is the asymptotic Imbalance:

$$I = \lim_{t\to\infty} \frac{1}{t} \int_0^t dt' \frac{N_e(t') - N_o(t')}{N_e(t') + N_o(t')} \tag{2.21}$$

where N_e and N_o are the number of particles in the even and odd sites respectively. A persistent Imbalance indicates a localised phase, while it obviously drops to 0 in absence of localisation, indicating that the system is ergodic as it does not retain the memory of its initial conditions.

To properly imitate the experiment we consider different realisations of the system each initially localised on a single even site and let them evolve separately under the Hamiltonian $H(t)$. The initial state in the Wannier states basis for each realisation $m = 1, ..., N/2$ reads:

$$\psi^{(2m)}(i, t = 0) = \langle i|\psi^{(2m)}(t = 0)\rangle = \delta_{i,2m} \tag{2.22}$$

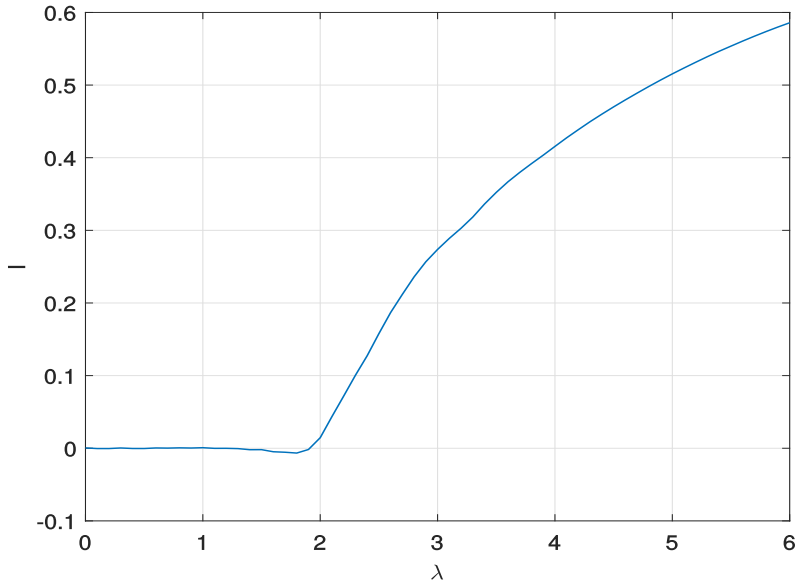

FIGURE 2.2: Imbalance in the time independent case as a function of the disorder strength λ, for lattice size $N = 50$, with periodic boundary conditions. We see a clear critical value at $\lambda_c = 2J$ indicating the localisation transition. The time of integration is $\tau = 1000\hbar/J$, at which the Imbalance has reached its asymptotic value

After a long evolution time we sum the modulus squared amplitudes of all the realisations to obtain the final density, namely:

$$n(i,t) = \sum_{m=1,\dots N/2} |\psi^{(2m)}(i,t)|^2 \tag{2.23}$$

The above definition is justified by the fact that the one-body density of a non interacting many-body system is the sum of the densities of the occupied single particle states Maruhn et al. (2010). The analogues to the occupation numbers N_e and N_o are then calculated by simply using this density function as a weight in the following sum:

$$N_e(t) = \sum_{i=1}^{N/2} n(2i,t) \tag{2.24}$$

and similarly

$$N_o(t) = \sum_{i=0}^{N/2-1} n(2i+1,t) \tag{2.25}$$

With these definitions we can calculate the Imbalance as defined in Eq. (2.21).

Before moving to the results for the driven lattice we show how the Imbalance behaves around the phase transition for the time independent model. Fig. (2.2) was obtained considering a lattice made of $N = 50$ sites and calculating the asymptotic Imbalance for different values of the disorder strength λ. It shows how the transition

is marked by a nonzero value of the Imbalance as a function of λ (all energies are in units of J), at the critical value $\lambda_c = 2J$.

The Imbalance is thus able to signal in a clear way the transition from the localised to the delocalised phase.

2.4.2.2 Inverse Participation Ratio

In this subsection we link the localisation properties of the model to the localisation of its Floquet states. The time periodicity of the full Hamiltonian $H(t)$ allows us to make use of the Floquet theorem, which states that we can write the time evolution of an arbitrary initial state as in Eq. (2.16) Shirley (1965), Sambe (1973):

$$|\psi(t)\rangle = \sum_n c_n e^{-i\epsilon_n(t)/\hbar} |u_n(t)\rangle \tag{2.26}$$

with $c_n = \langle u_n(0)|\psi(0)\rangle$ and ϵ_n are the quasienergies. We emphasize the fact that these coefficients do not depend on time.

We expand the Floquet states at $t = 0$ in the Wannier state basis yielding:

$$|\psi_n(0)\rangle = \sum_i b_i^{(n)} |i\rangle \,. \tag{2.27}$$

We define the averaged Inverse Participation Ratio (IPR) as the average of the IPRs of all the Floquet eigenmodes on the Wannier states, namely:

$$\text{IPR} = \frac{1}{N} \sum_{i,n} |b_i^{(n)}|^4 \tag{2.28}$$

where N represents the number of Floquet states which coincides with the number of sites of the lattice.

If each one of the Floquet states is localised on a single Wannier state then for any n there exists an i such that $|b_i^{(n)}| \approx 1$ and the sum approaches 1. If instead the eigenstates are distributed among many Wannier states then $|b_i^{(n)}| \approx 1/\sqrt{N}$ for all n, and i and the averaged IPR goes to 0 as $1/N$.

Thanks to the form of Eq. (2.26) we can expect a localised dynamics when very few Floquet states participate in the time evolution of an initial Wannier state. This would be the **analogue, in the context of time-periodic systems, to the phenomenon of Anderson localisation** for time independent Hamiltonians. Indeed, in a system that undergoes Anderson localisation, it is the localisation of the eigenstates of the Hamiltonian that implies non-ergodic dynamics Anderson (1958).

However at least in principle, one could have a localised dynamic without any localisation of the Floquet eigenstates, as it can occur as a consequence of the degeneracy of energy levels e.g. when the time average of the hopping parameter J becomes very small due to the driving. One is then left with an effective Hamiltonian, describing the time evolution over one period of the driving, where the hopping is completely suppressed. This particular mechanism is often referred to as *dynamic localisation* or *band collapse* (Drese and Holthaus (1997), Eckardt et al. (2009)). In Drese and Holthaus (1997), in particular, the authors propose to observe a dynamic localisation effect in a realization of the Aubry-André Hamiltonian by tuning the amplitude and frequency to a value for which the renormalized hopping would vanish. The periodic modulation that we are considering here is however different from theirs and doesn't allow to tune the time averaged hopping to zero. Comparing the Inverse Participation Ratio with the Imbalance allows us to verify that the localisation phase diagram of the model is not due to band collapse but to a time-periodic analogue of the Anderson localisation transition.

2.4.3 Results

In what follows we will indicate the disorder strength, λ, and the amplitude of the modulation, A, in units of J and times in units of $1/J$. The calculations below were done considering a lattice made of $N = 50$ sites, averaging over 20 different realisations of the disorder, which are obtained by varying the value of the phase ϕ in Eq. (2.19). In choosing β we decided to follow as close as possible the choice of the experiment in reference Bordia et al. (2017), so we chose $\beta = 532/738.2$. The simulations were made using the standard Matlab toolbox, solving the time evolution with the ode45 function in order to compute the Imbalance and exactly diagonalizing the propagator over one period to find the Floquet modes.

As a first step to outline the behaviour of this model we calculated the Imbalance for strong driving, i.e. $A = \lambda$, for a broad range of frequencies, keeping the disorder strength at a fixed value $\lambda = 5J$. The results are shown in Fig. (2.3), which highlights a delocalised regime for low frequencies while for high frequencies the Imbalance approaches that of the model in absence of driving. The similarity in the main features between this figure and the ones in Bordia et al. (2017) is already quite apparent. In particular the dip appearing after the Imbalance has started to rise, around $\hbar\omega = \lambda$, is present also in the many-body experiment, although less pronounced. We will give an heuristic explanation for the dip in Sec. (2.4.3.1), attributing the frequency dependence of the phase diagram to the spectrum of the time-independent model.

In order to better understand the phase diagram outlined by the Imbalance we have to consider the response of the model to various values of frequency and disorder. To this purpose we computed the time averaged Imbalance for different values of the

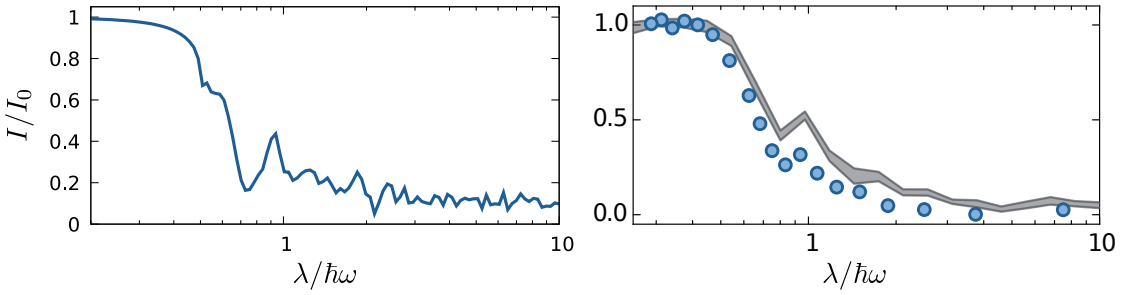

FIGURE 2.3: Imbalance as a function of frequency for $A = \lambda$, normalized to its value in the absence of driving. While for low frequencies the Imbalance is vanishing, it approaches its undriven value ($A = 0$) for high frequencies. The plot on the right is taken from Bordia et al. (2017) to allow comparison.

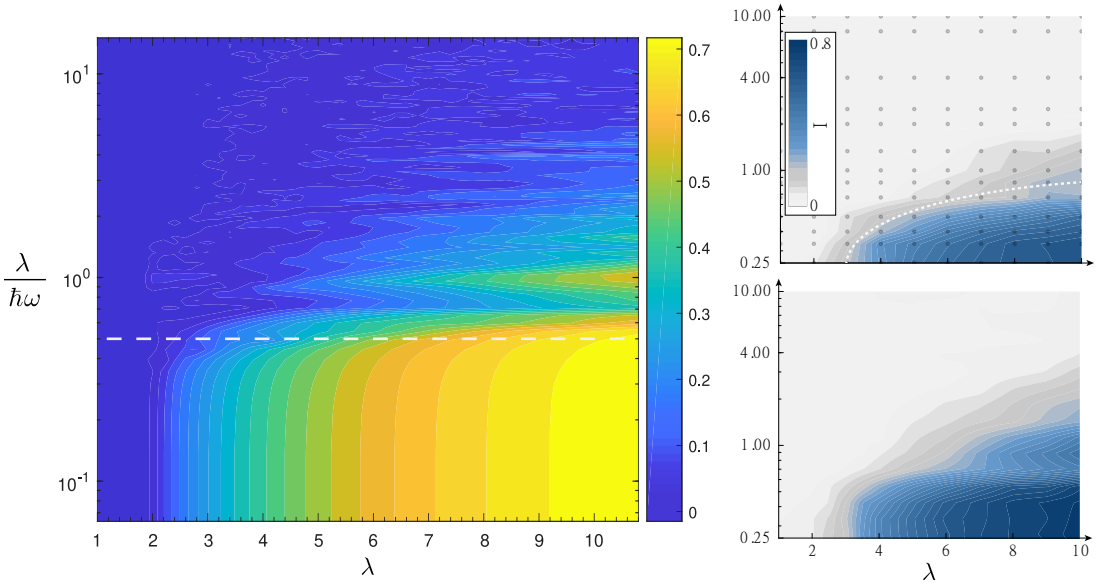

FIGURE 2.4: Imbalance as a function of frequency and disorder strength. On the vertical axis $\frac{\lambda}{\hbar\omega}$ is displayed in logarithmic scale to allow comparison with the experiment in Bordia et al. (2017), the results of which are displayed on the right of the figure. The dashed line is for $\hbar\omega_c = 2\lambda$, which is the approximate critical value for the frequency. The plots on the right are taken from Bordia et al. (2017) to allow comparison. The upper panel shows the experimental results, while the lower one shows results from numerical computations. The transition line for the model at $\hbar\omega_c = 2\lambda$ and the intermediate peak at $\hbar\omega = \lambda$ are present both in our single-particle model and in the many body one.

disorder strength λ and the angular frequency ω, setting the amplitude of the modulation in the strong driving regime i.e. $A = \lambda$. The evolution time is chosen to be 100 times the period of the modulation. In Fig. (2.4) and Fig. (2.5) the vertical axis shows $\lambda/\hbar\omega$ to allow comparison with the experiment in Bordia et al. (2017). In Fig. (2.6) the Inverse Participation Ratio is displayed as a function of λ and $\hbar\omega$ to more clearly show the relation between the frequency response and the spectrum.

Fig. (2.4) confirms that for very low frequencies the system is brought to a delocalised phase (marked by a vanishing Imbalance), while for high frequency the driving is not

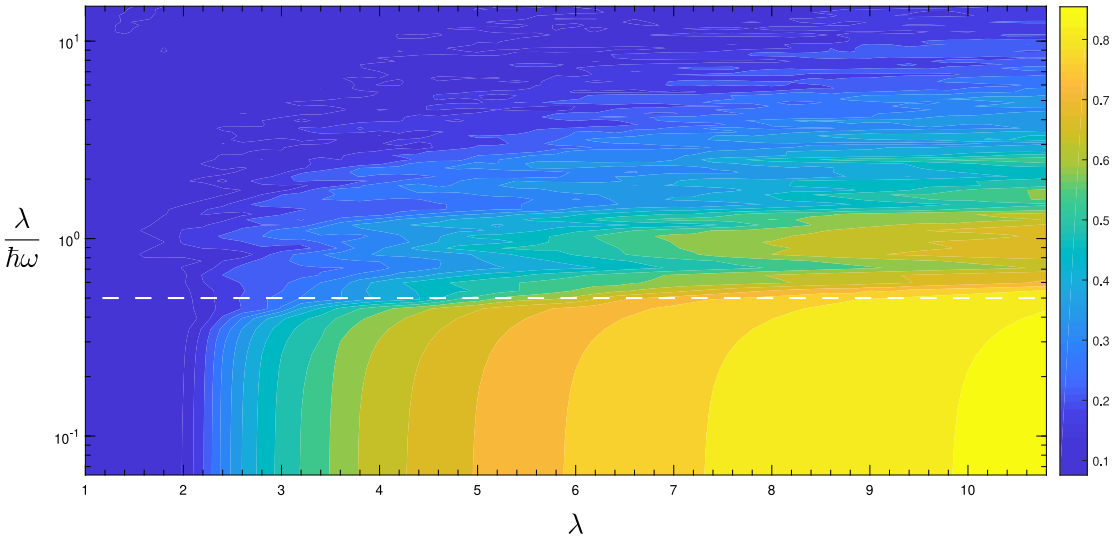

FIGURE 2.5: Inverse Participation Ratio as a function of frequency and disorder strength. On the vertical axis $\frac{\lambda}{\hbar\omega}$ is displayed in logarithmic scale to allow comparison with the experiment in Bordia et al. (2017). The dashed line is for $\hbar\omega_c = 2\lambda$, which is the approximate critical value for the frequency.

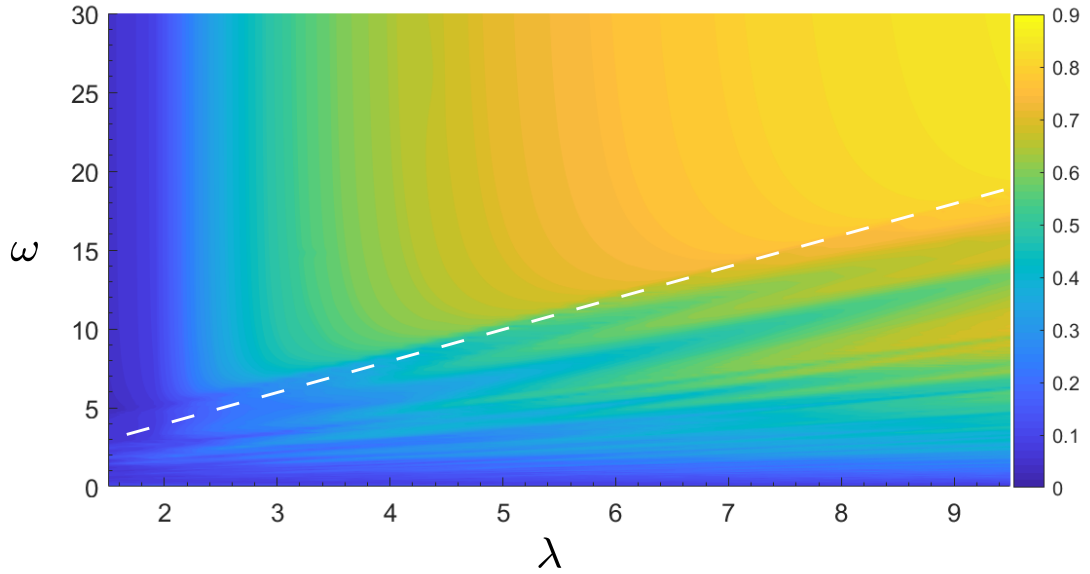

FIGURE 2.6: Inverse Participation Ratio as a function of frequency and disorder strength, for $A = \lambda$. The white dashed line is for $\hbar\omega_c = 2\lambda$, dividing the localised phase (yellow) from the delocalised one (blue).

able to bring the system to delocalisation anymore. Moreover it displays distinct analogy with the corresponding phase diagram in Bordia et al. (2017). The transition to a delocalised phase occurs for $\hbar\omega \approx 2\lambda$ both in the interacting and in the noninteracting case. The peak at $\hbar\omega = \lambda$ is also present in both cases, although it is more pronounced in the noninteracting case (see Fig. 2.3 for a better visual comparison).

As anticipated in the previous section we computed the Inverse Participation Ratio for various values of ω and λ. Figures (2.5) and (2.6) distinctly show the separation between the two phases. This also shows that the localisation properties of the Floquet eigenstates at initial time allow us to discern in a broad sense the different localisation properties of the system. This happens despite the fact that the initial Floquet states carry no information on the structure of the quasienergy spectrum which can contain accidental crossings of energy levels, causing the system to be partially localised.

The relatively small size of the system implies that the Inverse Participation Ratio will display finite size effects in the delocalised phase, where it vanishes as $1/N$. We run a simulation which computes the IPR as a function of frequency for different system sizes, going from $N = 50$ to $N = 500$. For each system size the IPR goes to 0 with the correct scaling with respect to N, while in the localised phase its behaviour is largely unchanged.

2.4.3.1 Critical frequency

In the results presented above there is a transition line (white dashed line in Fig. (2.4), Fig. (2.5) and Fig. (2.6) above which the system remains localised. This line appears for $\hbar\omega_c = 2\lambda$ which can be understood from the spectral properties of the Hamiltonian H_0 of Eq. (2.19). To better understand this, we refer to Fig. (2.1) showing the spectrum of the Aubry-André model as a function of the disorder strength for $N = 50$ lattice sites.

The bandwidth of the Aubry-André Model is $\approx 2\lambda$ for any disorder strength above the transition point $\lambda_c = 2J$. Thus the transition line in the time periodic case appears when the quanta of energy that the driving pumps into the system are too big for the system to absorb. Above the transition line the system's behaviour becomes that of the time independent model. This is because the period of the driving $T = 2\pi/\omega$ is now smaller than the fastest time scale present in the Aubry-André Hamiltonian, making the system unable to respond to the driving.

Below the transition line there are other smaller revivals of the localised phase. We attribute this intricate structure again to the spectrum of the Aubry-André model which is divided into smaller subbands divided by spectral gaps. In the intermediate range of frequencies where $\hbar\omega$ is comparable to the energy gaps present in the spectrum, the presence of a localised phase has a non monotonic dependence on the

frequency of the modulation. The most pronounced peak in the imbalance, that is apparent e.g. in Fig. (2.3), occurs around $\hbar\omega = \lambda$, compatibly with the energy difference between the two upper and lower bands and the central band in Fig. (2.1).

We mention that during the writing of this thesis we became aware of a paper Sinha et al. (2019) that complements our analysis. There, in an Aubry-Andrè model perturbed by multiple linear ramps of the disorder strength, the relation between the delocalisation transition and the spectrum of the undriven model is analysed in detal, and an argument in terms of the Kibble Zurek mechanism for the survival of some localised states is given.

All these results are consistent with what obtained in Bordia et al. (2017) and are well understood in terms of the single particle spectrum. This suggests that in this context the time averaged Imbalance, while providing a precise characterization of the phase diagram of the model, doesn't seem able to highlight the differences between an Anderson localised and a many body localised system.

2.4.3.2 Critical amplitude

Since for very low frequencies the system is brought to delocalisation we can define the following parameter:

$$\overline{\lambda}(t) \equiv \lambda + A\cos(\omega t) \tag{2.29}$$

If the frequency is low the global parameter $\overline{\lambda}(t)$ is changed adiabatically and sweeps through the transition point $\lambda_c = 2J$, bringing the system to delocalisation.

This intuitive picture helps us understand the role of the amplitude of the driving A: even for arbitrarily low frequencies the system does not delocalise if the amplitude is not big enough to make $\overline{\lambda}(t)$ sweep through the critical point $\lambda_c = 2J$. Following this reasoning we define the critical value for A to be such that $\min_t \left\{\overline{\lambda}(t)\right\} = \lambda_c = 2J$, namely:

$$A_c = \lambda - \lambda_c = \lambda - 2J \tag{2.30}$$

This picture is clearly confirmed by the contourplots of the Imbalance and the Inverse Participation Ratio as functions of the disorder strength and the amplitude, which are shown on Figures (2.7) and (2.8). For these plots we considered a frequency $\nu = \omega/2\pi = 0.005(1/J)$. The same value for the critical amplitude was found in Ray et al. (2018).

We stress that the very existence of a critical value of A as determined here is valid only in the case of a modulation of the form considered in this work, which corresponds to a modulation of the disorder strength. It is often stated in the literature (see Abanin et al. (2016), Gopalakrishnan et al. (2016), Rehn et al. (2016)) that a

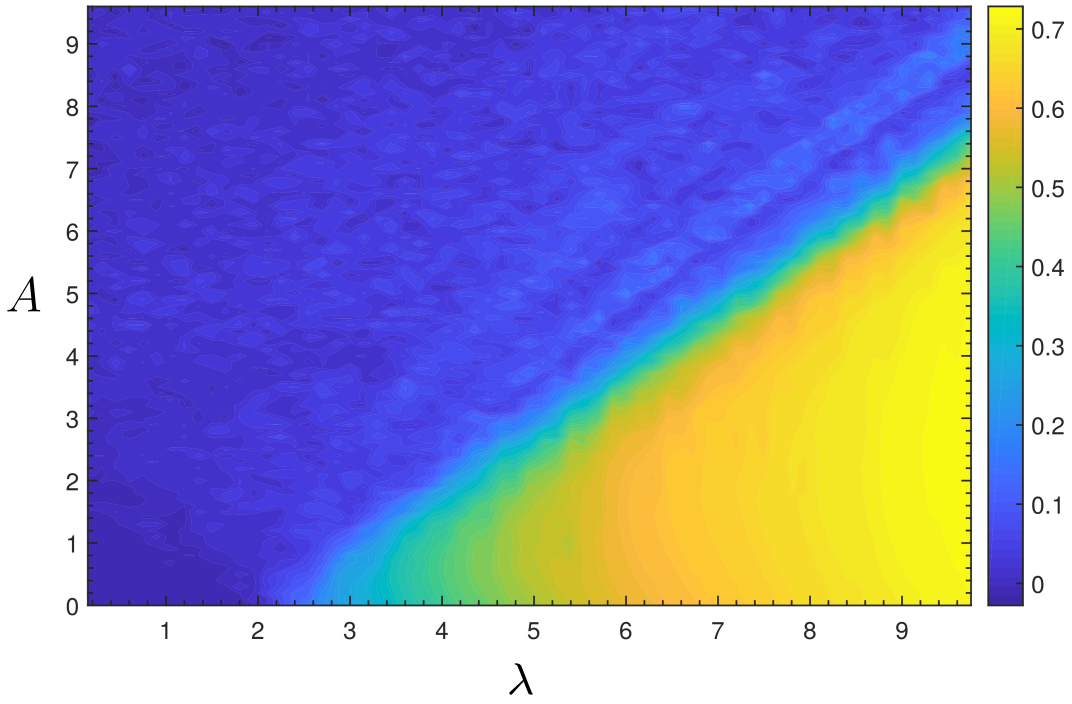

FIGURE 2.7: Imbalance as a function of amplitude and disorder strength, for $\nu = 0.005(1/J)$. There's a clear line for $A = \lambda - 2$ separating the localised phase (yellow) to the delocalised one (blue).

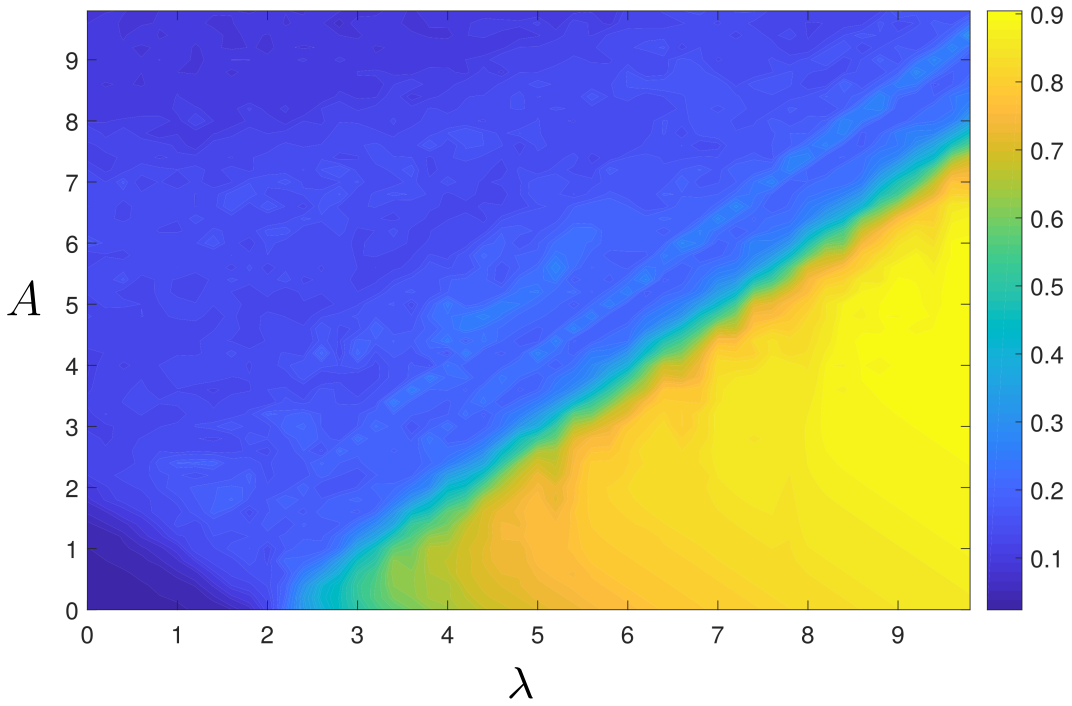

FIGURE 2.8: Inverse Participation Ratio of the Floquet eigenstates as a function of amplitude and disorder strength, for $\nu = 0.005(1/J)$. The result is consistent with the one in Fig. (2.7), confirming that the localisation properties of the model are due to the localisation of the Floquet eigenstates

modulation of arbitrarily small amplitude will always delocalise a many-body localised quantum system provided that the driving frequency is small enough. This statement however is not in contrast with our result as it refers to a driving of the form $A\cos(\omega t)\sum_i i\, c_i^\dagger c_i$.

2.4.3.3 Role of the interactions

Last, we want to briefly comment on the role of the interaction. In presence of the interaction U, we expect to retain most of the qualitative results displayed, as comparison with the many-body experiment seems to suggest. In particular, regarding the frequency response of the system we expect the description in terms of the spectrum to be still relevant, with the critical value ω_c to be shifted to be equal to the badwidth of the interacting model. According to Mastropietro (2016) the many-body interaction will change the size of the infinite number of spectral gaps of the non interacting spectrum, without closing any of them. This makes the interacting model very similar to the non interacting one, except for the intermediate frequency regime where the effect of the interaction in coupling the energy levels is crucial, possibly explaining the less sharp peaks displayed in the experiment in Bordia et al. (2017).

2.5 Conclusions

Our work shows that the driven non interacting Aubry-André model qualitatively reproduces many of the localisation phenomena which are found in the experiment Bordia et al. (2017) such as the presence of a delocalised phase for low frequency, the persistence of localisation for a high frequency driving, and the existence of a critical value of driving amplitude for the onset of the localisation transition.

We were able to determine the critical values for the frequency and the amplitude of the driving, and provide a physical explanation for their values. Further, we related the phases of the model to the localisation of its Floquet eigenstates. This shows that the localisation transition brought by the periodic driving is a time periodic analogue of the well known Anderson localisation transition. Future theoretical studies should focus on the role of interactions and the new qualitative aspects they bring.

3

Effective interactions among heavy fermions in presence of a light impurity - the N+1 bound problem

3.1 Introduction: the N+1 bound problem

How many atoms N of a species A can be bound by a single atom of a different species B?

In asking this question, we are assuming that the A atoms do not interact with each other since then the physics would be dominated by the intraspecies (A-A) interactions. We will rather consider that only the interspecies (A-B) interaction exists which makes this question rather nontrivial.

Theoretical works on few-body systems have shown that a single atom can bind together up to five noninteracting atoms of a different species Bazak and Petrov (2017), thus realizing a *pentamer* or $4+1$ *bound cluster*. While it is to a certain extent *expected* that there should be a limit to the number of atoms that can be bound this way, there is to our knowledge no simple argument that predicts its existence, even within the constraints of a sufficiently idealised model. In this chapter we attempt at tackling the question within such model. Similarly to the few body calculations that predict the $2+1$, $3+1$ and $4+1$ bound cluster we will assume zero-range interactions that can be described by a scattering length a (see appendix A). However we will approach the problem assuming a large number of atoms N. The result that we can obtain in this way are limited by our assumptions but provide a way to explore the problem within a simplified framework, avoiding the computational challenge of solving the exact few-body problem for increasing N.

Before we continue, we need to explain what it means for N type-A atoms to be bound by 1 type-B atom – forming an $N+1$ bound state. For a bound state of $N+1$ atoms to exist, its lowest energy state must obey

$$E_{N+1} < 0 \tag{3.1}$$

But this is only one first condition. We also need it to be energetically stable against fissioning into smaller parts. The requirement for that is that, for any way of partitioning the bound state, the total energy of the parts must be larger than the cluster's energy. For example, if we consider the possibility of fissioning into two parts N_1 and N_2 with $N_1 + N_2 = N + 1$ we must have :

$$E_{N+1} < E_{N_1} + E_{N_2} \tag{3.2}$$

and so on also for all partitions into three and more subclusters.

For correctly calculated ground state energies it is always true that $E_{N+1} \leq E_{N_1} + E_{N_2}$ since the N Hilbert space contains the smaller N_1 and N_2 spaces. What is relevant here is that we are restricting the search to states where all the atoms are located in the bound state, i.e. do not go off to infinity. Within this constraint, it is no longer necessarily true that $E_{N+1} \leq E_{N_1} + E_{N_2}$. If in fact we find that $E_{N+1} > E_{N_1} + E_{N_2}$ it means physically that the $N+1$ cluster can fission into N_1 and N_2 clusters. Of course we are assuming here that the ground state energies are reliably calculated with our scheme.

However in our case there is a great simplification: because we are taking the A atoms to be non-interacting, the energy of the subcluster which does not contain the B atom can be taken to be zero. This is because its energy is only kinetic in origin since there are no A-A interactions and therefore, is non-negative. So in our case the criterion for stability reduces to the following:

$$E_{N+1} < E_{N'+1}, \qquad \forall N' < N. \tag{3.3}$$

In other words, the energy must be a monotonic decreasing function of N. We remark however that this criterion is a sufficient condition to have a bound cluster and not a necessary one.

3.1.1 Outline

In this chapter we employ the Born-Oppenheimer approximation and the zero range approximation to analyse the $N+1$ bound problem. We will make a number of approximations in order to simplify the model. While this will limit the validity of our results, it will help us to gain physical insight into the problem and obtain results

within a simplified model. The strategy we will follow is to derive the energy of the impurity in presence of the N heavy fermions and check whether the energy of the $N+1$ system satisfies the stability criterion of Eq. (3.3). In order to estimate the energy of the impurity we will assume that it can be described as a polaron inside a background of noninteracting atoms.

Before moving to the actual problem we will first introduce a result in bosonic systems which shows that, for a model square well interaction potential, a single particle can bind an infinite amount of Bosons. Then we will mention the main result for Fermions which act as the starting point for this work.

The chapter is structured as follows. Secs. 3.2 and 3.3 introduce what we already know about the problem in the bosonic and in the fermionic case respectively. In sec. 3.4 we compute the binding energy and the kinetic energy of the impurity in the $N+1$ problem via the Born Oppenheimer approximation. In sec. 3.5 we compute the energy of the whole $N+1$ system and tackle the question that motivates this chapter.

3.2 The bosonic case

It is clear that the statistics of the A atoms plays a crucial role: if they are Bosons we can expect it is easier to bind them than if they are Fermions due to the Pauli repulsion.

Indeed, within a simple model of N type-A Bosons interacting with a single B atom through a finite-range attractive square well potential, **we can show rigorously that the B atom can bind an arbitrarily large number of Bosons**.

Suppose the A atoms do not interact among themselves and interact with the B atom with a potential $V(\mathbf{r})$ of depth V_0 and range r_0:

$$V(\mathbf{r}) = \begin{cases} -V_0 & r \leq r_0 \\ 0 & r > r_0 \end{cases}$$

Consider now a many-body wavefunction ψ defined as the product of single-particle wavefunctions of the A atoms $\psi(\mathbf{r}_i)$ and the wavefunction of the B atom, $\chi(\mathbf{r}_B)$:

$$\Psi\left(\mathbf{r}_1, ...\mathbf{r}_N, \mathbf{r}_B\right) = \chi\left(\mathbf{r}_B\right) \prod_{i=1}^{N} \psi\left(\mathbf{r}_i\right) , \tag{3.4}$$

where $\mathbf{r}_i$ is the position of the i-th A particle and $\mathbf{r}_B$ is the position of the B atom. Let us further suppose that the wavefunctions vanish outside a sphere of radius $R < 2r_0$. This implies that all the A atoms will feel the attractive potential $-V_0$. Under this

conditions the kinetic energy of the system is

$$E_k = K_B + NK_A\,, \tag{3.5}$$

where K_A is the kinetic energy of each A atom and K_B is the kinetic energy of the B atom. Crucially, both K_A and K_B do not depend on the depth of the potential V_0. The potential energy of the system is instead given by

$$U_b = -NV_0\,. \tag{3.6}$$

The total energy of the system is thus negative when

$$V_0 > K_A + \frac{K_B}{N} \tag{3.7}$$

Fixing the depth V_0 to satisfy Eq. (3.7) for $N = 1$ (i.e. $V_0 > K_A + K_B$) we get that the energy of the system is negative for any value of N and moreover it is a monotonically decreasing function of N. This fact, thanks to the criterion in Eq. (3.3) is enough to establish that a single atom B can bind an arbitrarily large number of Bosons, for a given attractive potential $V(r)$. Importantly, we can choose a value for V_0 that does not depend on N.

Experimentally, the question of the maximum bosonic cluster size is difficult to investigate with real ultracold bosonic atoms due to the large number of bound states in interatomic potentials, which can lead to rapid two-body loss when the interparticle scattering length is larger than the average distance between A-A atoms.

3.3 The fermionic case

The situation is considerably more interesting in the case of fermions where the A-B attractive interaction must compete with the Pauli repulsion. The simple trial wavefunction chosen in the previous subsection does not satisfy the stability criterion of Eq. (3.3) as the kinetic energy of the noninteracting A atoms scales as $N^{5/3}$. However, the $N + 1$ bound problem is motivated in this case by results in few-body physics for mass imbalanced Fermionic systems. This is the kind of systems that we will investigate in the remainder of the chapter.

In the context of few-body Fermions a system that has drawn theoretical interest is that of two heavy fermions (of mass M) interacting with a light one (of mass m) with a short range, nearly resonant potential. Kartavtsev and Malykh have shown that when the ratio between the masses $r = M/m$ satisfies the condition $8.172 < r < 13.607$ there exist a bound trimer, i.e. a cluster formed by two A particles of mass M and one B particle of mass m Kartavtsev and Malykh (2007). In this case the competition between

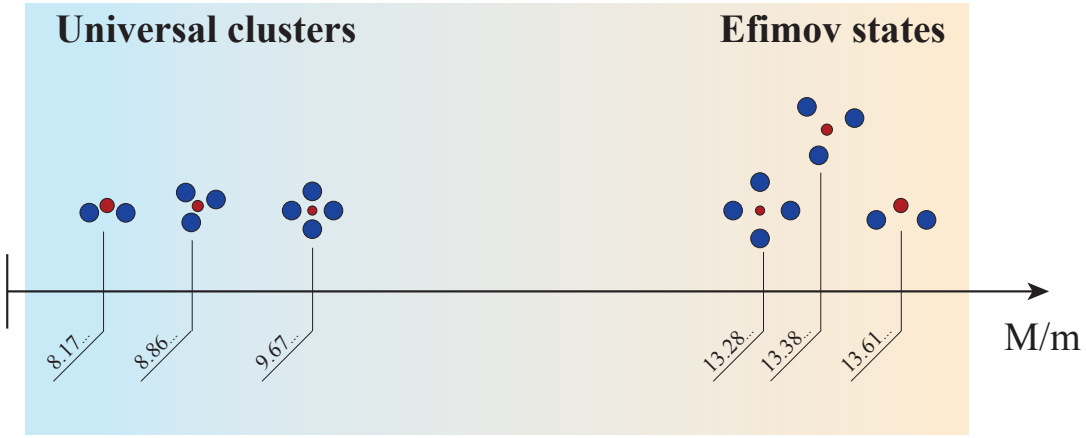

FIGURE 3.1: Schematic representation of the current results on few-body clusters. From small to higher mass ratios r the 2+1, 3+1, 4+1 bound universal clusters and the 4+1, 3+1, 2+1 Efimov states. Axis not to scale.

the interaction induced by the light B particle and the centrifugal barrier produce an effective potential with a local minimum which admits bound states that are stable against fissioning into subclusters. Other works have extended this result to bigger clusters. For $9.5 \lesssim r < 13.384$ a tetramer was found numerically by Doerte Blume in Blume (2012), which is the 4-body analogue of the trimers found in Kartavtsev and Malykh (2007). Bazak and Petrov Bazak and Petrov (2017) have recently proven the existence of a pentamer when the critical mass ratio satisfies $9.672 < r < 13.279$ respectively. These clusters are called in the literature *universal clusters* Naidon and Endo (2017) as they are completely described by a zero-range model of the interactions, thus their binding energy depends only on the scattering length and not on other details of the underlying potential.

For mass ratios bigger than the upper limits mentioned above, called *critical mass ratios* (13.28, 13.38 and 13.279) the zero-range model would predict an unphysical collapse of the few-body clusters (the *fall to the center problem*, see e.g. Landau and Lifshitz (1958)) and an infinitely negative energy at vanishing distances. The unphysical fall to the center is cured by taking into account an effective three-body interaction, which supports an infinity number of bound states, called *Efimov states*. Thus, the upper limits on the mass ratios for the existence of the universal clusters signal the presence of Efimov states. The situation is schematically summarized in Fig. (3.1).

The goal of this chapter is thus to consider what is a generalization of the few body problem, where a system of N heavy fermions of mass M interacts with a single light fermion of mass m, and see if we can provide an argument for the presence (or absence) of a $N+1$-body cluster. This question is justified in the first place by the results obtained in the few-body cases mentioned in the previous paragraphs, which are exact but limited to a small number of atoms. We are instead interested in the case of a large number of atoms where exact (numerical or analytical) computations are

unfeasible. We will disregard for the purpose of our analysis the existence of Efimov states, by considering mass ratios higher than the critical ones. This is because we are interested in **testing the validity of our model** in describing the basic physics behind the existence or absence of stable clusters. We stress that approaching the problem from the large N limit cannot provide a quantitatively accurate limit on the number of particles that can be bound but it allows to tackle the question of whether this limit exists.

3.4 Chemical potential and kinetic energy of the impurity in the Born-Oppenheimer approximation

We want to obtain an estimate of the binding and kinetic energies of a light impurity interacting with N heavy fermions. In order to do so we employ the Born Oppenheimer approximation which consists in finding the binding energy of the light impurity treating the positions of the heavy fermions as fixed. The latter appear thus as parameters in the Schrödinger equation of the impurity, representing fixed scatterers with which the impurity interacts. This procedure is justified by the large difference in mass between the two species, which allows us to think of the state of the light fermions as adiabatically adjusting to the (small) variation in positions of the heavy fermions.

We mention that through the Born-Oppenheimer approximation one can provide very good estimates of the critical mass ratio for the Efimov trimer and for the Universal trimers, as can be seen in Petrov (2013). Both phenomena are understood as a competition between the centrifugal repulsion and the exchange attraction induced by the impurity. Namely the universal trimer is formed when the total Born-Oppenheimer potential is repulsive both at short distances and long distances but has a minimum in between, while the Efimov effect occurs for nearly resonant interactions and larger mass ratios, when the attractive interaction ($\propto \frac{1}{r^2}$) completely overcomes the centrifugal barrier, leading to the fall to the center problem.

We consider the scattering of the light atom with the heavy ones in the zero range approximation, which is detailed in the appendix A. Here we quickly mention its most basic formulas in the case of the scattering of $N = 1$ (one heavy particle plus the impurity) in order to build an analogy for the general $N + 1$ case.

The Bethe-Peierls boundary conditions for a particle interacting with a potential described by a scattering length a read (see appendix A, Eq.(A.9)):

$$\lim_{\mathbf{r}\to 0} \psi(\mathbf{r}) \propto \frac{1}{r} - \frac{1}{a}, \tag{3.8}$$

where r is the relative position of the two scattering particles. We remind that this boundary condition replaces the interaction potential in the Schrödinger equation of the relative wavefunction. In the Born-Oppenheimer approximation the heavy atoms act as fixed scatterers, so the relative wavefunction $\psi(\mathbf{r})$ is just the wavefunction of the light atom.

The Schrödinger equation for the light impurity reads:

$$\nabla^2_{\mathbf{r}}\psi_{\mathbf{R}}(\mathbf{r}) = -\frac{\hbar^2\kappa^2(\mathbf{R})}{2m}\,\psi_{\mathbf{R}}(\mathbf{r})\,, \tag{3.9}$$

with $\mathbf{R}$ the position of the heavy atom and the wavefunction $\psi_{\mathbf{R}}(\mathbf{r})$ satisfying the Bethe Peierls boundary condition, Eq. (3.8). The solution to the above Schrödinger equation is given by:

$$\psi_{\mathbf{R}}(\mathbf{r}) = C\,\frac{\exp\left(-\kappa(R)|\mathbf{r}-\mathbf{R}|\right)}{|\mathbf{r}-\mathbf{R}|}\,, \tag{3.10}$$

with $\kappa(\mathbf{R})$ that must be chosen to satisfy Eq. (3.8) and C is a normalization constant. Analogously, in presence of N fixed scatterers (the heavy atoms) positioned at R_i we can write the wavefunction of the impurity as:

$$\psi_{\{\mathbf{R}_i\}}(\mathbf{r}) = \sum_{i=1}^{N} C_i \frac{\exp\left(-\kappa(R_i)|\mathbf{r}-\mathbf{R}_i|\right)}{|\mathbf{r}-\mathbf{R}_i|}\,. \tag{3.11}$$

We will drop in what follows the subscript $\{\mathbf{R}_i\}$. We can now impose the boundary conditions forced upon this wavefunction by the Bethe-Peierls boundary condition, namely that, for $\mathbf{r}\to\mathbf{R}_j$,

$$\psi(\mathbf{r}) \propto \frac{1}{|\mathbf{r}-\mathbf{R_j}|} - \frac{1}{a} \tag{3.12}$$

Expanding in powers of $\mathbf{r}-\mathbf{R_j}$ the wavefunction in Eq. (3.11) we obtain the following matrix equation:

$$C_j(\kappa - \frac{1}{a}) = \sum_{i\neq j}^{N} C_i \frac{\exp\left(-\kappa|\mathbf{R}_i-\mathbf{R}_j|\right)}{|\mathbf{R}_i-\mathbf{R}_j|} \tag{3.13}$$

Equation (3.13) is quite general and relies only on the assumptions underlying the Born-Oppenheimer approximation (namely that $M \ll m$) and the existence of a well defined zero-range approximation that allows, at low energies, to describe the short range interaction potential between the particles by means of the s-wave scattering length a.

In the case of N sufficiently big we take the continuum approximation of Eq. (3.13). In order to do so, we first of all define the density for the heavy fermions as:

$$\rho(\mathbf{r}) = \sum_i \delta(\mathbf{r}-\mathbf{R}_i) \tag{3.14}$$

Inserting this into Eq. (3.13) we obtain the following integral equation:

$$C(\mathbf{r})(\kappa - \frac{1}{a}) = \int d^3\mathbf{r}' C(\mathbf{r}') \frac{\exp(-\kappa|\mathbf{r} - \mathbf{r}'|)}{|\mathbf{r} - \mathbf{r}'|} \rho(\mathbf{r}') \tag{3.15}$$

The natural way to take the continuum approximation consists in considering $\rho(\mathbf{r})$ as a smooth function of the coordinate $\mathbf{r}$ and not as a sum of Dirac deltas centered at each fermions' position $\mathbf{R}_j$.

We can recast the integral equation obtained in Eq. (3.15) into a differential equation by applying the operator $\hat{L} = \nabla^2 - k^2$ on both sides, yielding:

$$(\nabla^2 - \kappa^2) C(\mathbf{r}) = 4\pi \frac{C(\mathbf{r})\rho(\mathbf{r})}{\frac{1}{a} - \kappa} \tag{3.16}$$

Where we used the fact that:

$$\hat{L}\left(\frac{\exp(-\kappa|\mathbf{r}|)}{|\mathbf{r}|}\right) = (\nabla^2 - \kappa^2)\left(\frac{\exp(-\kappa|\mathbf{r}|)}{|\mathbf{r}|}\right) = -4\pi\delta(\mathbf{r}) \tag{3.17}$$

We can now find the groundstate energy in the case where ρ does not depend on position. We further assume that the wavefunction $C(\mathbf{r})$ and $\rho(\mathbf{r})$ are constant in the ground state and we are led to the equation

$$\kappa^2(\kappa - 1/a) = 4\pi\rho. \tag{3.18}$$

Solving this equation for κ we can find the chemical potential of the impurity, which is defined as:

$$\mu_{\text{imp}} \equiv -\frac{\hbar^2\kappa^2}{2m}. \tag{3.19}$$

From Eq. (3.18) we get the following equation for $\eta = |\mu_{\text{imp}}|/E_F$

$$\frac{1}{k_F a} = \sqrt{\frac{\eta}{r}} - \frac{2}{3\pi}\frac{r}{\eta}, \tag{3.20}$$

where $r = M/m$ is the ratio between the masses of the heavy fermions and the light atoms. This equation is the same as Eq. (9) from Combescot et al. (2007) in the limit of large M/m, i.e. the energy of a Fermi polaron. The binding energy or chemical potential of the impurity can be regarded, in the spirit of the Born-Oppenheimer approximation, as an effective interaction between the heavy atoms.

In order to find the effective mass of the impurity we imagine to impart a small momentum q to it, which amounts to choosing in Eq. (3.16) a plane wave solution for $C(\mathbf{r})$, namely:

$$C'(\mathbf{r}) = C\, e^{-i\mathbf{q}\cdot\mathbf{r}}, \tag{3.21}$$

where q must satisfy $q^2 \ll \kappa^2$. The energy upon this small boost is then shifted from μ_{imp} to some μ'_{imp} depending on q, which satisfies:

$$\mu'_{\text{imp}}(q) = \mu_{\text{imp}} + \frac{\hbar^2 q^2}{2m^*}\,, \tag{3.22}$$

where m^* is the effective mass. Then the effective mass reads:

$$m^* = m \lim_{q\to 0} \left[\left(\kappa^2(q=0) - \kappa^2(q)\right)^{-1} q^2 \right] \tag{3.23}$$

which yields:

$$m^* = \frac{3}{2} m \left(\frac{1 - \left(\frac{4\pi}{9}\right)^{1/3} \frac{1}{k_F a}}{1 - \left(\frac{3\pi}{2}\right)^{1/3} \frac{1}{k_F a}} \right)\,. \tag{3.24}$$

In Fig. (3.2) we plot the inverse of the effective mass as a function of $1/k_f a$. The effective mass becomes negative for $1/k_F a = (2/3\pi)^{1/3}$ which indicates an instability. This is due to the formation of a dimer composed of the light impurity and one of the heavy atoms.

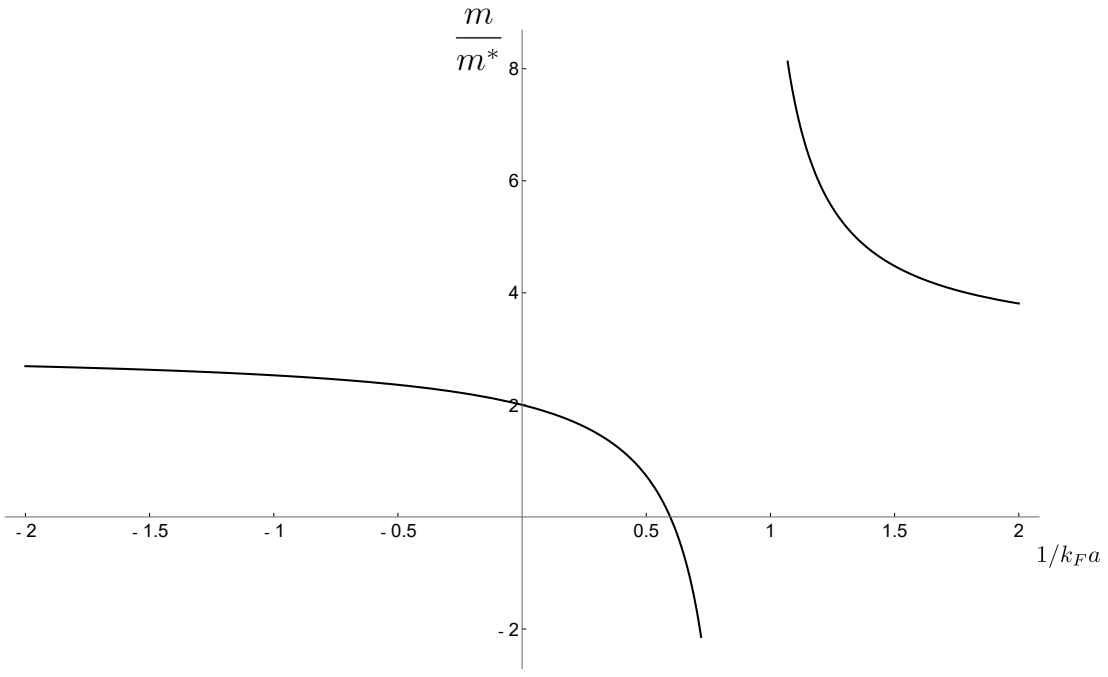

FIGURE 3.2: Inverse effective mass m/m^* as a function of $1/k_F a$. At $1/k_F a = (2/3\pi)^{1/3} \approx 0.6$ the effective mass becomes negative, indicating an instability corresponding to the polaron-dimer threshold.

3.5 Energetic analysis of the N+1 bound problem

3.5.1 Local density approach

To investigate the problem of whether there exists a bound state for arbitrarily large N, we would need to exactly solve the many-body problem in the large N limit. However, as we have mentioned in section 3.3, the computations of the exact energies are already challengin for few-body atoms, and have been obtained so far only up to $N = 5$. To overcome this we will make some assumptions about the energy functional in the large N limit and we will then work out their consequences in this chapter. These assumptions are based on a key idea, which we are putting to test: *in the case of large N bound states, the impurity behaves as a polaron inside the cluster, in the sense that its energy is given by a similar formula as in the usual extended gas case.* Moreover, rather than obtaining a quantitatively accurate estimate of the energy of the cluster, we are interested in deriving its scaling behaviour with respect to the parameters of the system, i.e. the interparticle distance (or equivalently the Fermi wavevector k_F) and the number of particles.

So we *assume* that the energy of the $N + 1$ system can be written in the following form:

$$E = \frac{3}{5}N\frac{\hbar^2 k_F^2}{2M} + \int_V d\mathbf{r}^3 \left(\frac{\hbar^2}{2m^*}|\nabla\Psi|^2 + \mu_{\text{imp}}|\Psi(\mathbf{r})|^2 \right) , \tag{3.25}$$

where the integration is carried out over the volume V of the purported cluster, which we assume to be a cubic box with linear size L, while k_F is the wavevector of the heavy Fermi atoms $k_F = (6\pi^2 N/V)^{1/3}$. The first term is the energy of the noninteracting Fermions which are assumed to be homogeneously distributed inside the box, $\Psi(\mathbf{r})$ is the wave function of the impurity and μ_{imp} is its chemical potential. In the usual case the wavefunction of a polaron is a plane wave. Here it is a localised wave packet centred around the cluster of N particles.

The scaling of the momentum of the impurity $p\Psi = -i\hbar\nabla\Psi$ with respect to the linear size L can be estimated from the Heisenberg uncertainty principle to be:

$$p^2 = \frac{3\hbar^2}{4L^2} = 3\hbar^2 \left(\frac{\pi}{6N}\right)^{2/3} \left(\frac{k_F}{2\pi}\right)^2 , \tag{3.26}$$

where we expressed the result in terms of the Fermi wavevector, proportional to the inverse of the interparticle distance $\approx (V/N)^{1/3}$.

Carrying out the integration in Eq. (3.25) we obtain:

$$E = \frac{3}{5}N\frac{\hbar^2 k_F^2}{2M} + \frac{3\hbar^2}{2m^*}\left(\frac{\pi}{6N}\right)^{2/3} \left(\frac{k_F}{2\pi}\right)^2 + \mu_{\text{imp}} . \tag{3.27}$$

The chemical potential of the impurity in Eq. (3.27) is the solution to Eq. (3.20) and the effective mass is given by Eq. (3.24). It is important to notice that both the chemical potential and the effective mass do not depend on the mass ratio r and the number of particles N.

Eq. (3.27) is based on three assumptions: that the N fermions are heavy compared to the single impurity, i.e. $M/m \gg 1$; that we are dealing with a system of many particles, i.e. $N \gg 1$ and that the polaron description valid for homogeneous systems can be used to describe the bound cluster.

Before looking for possible bound states it is worthwhile to comment on how the terms in Eq. (3.27) contribute to the energy of the system. A bound state can be formed when the effective attraction coming from the chemical potential of the impurity overcomes both the kinetic energy of the heavy fermions and of the impurity at long distances. Conversely, the kinetic energies must overcome the chemical potential to provide a barrier at short distances, in order to prevent an infinitely negative energy. From Eq. (3.27) it is clear that **increasing the mass ratio will favour the negative contribution from the chemical potential**, while **increasing the number of particles at fixed density ($\rho \propto k_F^{1/3}$) will favour the positive contribution from the kinetic energies**.

In the particular limit $a \to \infty$, when the scattering length is bigger than any other length scale in the system, Eq. (3.27) contains only terms that are quadratic in k_F. In this case there are only two possible outcomes, the total energy is either:

- **always positive**, when the number of particles makes the kinetic energy of the fermions bigger than the binding energy, causing the cluster to be unbound.
- **negative and unbounded from below** for vanishing interparticle distance, when a big mass ratio makes the kinetic energy of the fermions smaller than the binding energy. A negative infinite energy signals a fall to the center problem and possibly the presence of Efimov states.

For the stability of the system against fission into smaller clusters (see Eq. (3.3)) the dependence on the number of particles N is the crucial point. The number of particles appears in two terms: the kinetic energy of the heavy fermions and the kinetic energy of the impurity. For fixed mass ratio $r = M/m$ and density the kinetic energy of the heavy fermions increases linearly in N, as each of the non-interacting fermions has a kinetic energy which does not depend on N. On the contrary, the kinetic energy of the impurity is a decreasing function of N, as increasing N at fixed density will increase the available volume for the impurity, lowering its kinetic energy.

All the considerations made above qualitatively agree with the results on few-body clusters that we outlined in section 3.3. We will now divide our search into two

directions which is the positive scattering length and the negative scattering length case.

3.5.2 Positive scattering length near unitarity

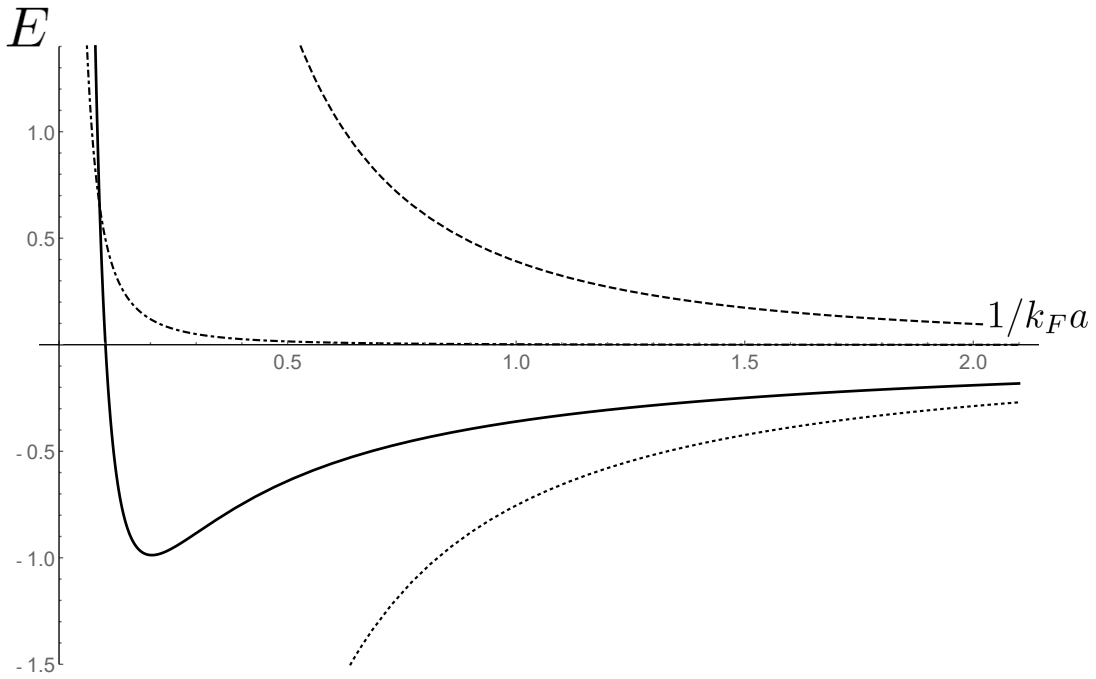

FIGURE 3.3: Energy (thick line) of the N+1 system as a function of $1/k_F a$, for mass ratio $r = 23$ and $N = 15$, in the unitary limit. The dashed line is the contribution from the kinetic energy of the heavy fermions, the dash-dotted line is the kinetic energy of the light fermion and the dotted line is the chemical potential of the light fermion.

The presence of the instability due to the polaron-dimer treshold illustrated in Fig. (3.2) constrains our search to the range $1/k_F a < 0.6$. For this reason, it is worthwhile to consider here the case where the scattering length is positive and the interactions are close to the unitary limit, i.e. $1/k_F a \ll 1$.

To first order in the small parameter $1/k_F a$, the chemical potential reads:

$$\frac{\mu_{\text{imp}}}{E_F} \approx -\left(\left(\frac{2}{3\pi}\right)^{2/3} + \frac{2}{3}\left(\frac{2}{3\pi}\right)^{1/3}\frac{1}{k_F a}\right) r\,, \tag{3.28}$$

where $E_F = (6\pi^2\rho)^{2/3}\hbar^2/2M$ is the Fermi energy of the medium and $r = M/m$ is the ratio between the masses. Note that in the equal mass case, $\mu_{\text{imp}} \simeq -0.6E_F$. This does not invalidate Eq. (3.28) since that equation is derived for large mass rations r.

The effective mass near unitarity reads:

$$m^* = \frac{3}{2}m\left(1 + \left(\frac{\pi}{18}\right)^{1/3}\frac{1}{k_F a} + ...\right) \simeq \frac{3}{2}m\left(1 + \frac{0.559}{k_F a}\right)\,. \tag{3.29}$$

Plugging this results into Eq. (3.25) we obtain the expression for the energy of the system near unitarity, to first order in $1/k_F a$:

$$E = \frac{3}{5}N\frac{\hbar^2 k_F^2}{2M} + \frac{\hbar^2}{m}\left(\frac{\pi}{6N}\right)^{2/3}\left(1 - \frac{d}{k_F a}\right)\left(\frac{k_F}{2\pi}\right)^2 - \left(b + \frac{c}{k_F a}\right)\frac{\hbar^2 k_F^2}{2m}, \tag{3.30}$$

where $b = 0.356$, $c = 0.398$ and $d = 0.559$. This expression, compared with Eq. (3.27) requires the additional assumption that $1/k_F a \ll 1$

We will look for minima with respect to k_F by imposing that:

$$\frac{\partial E}{\partial k_F} = 0 \tag{3.31}$$

$$\frac{\partial^2 E}{\partial k_F^2} > 0 \tag{3.32}$$

Moreover we have to make sure that the condition for stability against fissioning, Eq. (3.3), is satisfied at the minimum in k_F. The condition in Eq. (3.32) is verified when the following condition is met:

$$\frac{3}{5}Nr^{-1} + \frac{1}{2\pi^2}\left(\frac{\pi}{6N}\right)^{2/3} > b \tag{3.33}$$

We differentiate with respect to k_F and find that the minimum is given by:

$$\frac{1}{k_F a} = \frac{2\left(\frac{3}{5}Nr^{-1} + \frac{2}{(2\pi)^2}(\frac{\pi}{6N})^{2/3} - b\right)}{\left(\frac{2d}{(2\pi)^2}(\frac{\pi}{6N})^{2/3} + c\right)} \tag{3.34}$$

where $r = M/m$.

The energy at the minimum reads:

$$E_{min} = -\frac{\frac{d}{2\pi^2}\left(\frac{\pi}{6N}\right)^{2/3} + c}{4\left(\frac{3N}{5r} + \left(\frac{\pi}{6N}\right)^{2/3}\frac{1}{2\pi^2} - b\right)}. \tag{3.35}$$

The energy at the minimum is displayed in Fig. (3.4). The plot in Fig. (3.4) shows that for $N > 6$ the energy of the cluster is an increasing function of N, suggesting that any $N + 1$ cluster beyond $N = 6$ is unstable and will fission into smaller parts. Thus, our model predicts that there is a limit to the number of atoms that can be bound.

For $N < 6$ our model produces an unphysical infinitely negative energy, which is in general an artifact of the zero-range approximation. Moreover, the region for small N is outside the range of validity of our model. A more detailed study which takes into account a proper model potential could reproduce the results that are available from

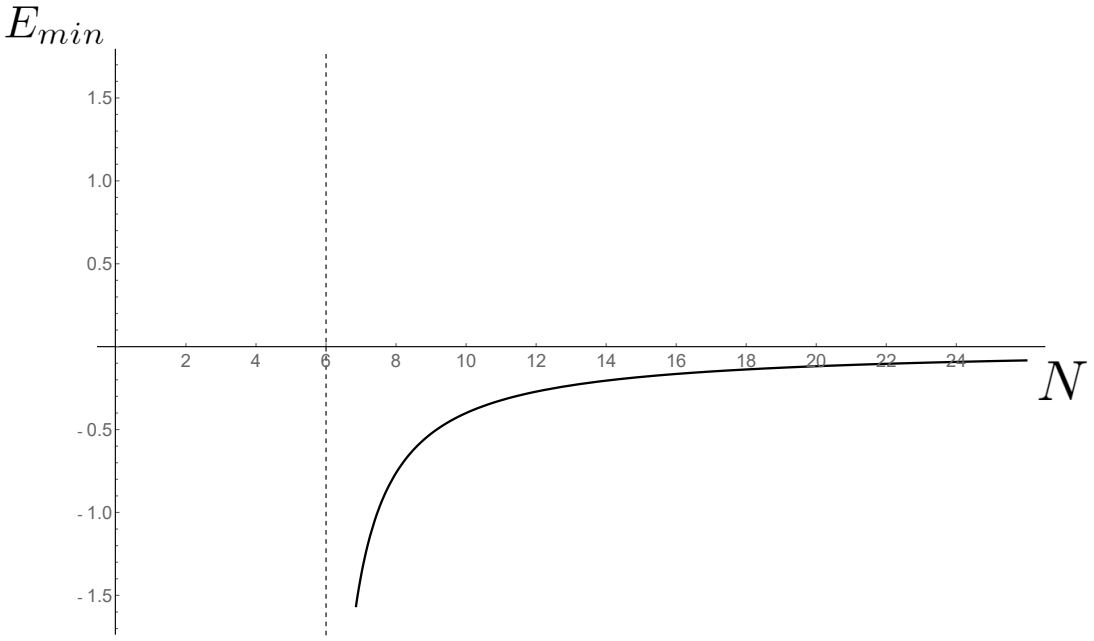

FIGURE 3.4: Energy at the minimum for positive scattering length a as a function of the number of particles N, with mass ratio $r = 10$. In the region before the dashed line the energy has no minimum and goes to negative infinity.

few-body calculations, predicting the existence of stable clusters up to $N = 5$ Bazak and Petrov (2017).

3.5.3 Negative scattering length

An interaction potential with negative scattering length cannot accommodate any bound dimer in 3 dimension. Moreover, while for Bosons it has been shown that there exist N-body bound states up to $N = 6$ for negative scattering lenght Naidon and Endo (2017), for fermions no such result has been found. Indeed, applying the Born-Oppenheimer approximation to the case of $N = 2$ (two heavy fermions and one light atom) one can show that there is no three body bound state for negative scattering length. Nevertheless, there is not to our knowledge any particular physical argument to rule out the existence of bound states for $N > 3$. Petrov (2021).

We show the energy of the $N + 1$ system as a function of $1/k_F a$ for $r = 10$ and $N = 12$ to $N = 15$ in Fig. (3.5). Note that the minima occur for interparticle distances $l = (6\pi^2)^{1/3}/k_F$ that are approximately one order of magnitude greater than the scattering length and energies that are two order of magnitude smaller than the energy of a dimer $E_{\text{dimer}} \approx \hbar^2/2ma^2$. This means that the hypothetical clusters would be very large clouds of atoms held together by a weak interaction.

As displayed in Fig. (3.5) the minimum in energy becomes more shallow for higher number of particles. This is true down until $N \approx 1$ where the energy of the bound state reaches its minimum. We show this in Fig. (3.6), where we plot the minimum value of the energy as a function of the number of particles for $r = 10$. This result would indicate that there is a stable cluster at some value of $N \approx 1$ and that any other cluster with higher number of particles would be unstable. However, our approximation can be reliable only for a large number of particles.

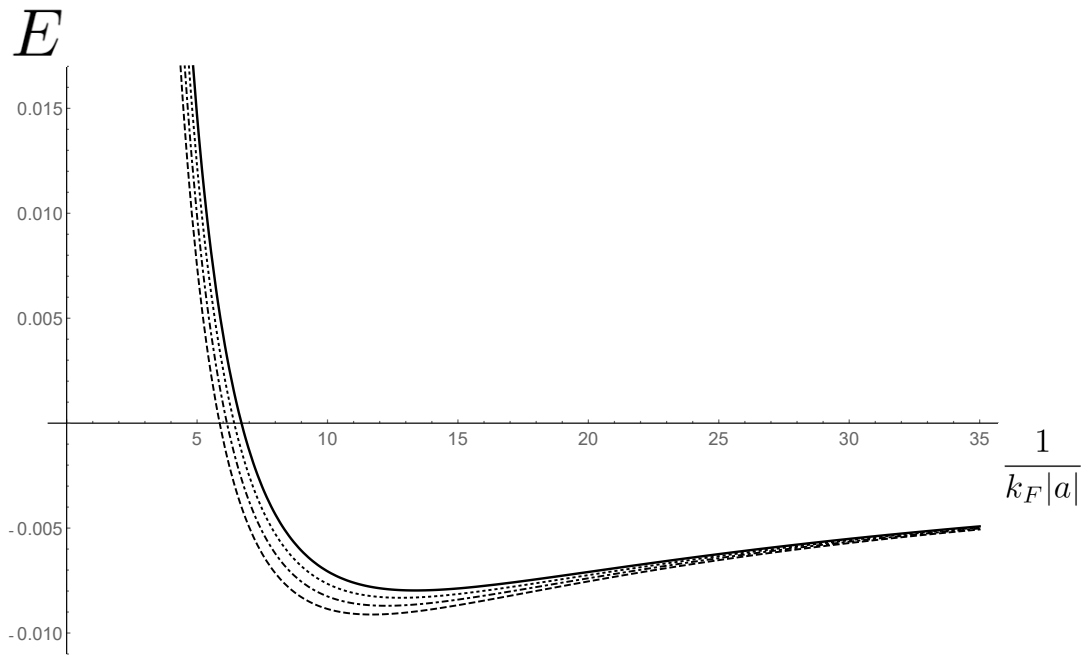

FIGURE 3.5: Energy of the N+1 system for negative scattering length as a function of $1/k_F|a|$, for $r = 10$. The number of particles for each curve is $N = 20$ (dashed), $N = 21$ (dashed dotted), $N = 22$ (dotted) and $N = 23$ (thick).

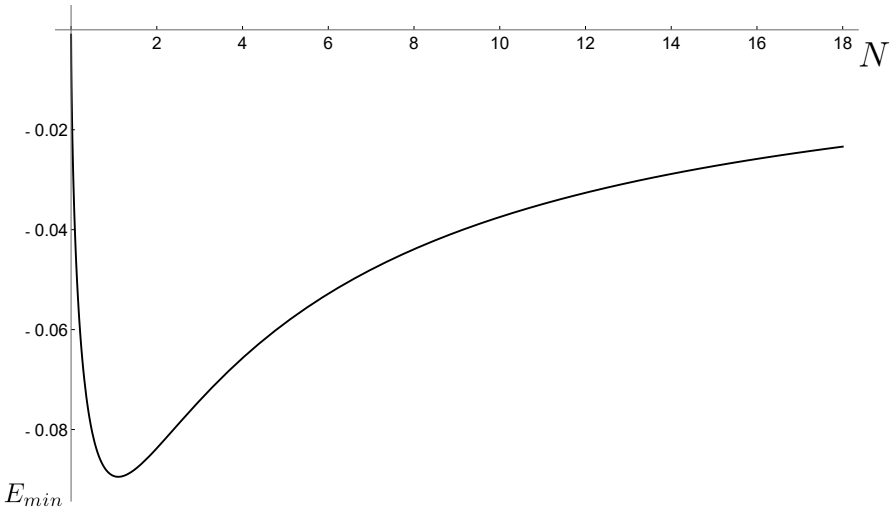

FIGURE 3.6: Energy at the minimum for negative scattering length a as a function of the number of particles N, for $r = 10$.

3.6 Conclusions

In this chapter we addressed a general question, that is whether the exchange of a light atom can bind together a large system of N heavy atoms. We exploited the difference in mass between the two species by making use of the Born-Oppenheimer

approximation and obtained the scaling of the binding energy in various regimes of scattering length.

The model we obtained, although based on a set of simplifying assumptions, predicts an interplay between the number of particles, the mass ratio and the scattering length that is compatible with currently known theoretical results obtained from more sophisticated few-body calculations.

Our results seem to indicate that there is no stable cluster for big N, as the $N-1$ cluster has systematically a lower energy than the former. This would imply that at some value of N a bound cluster, if existing at all, would have qualitatively different features from the ones that were found up to now.

4

Linear response study of the collisionless drag

The work contained in this chapter lead to the publication of the paper Romito et al. (2021).

4.1 Introduction

The superfluid drag was predicted by Andreev and Bashkin Andreev and Bashkin (1975) in 1975 for a two component superfluid mixture, correcting previous works by Khalatnikov Khalatnikov (1957). The effect predicts that, when two superfluid species in a mixture are interacting, superflow in one component will induce a superfluid current in the other one. In other words the superfluid currents of each component in a mixture depend on both superfluid velocities Andreev and Bashkin (1975). The intuitive idea behind the Andreev-Bashkin effect is that whenever a species A in the superfluid mixture is imparted a superfluid velocity the intraspecies interactions generate s quasiparticles which transport both the mass of the first species A and part of the mass of the species B. This effectively induces a mass current of the second species.

The Andreev-Bashkin drag should not be thought of in analogy with the drag between two classical fluids, which typically would be caused by microscopic collisions among individual particles. Indeed, in a superfluid the description in terms of individual particles loses all meaning and the Andreev-Bashkin effect requires no collisions to take place. Rather, it is a distinctly quantum mechanical effect where excited states have a *mixed* nature to which both species in the superfluid mixture contribute.

Although the Andreev-Bashkin effect was first predicted in the context of ^{3}He-^{4}He mixtures, a mixture of these two components where both are in the superfluid state

cannot be achieved experimentally, due to their low miscibility. The Andreev-Bashkin effect has also been discussed in the hydrodynamics of neutron star cores (see Lattimer and Prakash (2004) for a review), which are believed to be made of a mixture of superfluid neutrons and protons. Cold atomic mixtures have also been proposed as a promising environment Fil and Shevchenko (2005); Linder and Sudbø (2009); Nespolo et al. (2017); Parisi et al. (2018); Karle et al. (2019); Sellin and Babaev (2018) where the effect could be observed, as they provide a more accessible platform compared to neutron stars. Nevertheless, an experimental observation of the drag is still missing, as the typical ultracold atoms mixtures are weakly interacting, which limits the size of the drag.

The main aim of this chapter is to describe how the drag effect arises from the general microscopic many-body theory of two interacting quantum fluids as well as its effect on their dynamics.

4.1.1 Outline

We will relate the superfluid drag density to the current-current response functions and distinguish between their transverse and longitudinal long wavelength limits. It is important to notice that this approach is not limited to weakly interacting gases but is applicable to any quantum mixture. The linear response formalism requires only that the motion that is induced on the fluid is small enough to be treated as a perturbation. Therefore the formalism presented in this chapter can be employed to predict the magnitude of the drag effect in a variety of systems such as Bose-Bose superfluid mixtures on a lattice, Bose-Fermi superfluid mixtures and Fermi-Fermi superfluid mixtures.

We also connect the linear response result with the formalism of sum rules, which is an established tool to study the elementary and collective excitations of (trapped) quantum gases (see Pitaevskii and Stringari (2016)). We show how the presence of the drag results in a correction to the energy weighted sum rule.

Then, we specialize to the case of a weakly interacting Bose mixture with $\mathbb{Z}_2$ symmetry. The weakly interacting Bose mixture serves as a testing ground for the formalism of the previous sections and we will derive the beyond mean field frequency shifts of elementary spin excitations, namely the spin speed of sound and the spin dipole mode in a trapped gas.

Finally we study the linear response at short times to a perturbation that is quickly switched on, showing that it can be used to measure the drag effect in experiments.

While we will mostly focus on homogeneous systems, our formalism applies to discrete space Hamiltonians alike, with just some small modifications as explained in Appendix C.

The structure of the chapter is as follows. In sec. 4.3 we provide the microscopic definition of the drag within linear response theory and rigorously derive its correction to the energy weighted sum rule. The results in these two sections are generic to superfluid mixtures and can in principle by applied for any interaction.

In sec. 4.4 we specialize to a $\mathbb{Z}_2$ symmetric Bose-Bose mixture in the weakly interacting limit. We recover the known value Fil and Shevchenko (2005) of the superfluid drag in sec. 4.4.1 and calculate its effect on the spin speed of sound and on the spin dipole frequency in subsecs. 4.5.1 and 4.5.2, respectively. In sec. 4.6 we devise an efficient way to measure the drag by studying the short-time response to a quick perturbation.

Appendix D includes results for thermodynamic quantities such as the susceptibility and the chemical potential for a weakly interacting mixture. These results are used in subsecs. 4.5.1 and 4.5.2. Appendix C is devoted to generalizing the results for Bose-Hubbard Hamiltonians, which will be of great use in chapter 5.

Throughout the rest of this thesis we will use the more generic term "collisionless drag" interchangeably with "Andreev-Bashkin drag".

4.2 The Andreev-Bashkin effect: three fluid hydrodynamics

In 1957 Khalatnikov Khalatnikov (1957), inspired by the Landau two fluid model Landau (1941) used in single component superfluidity, described a mixture of *two* components in terms of a three fluid model, i.e. the normal fluid and the two superfluids. The resulting equation predict that the superfluid currents of the two species are uncoupled from each other. Later, in 1975, Andreev and Bashkin Andreev and Bashkin (1975) pointed out that the two superfluid motions must be coupled, and introduced such coupling in the three-fluid model. The intuition of Andreev and Bashkin is based on the example of a single ^{3}He atom surrounded by ^{4}He, not necessarily in the superfluid state. In this case the ^{3}He atom becomes a quasiparticle (a *polaron*) whose mass is renormalized to account for the transport of a portion of the mass of the surrounding ^{4}He Bardeen et al. (1967). In their paper, they prove that this picture is unchanged at the onset of superfluidity and should be valid when the number of ^{3}He atoms is comparable with that of ^{4}He. The Andreev-Bashkin drag is thus *collisionless*: it results from the mixed nature of quasiparticles of one component, which are renormalized by the interaction with the other component. Thus the flows of the two speices are coupled without any dissipation of energy. This peculiarity is what makes the drag non vanishing even at zero temperature.

For the case of a homogeneous system in the hydrodynamic limit, to describe the relation between the mass current densities $m_\alpha \mathbf{j}_\alpha$ of each component $\alpha = A, B$ and the velocities, they introduced the matrix of the superfluid densities $\rho_{\alpha\beta}$ defined such that:

$$\begin{aligned} m_A \mathbf{j}_A &= \rho_{nA}\mathbf{v}_n + \rho_{AA}\mathbf{v}_A^{(s)} + \rho_{AB}\mathbf{v}_B^{(s)}, \\ m_B \mathbf{j}_B &= \rho_{nB}\mathbf{v}_n + \rho_{BB}\mathbf{v}_B^{(s)} + \rho_{BA}\mathbf{v}_A^{(s)}. \end{aligned} \tag{4.1}$$

In Eq. (4.1) m_α are the bare masses of the constituent atoms of component α, n_α the number densities and $\mathbf{v}_\alpha^{(s)}$ are the superfluid velocities defined as $\mathbf{v}_\alpha^{(s)} = \hbar/m_\alpha \nabla\varphi(\mathbf{r}, t)$, with $\varphi(\mathbf{r}, t)$ the condensate phase. In the hydrodynamic regime, it is assumed that both the A and B normal components are in local thermal equilibrium due to their mutual collisions, implying that there is only one normal component $\rho_n = \rho_{nA} + \rho_{nB}$ moving with velocity $\mathbf{v}_n$. Eq. (4.1) describes the fact that the superflow of one component takes part in the mass current density of the other. The off-diagonal terms of the matrix represent the drag that one component forces upon the other. The matrix $\rho_{\alpha\beta}$ is symmetric Andreev and Bashkin (1975) – as will be also clear from the linear response formalism, so that $\rho_{AB} = \rho_{BA}$. Moreover, the superfluid densities satisfy the inequality:

$$\rho_{AB}^2 < \rho_{AA}\,\rho_{BB}\,. \tag{4.2}$$

Eq. (4.2) comes from the requirement that the matrix of superfluid densities is positive definite, hence its determinant is strictly positive.

It is worthwhile to comment on the physical meaning of the upper bound on the drag given by Eq. (4.2), i.e. $\rho_{AB}^2 = \rho_{AA}\,\rho_{BB}$. In order to make the discussion more clear we will focus on the case of a symmetric mixture, where $\rho_{AA} = \rho_{AB}$, but the following considerations generally apply to any superfluid mixture. For a symmetric mixture the upper bound reduces to $\rho_{AB} = \pm\rho_{AA}$, where the plus and minus sign correspond to two distinct phases of the superfluid mixture (see e.g. Kuklov and Svistunov (2003); Kuklov et al. (2004); Sellin and Babaev (2018)). One phase, for $\rho_{AA} = \rho_{AB}$ corresponds to paired superfluidity, where the two species undergo a pairing transition and consequently the flow in one component induces an equal flow in the other component. We will investigate this phase in relation to the drag coefficient in chapter 5, particularly in Sec. (5.2.4). The other phase, for $\rho_{AA} = -\rho_{AB}$, is the counterflow superfluid one, where the superflows are equal in value but they have opposite directions. In both cases the Andreev-Bashkin drag loses its meaning as the system becomes a superfluid of pairs, rather than a mixture of two coupled superfluids.

For a homogeneous system, galilean invariance Andreev and Bashkin (1975) requires that:

$$\rho_{n\alpha} = m_\alpha n_\alpha - \rho_{\alpha\alpha} - \rho_{AB}\,. \tag{4.3}$$

So that at zero temperature where the normal component vanishes Leggett (1998), the sum of all the superfluid densities is the total mass density of the system ρ, namely:

$$\rho \equiv m_A n_A + m_B n_B = \rho_{AA} + \rho_{BB} + 2\rho_{AB} \,. \tag{4.4}$$

This relation is modified in presence of a lattice which breaks translational invariance, as shown in Appendix C.

4.3 Microscopic description of the collisionless drag from linear response theory

In this section the three-fluid hydrodynamics of Eq. (4.1) is connected to the microscopic theory by means of linear response. Linear response theory allows to relate the superfluid and normal densities of the Landau two-fluid model with current-current response functions, as it is well described in the case of a single component (see, e.g., Baym (1968); Nozieres and Pines (1999); Pitaevskii and Stringari (2016)). In sec. 4.3.1 we generalize this concept to the case of a two component superfluid mixture, without referring to any specific microscopic model. We shall closely follow the formalism of Refs. Baym (1968); Nozieres and Pines (1999); Pitaevskii and Stringari (2016)). The basic idea is to start with the fluid in equilibrium and then to subject it to a weak transverse field whose intensity increases adiabatically from zero. We then can identify the current density that is imparted by the field, proportionally to the relevant superfluid density. We will show that this is formally the same as calculating the current density average with a perturbed Hamiltonian where the perturbation depends on the field. This can then be expressed in terms of a current-current response function. Finally, using Eq. (4.1), we express the current density in terms of the $\rho_{\alpha\beta}$ and ρ_n, thereby relating the latter to the transverse current response function in the long wave length limit. Although we will derive the general linear response expressions for the densities of the three-fluid model, we will mostly restrict to the zero temperature case to make the distinction with the single component case more apparent.

Aside from giving an intuitive account of the effect and making a clear connection to the existing literature on superfluidity, this approach could prove useful to make predictions on the value of the collisionless drag in various systems, thus identifying those which are the best candidates to display it in a significant way. Another strength of this formalism is that response functions can be generally computed making use of diagrammatic theory and numerical techniques.

In the second part of this section – sec. 4.3.2 – we will predict the effect of the drag on sum rules of the structure factor. Sum rules provide an established method to compute

the frequencies of collective oscillations for various physical systems (Pitaevskii and Stringari (2016) and references therein). We will show that the Andreev-Bashkin drag is proportional to the multiparticle contribution to the first moment spin structure factor. This results in a correction to the frequency of collective oscillations that could be measured in experiments to detect the drag.

4.3.1 Superfluid densities as current-current response functions

We take the approach described in Baym (1968) and generalize it to a two component superfluid mixture. The system considered here is described by an Hamiltonian in the form $\hat{H} = \hat{K} + \hat{U}$ where the kinetic term is

$$\hat{K} = \sum_{\alpha=A,B} \int \left(\frac{\hbar^2}{2m_\alpha} \nabla \hat{\Psi}_\alpha^\dagger \nabla \hat{\Psi}_\alpha \right) d\mathbf{r} \tag{4.5}$$

and the interaction reads

$$\hat{U}_{\alpha\beta} = \frac{1}{2} \sum_{\alpha,\beta} \int d\mathbf{r}\, d\mathbf{r}' \hat{\Psi}_\alpha^\dagger(\mathbf{r}) \hat{\Psi}_\beta^\dagger(\mathbf{r}') U_{\alpha\beta}(\mathbf{r}-\mathbf{r}') \hat{\Psi}_\beta(\mathbf{r}') \hat{\Psi}_\alpha(\mathbf{r}) \,, \tag{4.6}$$

with $U_{\alpha\beta}$ the two-body intra- and interspecies potential and $\hat{\Psi}_\alpha(\mathbf{r})$ and $\hat{\Psi}_\alpha^\dagger(\mathbf{r})$ quantum annihilation and creation fields of each species at position $\mathbf{r}$. In order to define the superfluid densities microscopically, we will express the currents of Eq. (4.1) as averages of the corresponding quantum operator:

$$\hat{\mathbf{j}}_\alpha(\mathbf{r}) = \frac{\hbar}{2m_\alpha i} \left(\hat{\Psi}_\alpha^\dagger(\mathbf{r}) \nabla \hat{\Psi}_\alpha(\mathbf{r}) - H.c. \right), \tag{4.7}$$

namely we will ensure that $\langle \hat{\mathbf{j}}_\alpha(\mathbf{r}) \rangle = \mathbf{j}_\alpha$.

To study the linear response of the system we consider the situation in which the superfluid is subject to a static transverse probe, described by a magnetic vector potential $\mathbf{A}(\mathbf{r})$. In the case of neutral cold atoms the magnetic vector potential probe can be generated by an artificial gauge field, which can be obtained in various ways, such as rotating the mixture or coupling the energy states of the atoms with a laser Dalibard et al. (2011). We study the problem in the London gauge London (1948) where the magnetic potential satisfies the condition:

$$\mathbf{q} \cdot \mathbf{A}(\mathbf{q}) = 0 \,, \tag{4.8}$$

where $\mathbf{A}(\mathbf{q})$ is the Fourier transform of $\mathbf{A}(\mathbf{r})$. In presence of this field the superfluid velocities $\mathbf{v}_\alpha^{(s)}$ read:

$$\mathbf{v}_\alpha^{(s)}(\mathbf{r}) = \frac{1}{2m_\alpha} \left(\nabla \varphi_\alpha - 2e_\alpha \mathbf{A}(\mathbf{r}) \right) . \tag{4.9}$$

In the case of a charged superconductor e_α is the electrical charge, while for a neutral superfluid it can be simply thought of as a constant that quantifies the coupling of the artificial gauge field with the species α. In the ground state the condensate phase is a constant, thus $\nabla\varphi_\alpha = 0$.

The hydrodynamic equations in Eq. (4.1) for the current densities of the two species read:

$$m_\alpha \mathbf{j}_\alpha(\mathbf{r}) = -\left(\rho_{\alpha\alpha}\frac{e_\alpha}{m_\alpha} + \rho_{\alpha\beta}\frac{e_\beta}{m_\beta}\right)\mathbf{A}(\mathbf{r})\,. \tag{4.10}$$

Eq. (4.10) is the London equation for a two component superfluid London (1948).

We will now compare this equation with the current response to a probe $\mathbf{A}(\mathbf{r})$ in order to identify the superfluid densities. In presence of a transverse probe the current density operators transform in the following way:

$$\hat{\mathbf{j}}_\alpha(\mathbf{r}) \to \hat{\mathbf{j}}_\alpha(\mathbf{r}) - \frac{e_\alpha}{m_\alpha}\hat{n}_\alpha(\mathbf{r})\mathbf{A}(\mathbf{r})\,, \tag{4.11}$$

where $\hat{n}_\alpha(\mathbf{r}) = \hat{\Psi}^\dagger_\alpha(\mathbf{r})\hat{\Psi}_\alpha(\mathbf{r})$ is the density operator at position $\mathbf{r}$. The Hamiltonian gets transformed to:

$$\begin{aligned}\hat{H} \to \hat{H} &- \sum_{\alpha=A,B}\frac{e_\alpha}{m_\alpha}\int d\mathbf{r}\,\hat{\mathbf{j}}_\alpha(\mathbf{r})\cdot\mathbf{A}(\mathbf{r}) \\ &+ \sum_{\alpha=A,B}\frac{e_\alpha^2}{2m_\alpha}\int d\mathbf{r}\,\hat{n}_\alpha(\mathbf{r})A^2(\mathbf{r})\,.\end{aligned} \tag{4.12}$$

Let us suppose, without loss of generality, that the vector potential A is along the x direction. We obtain the average of the current density operator to first order in the perturbation $\mathbf{A}(\mathbf{r})$:

$$\begin{aligned}\langle\hat{j}_{x,\alpha}(\mathbf{r})\rangle &= -n_\alpha(\mathbf{r})\frac{e_\alpha}{m_\alpha}A(\mathbf{r}) \\ &+ \sum_{\beta=A,B} e_\beta\int d\mathbf{r}'\chi_{j_{x,\alpha},j_{x,\beta}}(\mathbf{r},\mathbf{r}')A(\mathbf{r})\,,\end{aligned} \tag{4.13}$$

where $\chi_{j_{x,\alpha},j_{x,\beta}}(\mathbf{r},\mathbf{r}')$ are the static current-current response functions.

For a homogeneous system of volume V and number of atoms N we have that $n_\alpha(\mathbf{r}) = n_\alpha = N/V$ and we can recast (4.13) in terms of the Fourier transform of the current-current response function at $T = 0$ Pitaevskii and Stringari (2016):

$$\chi_{j_{x,\alpha},j_{x,\beta}}(\mathbf{q}) = \frac{1}{V}\sum_{n\neq 0}\left(\frac{\langle n|j^\dagger_{x,\alpha}(\mathbf{q})|0\rangle\,\langle 0|j_{x,\beta}(\mathbf{q})|n\rangle}{E_n - E_0} - \frac{\langle n|j_{x,\alpha}(\mathbf{q})|0\rangle\,\langle 0|j^\dagger_{x,\beta}(\mathbf{q})|n\rangle}{E_0 - E_n}\right)\,, \tag{4.14}$$

where $|n\rangle$ and E_n are respectively the eigenstates and eigenergies in absence of the velocity perturbation, and $n = 0$ corresponds to the ground state. The operator $\hat{\mathbf{j}}_\alpha(\mathbf{q})$

is the Fourier transform of the current density operator of Eq. (4.7):

$$\hat{\mathbf{j}}_\alpha(\mathbf{q}) = \frac{\hbar}{2m_\alpha}\sum_{\mathbf{k}}(2\mathbf{k}+\mathbf{q})\,\hat{a}^\dagger_{\mathbf{k},\alpha}\hat{a}_{\mathbf{k}+\mathbf{q},\alpha}\,, \tag{4.15}$$

with $\hat{a}_{\mathbf{k},\alpha} = V^{-1/2}\int d\mathbf{r}\, e^{i\mathbf{k}\cdot\mathbf{r}}\hat{\Psi}_\alpha(\mathbf{r})$. We point out that the current response function defined in Eq. (4.14) is intensive.

Because of Eq. (4.8) the Fourier transform of Eq. (4.13) will give the *transverse* response function Nozieres and Pines (1999). For an arbitrary direction of $\hat{\mathbf{j}}_\alpha(\mathbf{q})$ we have the following definitions for the transverse and longitudinal response functions:

$$\begin{aligned}\chi_{\mathbf{j}_\alpha,\mathbf{j}_\beta}(q^T, q^L = 0) &\equiv \chi^T_{\mathbf{j}_\alpha,\mathbf{j}_\beta}(\mathbf{q})\,,\\ \chi_{\mathbf{j}_\alpha,\mathbf{j}_\beta}(q^T = 0, q^L) &\equiv \chi^L_{\mathbf{j}_\alpha,\mathbf{j}_\beta}(\mathbf{q})\,,\end{aligned} \tag{4.16}$$

where q^T and q^L are the components of $\mathbf{q}$ perpendicular and parallel to $\mathbf{j}$ respectively. The linear response result for the current carried by each component reads:

$$\langle\hat{\mathbf{j}}_\alpha\rangle = -n_\alpha\frac{e_\alpha}{m_\alpha}\mathbf{A} + \sum_{\beta=A,B} e_\beta\chi^T_{j_\alpha,j_\beta}(\mathbf{q}=0)\mathbf{A}\,, \tag{4.17}$$

with $\mathbf{A} \equiv \mathbf{A}(\mathbf{q}=0)$.

We can now match this result of linear response theory with the hydrodynamics predicted by Eq. (4.10). Comparing Eq. (4.10) and Eq. (4.17) we get the desired results for the superfluid densities in terms of linear response functions:

$$-m_A m_B \lim_{\mathbf{q}\to 0}\chi^T_{\mathbf{j}_A,\mathbf{j}_B}(\mathbf{q}) = \rho_{AB}\,, \tag{4.18}$$

$$m_\alpha n_\alpha - m_\alpha^2 \lim_{\mathbf{q}\to 0}\chi^T_{\mathbf{j}_\alpha,\mathbf{j}_\alpha}(\mathbf{q}) = \rho_{\alpha\alpha}\,, \tag{4.19}$$

$$\sum_{\alpha,\beta=A,B} m_\alpha m_\beta \lim_{\mathbf{q}\to 0}\chi^T_{\mathbf{j}_\alpha,\mathbf{j}_\beta}(\mathbf{q}) = \rho_n\,. \tag{4.20}$$

Where the last equation can be obtained from the other two by using the normalization condition of Eq. (4.4). For a translational invariant system at zero temperature $\rho_n = 0$, as the system is completely superfluid Leggett (1998).

Note that in a single component superfluid, the zero temperature transverse response is zero, since the superfluid fraction is equal to the total mass density of the system. Here, we can also consider the relative response of the current of B-atoms $\hat{\mathbf{j}}_B(\mathbf{r})$ to a probe coupling with A-atoms $\hat{\mathbf{j}}_A(\mathbf{r})\cdot\mathbf{A}(\mathbf{r})$ i.e. $\chi^T_{\mathbf{j}_A,\mathbf{j}_B}$ which is nonzero even in the groundstate as we see from (4.18). This effect has no analogy with the single component case and results from the impossibility of uncoupling the motion of two interacting components of a superfluid. In this sense the drag behaves as a sort of normal component at zero temperature decreasing the value of the diagonal

superfluid densities $\rho_{\alpha\alpha}$ and taking part in the transverse response. Nevertheless, as in the case of a single species, the total response to a transverse field coupling to both currents, $\chi^T_{\mathbf{j}_A,\mathbf{j}_A} + \chi^T_{\mathbf{j}_B,\mathbf{j}_B} + 2\chi^T_{\mathbf{j}_A,\mathbf{j}_B}$ is zero.

The formalisation of Eqs. (4.18), (4.19), (4.20) is an important result of this chapter. They provide the full microscopic expressions of the hydrodynamic coefficients to linear order in the superfluid velocities. The only assumption required for their validity is to deal with a homogeneous superfluid mixture with nonvanishing interspecies interactions. In particular, Eq. (4.18) describes the drag as a mutual correlation between currents in the two species.

In the case of a lattice described by a single-band Hubbard Hamiltonian Eqs. (4.18), (4.19), (4.20) are slightly modified due to the lack of continuous translational invariance. As we show in Appendix C, the number density $\hat{n}_\alpha$ has simply to be replaced by the kinetic energy density $\hat{K}_\alpha$.

4.3.2 Current response and sum rules

In a system where a single species is present the longitudinal current response function in the static limit is proportional to the first moment of the structure factor (see, e.g., Pitaevskii and Stringari (2016)), which in turn is proportional to the density of particles. In what follows we will extend this notion to the case of a two component system and relate it to the drag coefficient.

The structure factor at zero temperature for an operator $\hat{F}$ is defined as:

$$S_F(\omega) = \sum_n |\, \langle n|\hat{F}|0\rangle \,|^2\, \delta(\hbar\omega - \hbar\omega_{n0})\,, \tag{4.21}$$

where $\hbar\omega_{n0} = E_n - E_0$. We will be concerned here with the cases in which the operator $\hat{F}$ is the density operator (with corresponding structure factor S_d)

$$\hat{\rho}_{\mathbf{q}} = \sum_{\mathbf{k}} \left(\hat{a}^\dagger_{\mathbf{k}+\mathbf{q},A}\hat{a}_{\mathbf{k},A} + \hat{a}^\dagger_{\mathbf{k}+\mathbf{q},B}\hat{a}_{\mathbf{k},B} \right)\,, \tag{4.22}$$

or the spin operator (respectively S_s)

$$\hat{s}_{\mathbf{q}} = \sum_{\mathbf{k}} \left(\hat{a}^\dagger_{\mathbf{k}+\mathbf{q},A}\hat{a}_{\mathbf{k},A} - \hat{a}^\dagger_{\mathbf{k}+\mathbf{q},B}\hat{a}_{\mathbf{k},B} \right)\,. \tag{4.23}$$

Excited states created by the density operator are said to belong to the *density channel* and those created by the spin operator are said to belong to the *spin channel*. Fig. 4.1 shows a representation of the single particle excitations created by the density and spin operator, where only one (spin or density) quasiparticle is excited. In general, the density operator can create multiple quasiparticles or quasiholes in both species

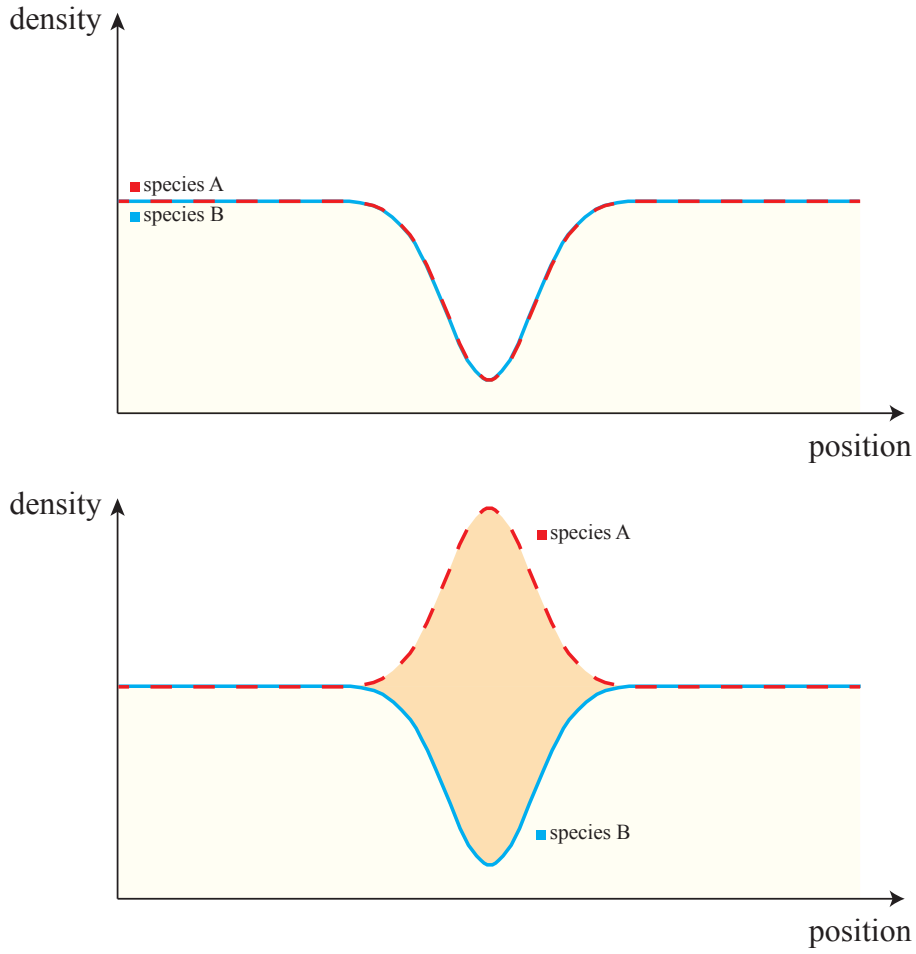

FIGURE 4.1: (Adapted from Shin et al. (2006)). Representation of the elementary, single particle excitations created by the density and spin operator respectively, displayed as "bumps" in the density of the two species. On the left, a density quasihole (composed of a quasihole of species A and a species B). On the right a spin quasiparticle (composed of a quasiparticle of species A and a quasihole of species B). The spin and density single particle excitations will propagate as phonons with corresponding speed of sound.

(which correspond to density channel excitations), while the spin operator creates multiple instances of a quasiparticles in one species and a quasiholes in the other one (which correspond to spin channel excitations). We will see in this section the distinction between single quasiparticle excitations and multiple quasiparticle excitations is a crucial one.

Let us specialize here to the case where the two components have equal masses $m_A = m_B = m$ and densities $n_A = n_B = n$, the generalization being quite straightforward. The density structure factor satisfies the f-sum rule (see, e.g.,

Nozieres and Pines (1999), Vol. I, Chapter 4):

$$\begin{aligned} M_{1,d}(\mathbf{q}) &= \frac{1}{V}\int_0^\infty \omega S_d(\mathbf{q},\omega)\, d\omega = \\ &= \frac{1}{2V\hbar^2}\left\langle \left[\hat{\rho}^\dagger_{\mathbf{q}}, \left[\hat{H}, \hat{\rho}_{\mathbf{q}}\right]\right]\right\rangle = \frac{n}{m}q^2\,, \end{aligned} \tag{4.24}$$

where we defined $M_{1,d}(\mathbf{q})$ the first moment of the density structure factor. An analogous result, the spin f-sum rule, is valid for the spin structure factor, namely:

$$\begin{aligned} M_{1,s}(\mathbf{q}) &= \frac{1}{V}\int_0^\infty \omega S_s(\mathbf{q},\omega)\, d\omega = \\ &= \frac{1}{2V\hbar^2}\left\langle \left[\hat{s}^\dagger_{\mathbf{q}}, \left[\hat{H}, \hat{s}_{\mathbf{q}}\right]\right]\right\rangle = \frac{n}{m}q^2\,, \end{aligned} \tag{4.25}$$

where $M_{1,s}(\mathbf{q})$ is the first moment of the spin structure factor. The f-sum rule can be interpreted as a constraint on the total "strength" of the response of a system to a probe. It consists of a sum of all the transition probabilities from the ground state to the excited states that can be coupled by the relevant operators ($\hat{s}^\dagger_{\mathbf{q}}$, and $\hat{s}^\dagger_{\mathbf{q}}$ in this case) weighted by the respective transition energies.

The first moment of the density (respectively spin) structure factor are related to longitudinal density (respectively spin) current response functions Nozieres and Pines (1999). Consider in fact the density (respectively spin) current $\mathbf{j}_{d(s)}(\mathbf{q}) = \mathbf{j}_A(\mathbf{q}) \pm \mathbf{j}_B(\mathbf{q})$ and its longitudinal response function:

$$\chi^L_{\mathbf{j}_{d(s)}\mathbf{j}_{d(s)}}(\mathbf{q}) \equiv \chi^L_{\mathbf{j}_A,\mathbf{j}_A}(\mathbf{q}) + \chi^L_{\mathbf{j}_B,\mathbf{j}_B}(\mathbf{q}) \pm 2\chi^L_{\mathbf{j}_A,\mathbf{j}_B}(\mathbf{q})\,. \tag{4.26}$$

Using the definition of the structure factor, Eq. (4.21), and the continuity equation we obtain:

$$\begin{aligned} \chi^L_{\mathbf{j}_{d(s)}\mathbf{j}_{d(s)}}(\mathbf{q}) &= \frac{2}{Vq^2}\sum_n \frac{|\,\langle 0|\mathbf{q}\cdot\mathbf{j}_{d(s)}(\mathbf{q})|n\rangle\,|^2}{E_n - E_0} = \\ &= \frac{2}{Vq^2}\int_0^\infty \omega S_{d(s)}(\mathbf{q},\omega)d\omega = \frac{2}{q^2}M_{1,d(s)}(\mathbf{q})\,. \end{aligned} \tag{4.27}$$

In order to find an expression for the drag in terms of the first moment of the structure factor we need now to relate the longitudinal response to the transverse response as it is the latter which is proportional to ρ_{AB} by Eq. (4.18). To do so, it is necessary to separate the contributions of *single (quasi)particle* and *multi(quasi)particle excitations* to the response functions, as they allow to discriminate between the longitudinal and transverse response.

At zero temperature the excited states that will contribute to the matrix elements of the response functions in Eqs. (4.24), (4.25) and (4.27) should be divided in two categories: *single particle* and *multiparticle excitations* Nozieres and Pines (1999). The

former are obtained from the ground state by adding a single quasiparticle of momentum $\mathbf{q}$ to the ground state, which will then propagate as a sound wave (a *phonon*) of momentum q and energy $\omega = cq^2$, where c is the speed of sound. The latter consist instead of several excited quasiparticles with total momentum $\mathbf{q}$.

If we focus on the long wavelength limit, i.e. $\mathbf{q} \to 0$, in a single component superfluid, conservation of total current allows us to conclude that **multiparticle excitations give a negligible contribution to the first moment of the structure factor**. In other words, when computing the integral of the structure factor in Eq. (4.24), one needs to compute only matrix elements with excited states that differ from the ground state for a single excited quasiparticle, with well defined momentum $\mathbf{q}$. All other contributions will disappear when taking the limit $\mathbf{q} \to 0$ Nozieres and Pines (1999). The single particle excitations are then said to *exhaust* the sum rule, meaning that they are the only excited states to take into account in order to reproduce it.

In two component superfluids the situation is different. While the same considerations as in single species superfluids apply to the density channel of a two species one, with density phonons exhausting the corresponding sum rule, **multiparticle states in the spin channel are not negligible** even at long wavelengths. This is a consequence of the fact that, unlike the total current $\mathbf{j}_d(\mathbf{q})$, the spin current $\mathbf{j}_s(\mathbf{q})$ is not conserved Leggett (1965).

Indeed, conservation laws define the long wavelength behaviour of the matrix elements that appear in the f-sum rule (we refer here to the approach contained in Nozieres and Pines (1999)). For the density current we have that

$$\lim_{\mathbf{q}\to 0} \langle 0|\mathbf{j}_d(\mathbf{q})|n\rangle = 0\,, \tag{4.28}$$

when $|n\rangle$ is a multiparticle excited state, since the total current is a good quantum number. Using the continuity equation we obtain:

$$(\omega_n - \omega_0)\,\langle 0|\rho_{\mathbf{q}}(\mathbf{q})|n\rangle = -\,\langle 0|\mathbf{q}\cdot\mathbf{j}_d(\mathbf{q})|n\rangle\ . \tag{4.29}$$

Since the frequency $\omega_n - \omega_0$ will be constant at long wavelengths for multiparticle excitations this allows to conclude that the matrix element $\langle 0|\rho_{\mathbf{q}}|n\rangle$ will tend to 0 at least as fast as q^2. A similar argument is not valid for the spin operator as the corresponding spin current is not conserved, so Eq. (4.28) does not hold.

Further analysis of conservation laws allows us to completely identify the low $\mathbf{q}$ limit of the contributions to $M_{1,s}$ coming from $\langle 0|\hat{s}_{\mathbf{q}}|n\rangle$ and $(\omega_n - \omega_0)$ for long wavelengths. These results are summarized in table 4.1 with the corresponding results for the density operator.

	Single Particle	Multiparticle
$\mid \langle 0 \mid \hat{\rho}_{\mathbf{q}} \mid n \rangle \mid^2$	q	q^4
$\mid \langle 0 \mid \hat{s}_{\mathbf{q}} \mid n \rangle \mid^2$	q	q^2
$(\omega_n - \omega_0)$	q	const.
$M_{1,d}$	q^2	q^4
$M_{1,s}$	q^2	q^2

TABLE 4.1: Contributions to the sum rule in the low q limit.

The table shows how, in the f-sum rule for the spin moment $M_{1,s}$, single particle and multiparticle excitations contribute at the same order in $\mathbf{q}$. For the density moment $M_{1,d}$, as argued from the conservation of the density current, single particle excitations are dominant and so they exhaust the sum rule in the long wavelength ($\mathbf{q} \to 0$) limit.

Since the longitudinal current response is connected to the first moment by Eq. (4.27), the result summarized in table 4.1 implies that longitudinal current response is determined by single particle and multiparticle excitations in the spin channel, and by single particle excitations only in the density channel. We will see in what follows that the situation is different for the transverse response function.

The correlation functions $\chi^T_{\mathbf{j}_\alpha \mathbf{j}_\beta}(\mathbf{q})$ are determined in the low $\mathbf{q}$ limit by matrix elements which connect multiparticle excited states only. Single particle excitations cannot contribute to the transverse response because they have a defined axial symmetry determined by their momentum $\mathbf{q}$ (see Nozieres and Pines (1999), Vol. II, Chapter 4), and a transverse current cannot excite them. On the other hand, multiparticle excitations do not possess any symmetry around the $\mathbf{q}$ axis and can contribute to the transverse response $\chi^T_{\mathbf{j}_\alpha \mathbf{j}_\beta}(\mathbf{q})$. Thus, we can write:

$$\lim_{\mathbf{q}\to 0} \chi^T_{\mathbf{j}_\alpha \mathbf{j}_\beta}(\mathbf{q}) = \lim_{\mathbf{q}\to 0} \chi^T_{\mathbf{j}_\alpha \mathbf{j}_\beta}(\mathbf{q})^{(m.p.)} . \tag{4.30}$$

With the superscript "m.p." we indicate that the only contributions are matrix elements connecting the ground state to multiparticle excited states.

A nonzero response of the superfluid to a transverse probe is thus strictly connected with the presence of multiparticle excitations in the multicomponent system, while in the case of a single component single particle excitations are the only low lying excited states at zero temperature and cannot be excited by such a probe. This important result will also be used in calculating the drag for a weakly interacting Bose mixture in sec. 4.4.1. There, only matrix elements which connect excited states made of a density and a spin phonon will appear in the transverse response.

The same reasoning does not apply to the longitudinal response where single particle excitations have the same axial symmetry as the probe. Nevertheless we should expect that the contribution of multiparticle excitations to the transverse and the longitudinal response is the same as they do not have any axial symmetry that can

discriminate between the two. We can write that:

$$\lim_{\mathbf{q}\to 0} \chi^{T}_{\mathbf{j}_\alpha \mathbf{j}_\beta}(\mathbf{q})^{(m.p.)} = \lim_{\mathbf{q}\to 0} \chi^{L}_{\mathbf{j}_\alpha \mathbf{j}_\beta}(\mathbf{q})^{(m.p.)} \,. \tag{4.31}$$

Using Eqs. (4.31) and (4.18) we can now write ρ_{AB} in terms of the longitudinal response:

$$\frac{\rho_{AB}}{m^2} = -\lim_{\mathbf{q}\to 0} \chi^{T}_{\mathbf{j}_\alpha \mathbf{j}_\beta}(\mathbf{q})^{(m.p.)} = -\lim_{\mathbf{q}\to 0} \chi^{L}_{\mathbf{j}_A \mathbf{j}_B}(\mathbf{q})^{(m.p.)}. \tag{4.32}$$

This equation allows the drag to be expressed directly from the multiparticle contributions to the sum rule $M_{1,s}$. Using Eqs. (4.26), (4.27) and (4.32) one has:

$$\begin{aligned} \frac{\rho_{AB}}{m^2} &= 4\left(\chi^{L}_{\mathbf{j}_d \mathbf{j}_d}(\mathbf{q})^{(m.p.)} - \chi^{L}_{\mathbf{j}_s \mathbf{j}_s}(\mathbf{q})^{(m.p.)}\right) \\ &= \lim_{\mathbf{q}\to 0} \frac{1}{2q^2} M^{(m.p.)}_{1,s}(\mathbf{q}) \,, \end{aligned} \tag{4.33}$$

where we used the fact that the density sum rule is exhausted by single particle excitations in the low $\mathbf{q}$ limit, namely:

$$\lim_{\mathbf{q}\to 0} \frac{2}{q^2} M^{(m.p.)}_{1,d}(\mathbf{q}) = 0 \,. \tag{4.34}$$

Finally making use of the last equality in Eq. (4.25):

$$M^{(s.p.)}_{1,s} = \frac{nq^2}{m}\left(1 - \frac{2\rho_{AB}}{mn}\right) . \tag{4.35}$$

The superscript $(s.p.)$ indicates the fact that we are accounting for contributions to $M_{1,s}$ coming only from single particle excitations.

Eq. (4.35) expresses a crucial result for a two species superfluid: in the low $\mathbf{q}$ limit the single particle contribution to $M_{1,s}$ is reduced from the value predicted by the f-sum rule by a factor proportional to **the drag ρ_{AB}, which accounts for multiparticle excitations**. In a single component superfluid this contribution is absent and the response of the system in the static, long wavelength limit is accounted for by single particle excitations only.

By computing the single particle contribution to the first moment of the spin operator, using Eq. (4.35), we are able to estimate the frequency of collective spin excitations, as we will do in subsecs. 4.5.1 and 4.5.2, and show how the drag influences them. While we will work out the consequences of Eq. (4.35) in the following sections, we can already infer its fundamental implications, at least in an intuitive sense. In fact, if we interpret the f-sum rule as a normalization condition that sets the scale for the response of a system to a probe, **Eq. (4.35) implies a diminished strength of the single particle spin excitations, as part of the normalization constraint is fulfilled by the multiparticle excited states.**

The presence of a finite drag ρ_{AB} has also an implication on the low energy, long wavelength quantum hydrodynamic Hamiltonian for two superfluids contains off-diagonal superfluid densities (see, e.g., Nespolo et al. (2017)):

$$H_{eff} = \sum_{\alpha,\beta=A,B} \int d\mathbf{r} \left(\frac{\hbar^2 \rho_{\alpha\beta}}{2m^2} \nabla\hat{\phi}_\alpha \cdot \nabla\hat{\phi}_\beta + \frac{g_{\alpha\beta}}{2} \hat{\Pi}_\alpha \hat{\Pi}_\beta \right) . \tag{4.36}$$

In the previous expression $\hbar\nabla\hat{\phi}_\alpha / m_\alpha$ is the superfluid velocity fluctuation of component α, $\hat{\Pi}_\alpha$ the density fluctuation and $g_{\alpha\beta} = \partial^2\epsilon/\partial n_\alpha \partial n_\beta$ with ϵ the ground state energy is the compressibility matrix. The operators $\hat{\phi}_\alpha$ and $\hat{\Pi}_\alpha$ satisfy the commutation relations: $\left[\hat{\phi}_\alpha(\mathbf{r}), \hat{\Pi}_\beta(\mathbf{r}')\right] = i\hbar\delta_{\alpha\beta}\delta(\mathbf{r}-\mathbf{r}')$. Using the effective Hamiltonian the first moment of an operator $\hat{F}$ can be also calculated Pitaevskii and Stringari (2016) via the commutator:

$$M^{eff}_{1,F} = \frac{1}{2V\hbar^2} \left\langle \left[\hat{F}^\dagger, \left[\hat{H}_{eff}, \hat{F}\right]\right] \right\rangle . \tag{4.37}$$

In particular for a spin density perturbation where $\hat{F} = \hat{\Pi}_{A,\mathbf{q}} - \hat{\Pi}_{B,\mathbf{q}}$ and indeed Eq. (4.37) coincides with the single particle excitation result, Eq. (4.35). The theory presented in this section thus represents a microscopic justification for the effective Hamiltonian in Eq. (4.36).

4.4 Weakly interacting Bose-Bose mixture: drag and excitations

A strength of the linear response formalism we developed in sec. 4.3.1 is that it provides a method to compute easily the superfluid density matrix. To provide a benchmark for it we now compute the relevant response functions in the Bogoliubov approximation for a weakly interacting Bose-Bose mixture at zero temperature. With the computations in this subsection we reproduce in a easy way the results in Ref. Fil and Shevchenko (2005). For completeness, in Appendix C we also show how to easily recover the result for the Hubbard model obtained in Linder and Sudbø (2009). We mention that the linear response formalism we developed was recently used in Ota and Giorgini (2020) to compute the Andreev-Bashkin drag in a weakly interacting Bose mixture at finite temperature, within beyond mean field Popov theory.

We will compute the current response in one component to a probe current in the other component along the x direction. Since the system is isotropic, the response will also be along the x direction. For simplicity we will assume a $\mathbb{Z}_2$ symmetric mixture, meaning that the densities, the masses and the intraspecies contact interactions of the two components are equal, namely $n_A = n_B = n$, $m_A = m_B = m$ and $g_{AA} = g_{BB} = g$. Additionally, at zero temperature, Eq. (4.20) for the $\mathbb{Z}_2$ symmetry implies the

following useful equality:

$$\chi^T_{j_{x,A},j_{x,A}}(\mathbf{q},\omega) = \chi^T_{j_{x,B},j_{x,B}}(\mathbf{q},\omega) = -\chi^T_{j_{x,A},j_{x,B}}(\mathbf{q},\omega). \tag{4.38}$$

4.4.1 Drag in a uniform mixture

We consider the case of a homogeneous weakly interacting Bose-Bose mixture with volume V. The mixture is stable in the mean field approximation when $g > 0$ and $|g_{AB}| < g$, where g_{AB} is the interspecies coupling. Since linear response requires the ground state to be stable we will only consider the case $|g_{AB}| < g$. The Hamiltonian describing the system, written in the momentum space basis, is:

$$\begin{aligned}\hat{H} = &\sum_{\alpha=A,B}\sum_{\mathbf{k}} \epsilon_{\mathbf{k}} \hat{a}^\dagger_{\mathbf{k},\alpha}\hat{a}_{\mathbf{k},\alpha} \\ &+ \frac{g}{2V}\sum_{\alpha=A,B}\sum_{\mathbf{k}_1,\mathbf{k}_2,\mathbf{p}} \hat{a}^\dagger_{\mathbf{k}_1+,\alpha}\hat{a}^\dagger_{\mathbf{k}_2-\mathbf{p},\alpha}\hat{a}_{\mathbf{k}_1,\alpha}\hat{a}_{\mathbf{k}_2,\alpha} \\ &+ \frac{g_{AB}}{2V}\sum_{\mathbf{k}_1,\mathbf{k}_2,\mathbf{p}} \hat{a}^\dagger_{\mathbf{k}_1+\mathbf{p},A}\hat{a}^\dagger_{\mathbf{k}_2-\mathbf{p},B}\hat{a}_{\mathbf{k}_1,A}\hat{a}_{\mathbf{k}_2,B}\,,\end{aligned} \tag{4.39}$$

where $\hat{a}_{\mathbf{k},\alpha}$ and $\hat{a}^\dagger_{\mathbf{k},\alpha}$ respectively annihilate and create a particle of species α and momentum $\mathbf{k}$ and $\epsilon_{\mathbf{k}} = \hbar^2k^2/2m$.

The intraspecies and interspecies couplings are related to the scattering lengths by $g = 4\pi\hbar^2 a/m$ and $g_{AB} = 4\pi\hbar^2 a_{AB}/m$ respectively. In the weakly interacting limit, when $na^3 \ll 1$, quantum fluctuations are small and the Hamiltonian in Eq. (4.39) can be reduced to a quadratic form by means of the Bogoliubov approximation. We retain only terms which are quadratic in the operators $a_{\mathbf{p},\alpha}$ and $a^\dagger_{\mathbf{p},\alpha}$ for $\mathbf{p} \neq 0$ and replace $a_{\mathbf{p}=0,\alpha}$ and $a^\dagger_{\mathbf{p}=0,\alpha}$ with $\sqrt{N_0}$, where N_0 is the number of particles in the condensate. The quadratic Hamiltonian can be diagonalized by a canonical transformation to the basis of Bogoliubov quasiparticles $\hat{b}^\dagger_{d,\mathbf{k}}$ and $\hat{b}^\dagger_{s,\mathbf{k}}$ in a balanced two component mixture Tommasini et al. (2003):

$$\begin{aligned}\hat{a}_{\mathbf{k},A} &= \frac{1}{\sqrt{2}}(u_{d,\mathbf{k}}\hat{b}_{d,\mathbf{k}} + v_{d,\mathbf{k}}\hat{b}^\dagger_{d,-\mathbf{k}} + u_{s,\mathbf{k}}\hat{b}_{s,\mathbf{k}} + v_{s,\mathbf{k}}\hat{b}^\dagger_{s,-\mathbf{k}})\,, \\ \hat{a}_{\mathbf{k},B} &= \frac{1}{\sqrt{2}}(u_{d,\mathbf{k}}\hat{b}_{d,\mathbf{k}} + v_{d,\mathbf{k}}\hat{b}^\dagger_{d,-\mathbf{k}} - u_{s,\mathbf{k}}\hat{b}_{s,\mathbf{k}} - v_{s,\mathbf{k}}\hat{b}^\dagger_{s,-\mathbf{k}})\,.\end{aligned} \tag{4.40}$$

The labels d and s indicate density and spin quasiparticles and the coefficients $u_{d(s),\mathbf{k}}$ and $v_{d(s),\mathbf{k}}$ are:

$$\begin{aligned} u_{d(s),\mathbf{k}} &= \frac{1}{2}\left(\sqrt{\frac{\epsilon_{\mathbf{k}}}{\Omega_{d(s),\mathbf{k}}}} + \sqrt{\frac{\Omega_{d(s),\mathbf{k}}}{\epsilon_{\mathbf{k}}}}\right), \\ v_{d(s),\mathbf{k}} &= \frac{1}{2}\left(\sqrt{\frac{\epsilon_{\mathbf{k}}}{\Omega_{d(s),\mathbf{k}}}} - \sqrt{\frac{\Omega_{d(s),\mathbf{k}}}{\epsilon_{\mathbf{k}}}}\right), \end{aligned} \tag{4.41}$$

where $\Omega_{d,\mathbf{k}}$ and $\Omega_{s,\mathbf{k}}$ are the excitation energies of the density and spin excitations respectively, namely:

$$\Omega_{d(s),\mathbf{k}} = \sqrt{\frac{\hbar^2 k^2}{2m}\left(\frac{\hbar^2 k^2}{2m} + 2gn \pm 2g_{\mathrm{AB}}n\right)}. \tag{4.42}$$

The diagonalized Hamiltonian takes the form:

$$\hat{H} \approx E_0 + \sum_{\gamma=d,s}\sum_{\mathbf{k}\neq 0} \Omega_{\gamma,\mathbf{k}} \hat{b}^\dagger_{\gamma,\mathbf{k}} \hat{b}_{\gamma,\mathbf{k}}\,, \tag{4.43}$$

where E_0 is the ground state energy. We substitute the above expressions into Eqs. (4.18), (4.19) and (4.20) and use Eqs. (4.15) and (4.38) to find the expression of the drag in terms of the excitation spectra $\Omega_{d(s),\mathbf{k}}$:

$$\begin{aligned} \rho_{AB} &= -m^2 \lim_{\mathbf{q}\to 0} \chi^T_{j_{x,A}, j_{x,B}}(\mathbf{q}) \\ &= \frac{\hbar^2}{2V}\sum_{\mathbf{k}} \frac{(u_{d,\mathbf{k}} v_{s,\mathbf{k}} - u_{s,\mathbf{k}} v_{d,\mathbf{k}})^2}{\Omega_{d,\mathbf{k}} + \Omega_{s,\mathbf{k}}} k_x^2 \\ &= \frac{\hbar^2}{8V}\sum_{\mathbf{k}} \frac{(\Omega_{d,\mathbf{k}} - \Omega_{s,\mathbf{k}})^2}{(\Omega_{d,\mathbf{k}} + \Omega_{s,\mathbf{k}})\Omega_{s,\mathbf{k}}\Omega_{d,\mathbf{k}}} k_x^2\,. \end{aligned} \tag{4.44}$$

This coincides with the result obtained in Fil and Shevchenko (2005) where also the finite temperature result was derived. The expression of Eq. (4.44) is rather suggestive. The second line of the equation displays a result that we anticipated in sec. 4.3.2 and that holds in general: only matrix elements between multiparticle excited states ($\sim b^\dagger b^\dagger |0\rangle$) contribute to the transverse response, as expected from the previous discussion on sum rules. In the present case of a $\mathbb{Z}_2$ symmetric mixture the multiparticle excitations are composed of spin and density phonons.

The numerator on the third line of Eq. (4.44) implies that the collisionless drag strictly depends on the difference in the bare excitation energies in the spin and density channel. The result of Eq. (4.44) is an even function of the interspecies interaction g_{AB}, as a result of the Bogoliubov approximation, while the inclusion of higher order terms

should eliminate this symmetry. In particular one can expect the drag to be stronger in the attractive regime where density-density fluctuations are enhanced.

The sum in Eq. (4.44) can be turned into an integral which can be solved analytically, giving:

$$\rho_{AB} = mn\sqrt{na^3}\eta^2 F(\eta)\,, \tag{4.45}$$

where $\eta = \frac{|g_{AB}|}{g}$ and:

$$F(\eta) = \frac{256}{45\sqrt{2\pi}} \frac{2 + 3\sqrt{(1+\eta)(1-\eta)}}{(\sqrt{2(1-\eta)} + \sqrt{2(1+\eta)})^3}. \tag{4.46}$$

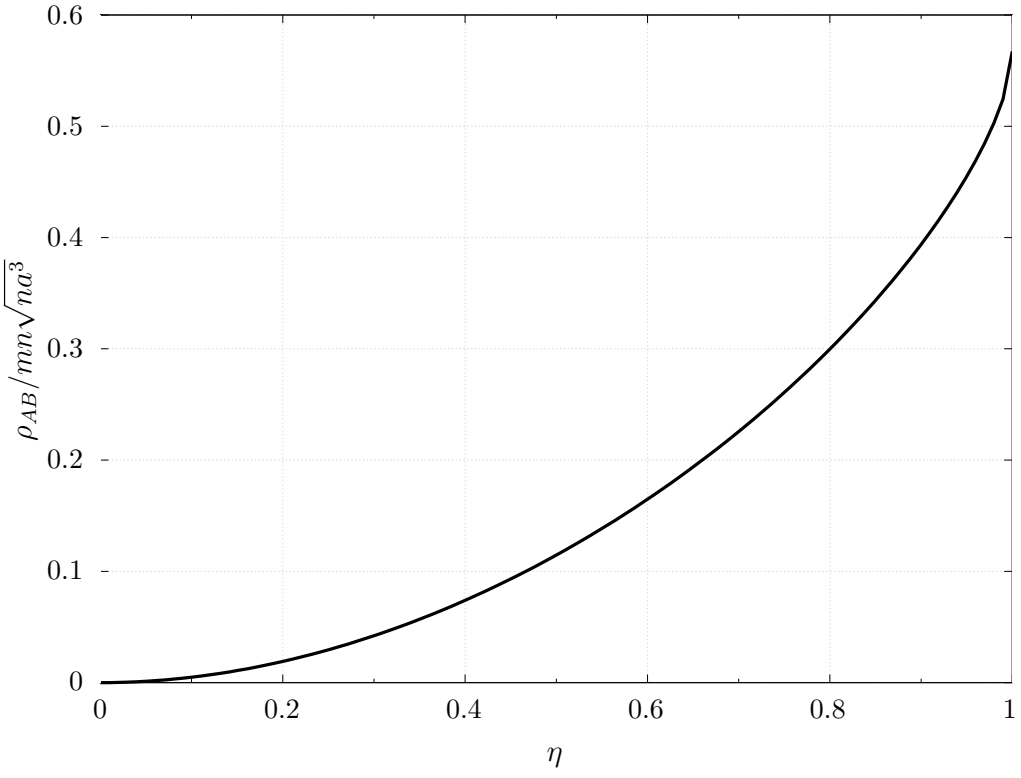

FIGURE 4.2: Superfluid drag as a function of the interspecies interaction strength $\eta = |g_{AB}|/g$. The drag is seen to increase monotonically with η to a maximum of $mn\sqrt{na^3}64/45\sqrt{2\pi}$. Note also that ρ_{AB} is an even function of g_{AB} and so it has the same behaviour for attractive and repulsive interactions.

We see from Eq. (4.45) that the drag coefficient is directly proportional to the gas parameter $\sqrt{na^3}$, making the effect very small for weakly interacting mixtures.

A couple of remarks are worth. In presence of a superfluid phase we would expect the response functions $\chi_{j_{x,A},j_{x,A}}(\mathbf{q})$ and $\chi_{j_{x,B},j_{x,B}}(\mathbf{q})$ to converge to the transverse (longitudinal) response when q_x goes to zero before (after) q_y and q_z (Eq. (4.16)). However within the Bogoliubov approximation all the long wavelength limits

commute, implying incorrectly that there is no distinction between the transverse and longitudinal response. While the prediction for the transverse response is valid, the Bogoliubov approximation gives an incorrect value for the longitudinal response functions. This is a known shortcoming of the Bogoliubov approximation, present also in the single component case, that can be cured by taking into account vertex corrections (see Schrieffer (1999) for a detailed treatment).

4.5 Effect of the drag on the excitations of a two component BEC

A fundamental task in order to make the Andreev-Bashkin effect measurable is to predict its effect on physical observables that are accessible to experiments. Here we address this point by computing the beyond mean field correction to the spin speed of sound in sec. 4.5.1 and the spin dipole mode frequency in sec. 4.5.2. Importantly for the ongoing experiments on spin superfluidity (see, e.g., Fava et al. (2018); Kim et al. (2020)) we show that for a weakly interacting repulsive Bose-Bose mixture the beyond mean field corrections to the spin speed of sound are dominated by the change in the susceptibility, while the collisionless drag gives a minor contribution. In the following sec. (4.5.2) we show instead that the two contributions are roughly of the same order for the spin dipole mode frequency for a trapped mixtures.

In order to estimate the excitation energies we use sum rules for which we provided a number of results in the previous sections. Within linear response, the energy of the lowest state excited by an operator $\hat{F}$ satisfies the inequality Pitaevskii and Stringari (2016):

$$\hbar\omega_s(q) \leq \sqrt{\frac{M_{1,F}}{M_{-1,F}}}\,, \tag{4.47}$$

with $M_{1,F}$ the first moment of the structure factor for the operator F and $M_{1,s}$ the so called *inverse energy weighted sum rule* for

$$M_{-1,F} = \int_0^\infty \frac{S_F(\mathbf{q},\omega)}{\omega} d\omega \tag{4.48}$$

Eq. (4.47) represents an upper bound on the energy of the lowest lying excitations. In the long wavelength limit ($\mathbf{q} \to 0$) the lowest lying excited states are the single particle excitations, as their energy vanishes with q^2. Moreover, Eq. (4.47) becomes an equality when only single particle excited states are accounted for in calculating $M_{1,F}$ and $M_{-1,F}$ Pitaevskii and Stringari (2016). Namely we may write:

$$\hbar\omega_s(q) = \sqrt{\frac{M_{1,F}^{(s.p.)}}{M_{-1,F}^{(s.p.)}}}\,, \tag{4.49}$$

where as in sec. 4.3.2 by the superscript $(s.p.)$ we indicate the fact that we are considering matrix elements where only single particle excited states appear.

From Eq. (4.49) the strategy of the next two subsections is made apparent. We will compute the relevant moments of the structure factors, including the correction coming from the drag, when the operator $\hat{F}$ is the spin operator (in sec. 4.5.1) or the dipole operator (in sec. 4.5.2). This will provide us with an expression for the energy of the low lying excited states created by these operators and the effect that the drag has on their magnitude.

4.5.1 Beyond mean field correction to the spin speed of sound in a homogeneous gas

For a homogeneous $\mathbb{Z}_2$ symmetric superfluid mixture the single particle excitations consist in sound waves that propagate through the gas. There are two sounds a two species superfluid mixture, the density sound and the spin sound, excited by the respective operators. They correspond to in phase and out of phase local fluctuations in the density of the two species, as depicted in fig. 4.1, and propagate through the gas with speed c_d and c_s respectively. While the density speed of sound is not affected by the drag, the spin speed of sound receives a correction at first order in the gas parameter $\sqrt{na^3}$.

By choosing as exciting operator the spin density operator (Eq. (4.23)) in Eq. (4.49) we can estimate the spin dispersion relation. We use for the the energy weighted sum rules the general expression Eq. (4.35) with the drag given by the weakly interacting result, Eq. (4.45):

$$M_{1,s}^{(s.p.)} = \frac{nq^2}{m}\left(1 - \sqrt{na^3}\,2\eta^2 F(\eta)\right) . \tag{4.50}$$

The inverse energy weighted moment, $M_{-1,s}$, is exhausted by single particle excitations as evident from table 4.1 and it is given by:

$$M_{-1,s} = M_{-1,s}^{(s.p.)} = \frac{\chi_s}{2} , \tag{4.51}$$

where χ_s is the spin susceptibility, defined as $\chi_s^{-1} = \frac{\partial^2(E/V)}{\partial(n_A - n_B)^2}$, and E is the energy of the superfluid in its ground state. The latter has to be determined to the same order of $M_{1,s}$ and therefore one must use the equation of state for the Bose-Bose mixtures including the Lee-Huang-Yang correction Larsen (1963). Eventually we find (see Appendix D for the derivation):

$$\frac{1}{M_{-1,s}} = (g - g_{AB})\left(1 + \sqrt{na^3}C(\eta)\right) , \tag{4.52}$$

where the function $C(\eta)$ is defined in Eq. (D.6). So we have that

$$\frac{M_{1,s}^{(s.p.)}}{M_{-1,s}} \equiv c_s^2 q^2 = c_{s,MF}^2 [1 + \sqrt{na^3}(C(\eta) - 2\eta^2 F(\eta))] q^2 \,, \tag{4.53}$$

where $c_{s,MF} = \sqrt{n(g - g_{AB})/m}$ is the mean field spin speed of sound. In Fig. (4.3) we report the quantity:

$$\delta c_s = \frac{c_s - c_{s,MF}}{c_{s,MF}} \tag{4.54}$$

which quantifies the deviation of the spin speed of sound from its mean field value.

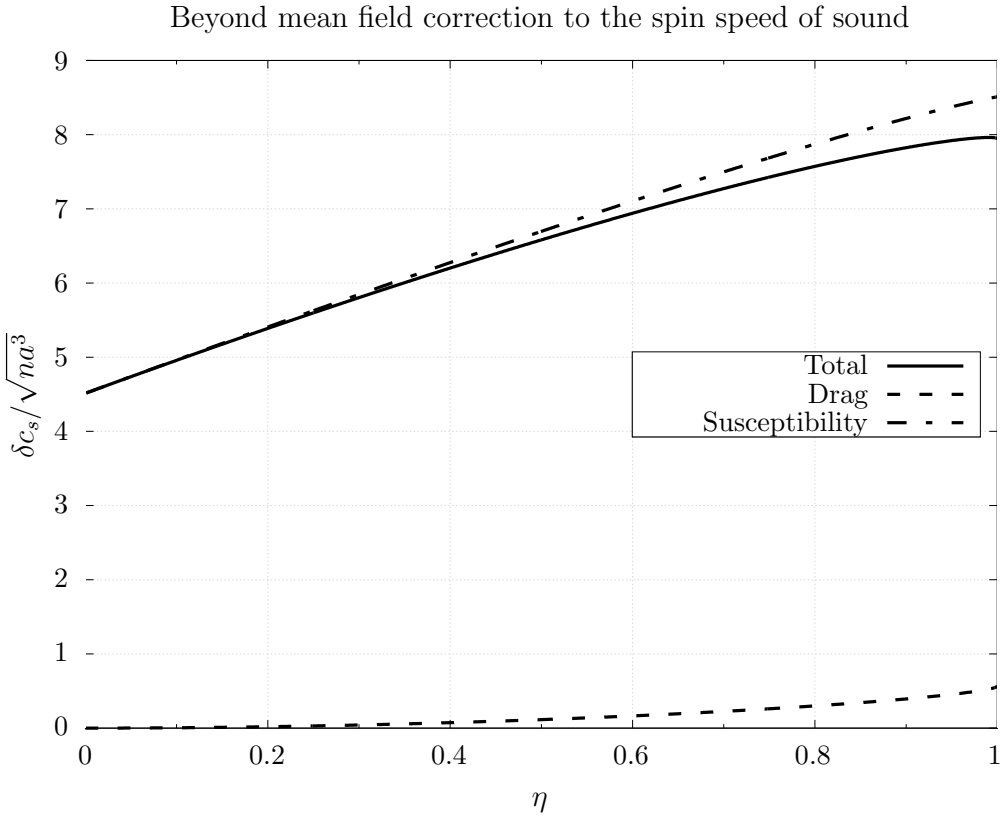

FIGURE 4.3: Beyond mean field correction to the spin speed of sound (full line) as a function of the interspecies interactions $\eta = |g_{AB}|/g$. We limited the analysis to values of η smaller than 1 to avoid the regimes of phase separation and collapse. The correction coming from the drag (dashed) is at least one order of magnitude smaller than that coming from Lee-Huang-Yang terms in the susceptibility (dotted).

From Fig. (4.3) it is clear that the beyond mean field correction to the spin speed of sound is dominated by the susceptibility contribution. The overall correction for typical values of the gas parameter $\sqrt{na^3} \approx 10^{-3}$ is of order $10^{-3} - 10^{-2}$ but the contribution from the drag is at least one order of magnitude smaller. We mention that a recent experiment Kim et al. (2020) has been able to measure the two (density and spin) sounds of a symmetric superfluid mixture, although with the current precision it is not possible to observe beyond mean field effects on the spin speed of sound.

4.5.2 Spin dipole modes in a trap

We can apply a similar reasoning to the determination of the frequency of dipole modes for the two species in the mixture trapped by spherically symmetric harmonic potentials:

$$V_\alpha(r) = \frac{m}{2}\omega_0^2(r - r_{0,\alpha})^2\,, \tag{4.55}$$

where ω_0 is the trapping frequency and $r_{0,\alpha}$ is the center of the trap for each species α. Initially the two species dependent traps are such that $r_{0,A} = r_{0,B} \equiv 0$. The so called *spin dipole mode* can be excited by separating by a small amount δx the center of the two traps, as illustrated in Fig. 4.4, inducing a *spin dipole moment* in the cloud, represented by the operator:

$$\hat{D}_s = \int d^3\mathbf{r}\, x\, (\hat{n}_A(\mathbf{r}) - \hat{n}_B(\mathbf{r}))\,. \tag{4.56}$$

After the displacement the density of the two species (and thus the spin dipole moment) will start to oscillate out of phase with a certain frequency ω_{D_s} which we set out to compute in this section. Before moving to the actual computations we shall briefly compare with the case of a single component superfluid. There the only dipole mode that exists corresponds to oscillations of the center of mass of the whole system and characterized by the frequency $\omega_D = \omega_0$ Stringari (1996), independently of the interactions. In the superfluid mixture the oscillation of the center of mass corresponds to in phase oscillations of the two species, i.e. the *density dipole mode*. While for the density dipole mode one recovers the same result as for the single component Bose gas, the spin dipole mode should be modified by beyond mean field corrections, as in the analogous case of Fermi-Liquid theory Recati and Stringari (2011).

We apply the formalism of sum rules to the spin dipole operator, i.e. we choose $\hat{F} = \hat{D}_s$ in Eq. (4.49). The spin dipole frequency can be computed as:

$$\hbar\omega_{D_s} = \sqrt{\frac{M^{(s.p.)}_{1,D_s}}{M^{(s.p.)}_{-1,D_s}}}\,. \tag{4.57}$$

Similarly to the case of the spin operator in the previous subsection, the single particle contribution to $M^{(s.p.)}_{1,D_s}$ is modified by the presence of the collisionless drag as is evident from evaluating the commutator (Eq. (4.37)):

$$\begin{aligned} M^{(s.p.)}_{1,D_s} &= \frac{1}{2V}\left\langle\left[\hat{D}_s,\left[\hat{H}_{eff},\hat{D}_s\right]\right]\right\rangle \\ &= \frac{1}{V}\int d^3\mathbf{r}\frac{n(\mathbf{r})}{m}\left(1 - \frac{2\rho_{AB}(\mathbf{r})}{mn(\mathbf{r})}\right)\,. \end{aligned} \tag{4.58}$$

where the Hamiltonian $\hat{H}_{eff}$ is the effective hydrodynamic Hamiltonian of Eq. (4.36) with the addition of the harmonic trapping potential. The local drag coefficient $\rho_{AB}(\mathbf{r})$

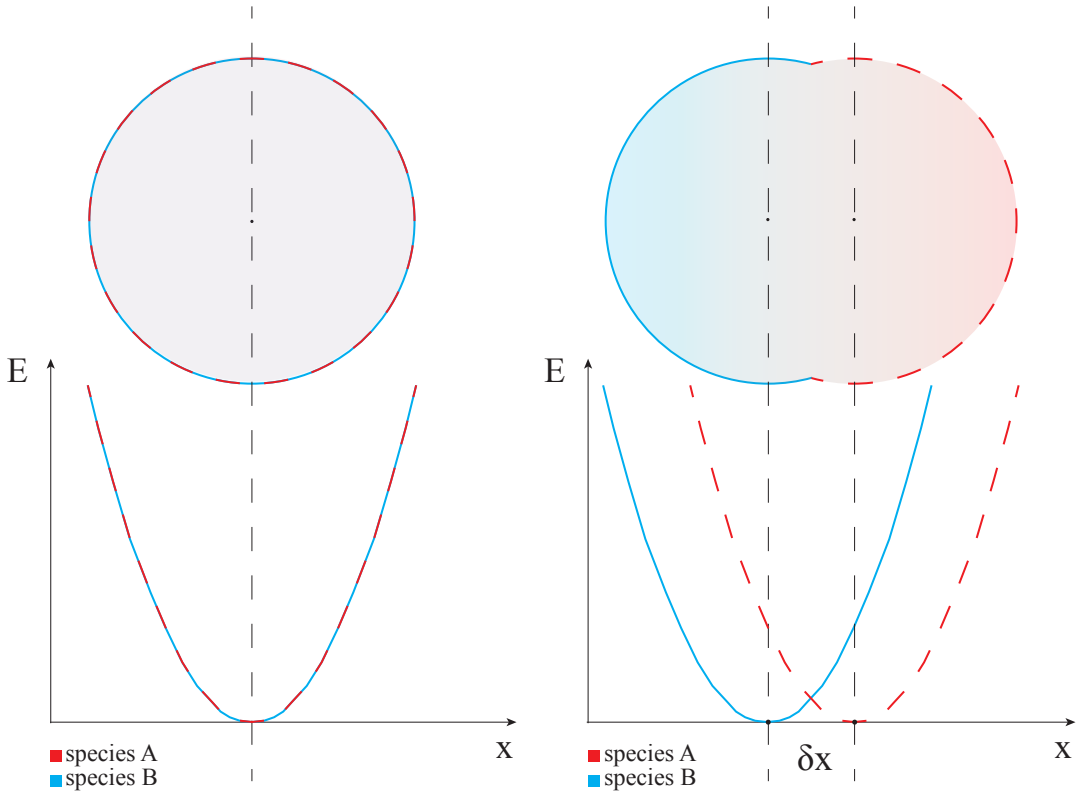

FIGURE 4.4: Representation of the excitation of a spin dipole mode. Initially (left panel) the two species are trapped in the same position. Then (right panel) the center of the two traps is displaced by a small amount $\delta x = r_{0,A} - r_{0,B}$, inducing a spin dipole moment D_s. The two species composing the mixture will start to oscillate inside the shaded region.

is a function of the coordinates $\mathbf{r}$ only through $n(\mathbf{r})$, i.e. the local density approximation of Eq. (4.45). The inverse energy weighted moment, M_{-1,D_s}, is determined by the spin susceptibility via the expression Sartori et al. (2015):

$$M_{-1,D_s} = \frac{1}{2V}\int d^3\mathbf{r}\, x^2 \chi_s(n(\mathbf{r}))\,. \tag{4.59}$$

Consistently the density profile is determined within the local density approximation of the Lee-Huang-Yang equation of state in presence of the harmonic potential (see Appendix D for the derivation)[1].

[1]The use of the local density approximation for ρ_{AB} and χ_s is valid as long as the spin healing length $\xi_s = \sqrt{8\pi n\,(a - a_{AB})}$ is much smaller than the size of the Bose-Bose mixture cloud, which we can identify with the Thomas-Fermi radius R_{TF} (see Eq. (4.61)).

Eventually we are able to write the sum rules as:

$$\begin{aligned} M_{1,D_s}^{(s.p.)} &= \frac{n}{m}\left(1-\frac{15\pi}{32}\sqrt{n(0)a^3}\eta^2 F(\eta)\right), \\ \frac{1}{M_{-1,D_s}} &= \frac{5(g-g_{AB})}{R_{TF}^2}\left(1+\frac{5\pi}{32}\sqrt{n(0)a^3}(C(\eta)-B(\eta))\right), \end{aligned} \tag{4.60}$$

where R_{TF} is the so-called mean-field Thomas-Fermi radius Pitaevskii and Stringari (2016) of the trapped mixture:

$$R_{TF} = \left(\frac{15N\,(g+g_{AB})}{8\pi m\omega_0^2}\right)^{1/5}. \tag{4.61}$$

The expression for the functions $C(\eta)$ and $B(\eta)$ can be found in Appendix D, Eqs. (D.6) and (D.4) respectively.

As for the homogeneous case we report in Fig. (4.5) the variation

$$\delta\omega = \frac{\omega_{D_S}-\omega_{MF}}{\omega_{MF}}, \tag{4.62}$$

which quantifies the deviation of the spin dipole frequency from its mean field value $\omega_{MF} = \omega_0\sqrt{(g-g_{AB})/(g+g_{AB})}$ and is always positive. Also in the trapped cases the correction to the spin dipole frequency due to the drag is extremely small: for typical values of the gas parameter $\sqrt{n(0)a^3} \approx 10^{-3}$ the relative correction given by the drag is of order $10^{-3}-10^{-4}$. However, differently from the case of the speed of sound the correction from the drag can become comparable to the susceptibility one, owing to the non monotonic behaviour of the latter. The correction coming from the susceptibility is not a monotonic function of η (contrarily to the homogeneous case) as a result of the competition between the functions $C(\eta)$ and $B(\eta)$. The former comes from the beyond mean field correction to the spin susceptibility (Eq. (D.5)), the latter comes from the beyond mean field correction to the size of the cloud (Eq. (D.10)). Finally notice that for $\eta = 0$ the two clouds oscillate independently and we get indeed $\omega_{D_s} = \omega_0$ as for the in phase oscillations.

The calculations of this section can be easily extended to an elongated trap. For an ellipsoidal trap with frequencies ω_x, ω_y and ω_z along the x, y and z direction Eq. (4.58) is unchanged while Eq. (4.59) has to be multiplied by a factor $\omega_x/\bar{\omega}_0$ where $\bar{\omega}_0 = \sqrt[3]{\omega_x\omega_y\omega_z}$. The relative size of the correction from the susceptibility and the drag is unchanged.

The major drawback of weakly interacting gases is apparent from our results. The Andreev-Bashkin effect is made elusive by the fact that, being due to beyond mean field quantum fluctuations, it is typically very small in cold gases settings. While increasing the strength of interactions would increase the magnitude of the drag, it

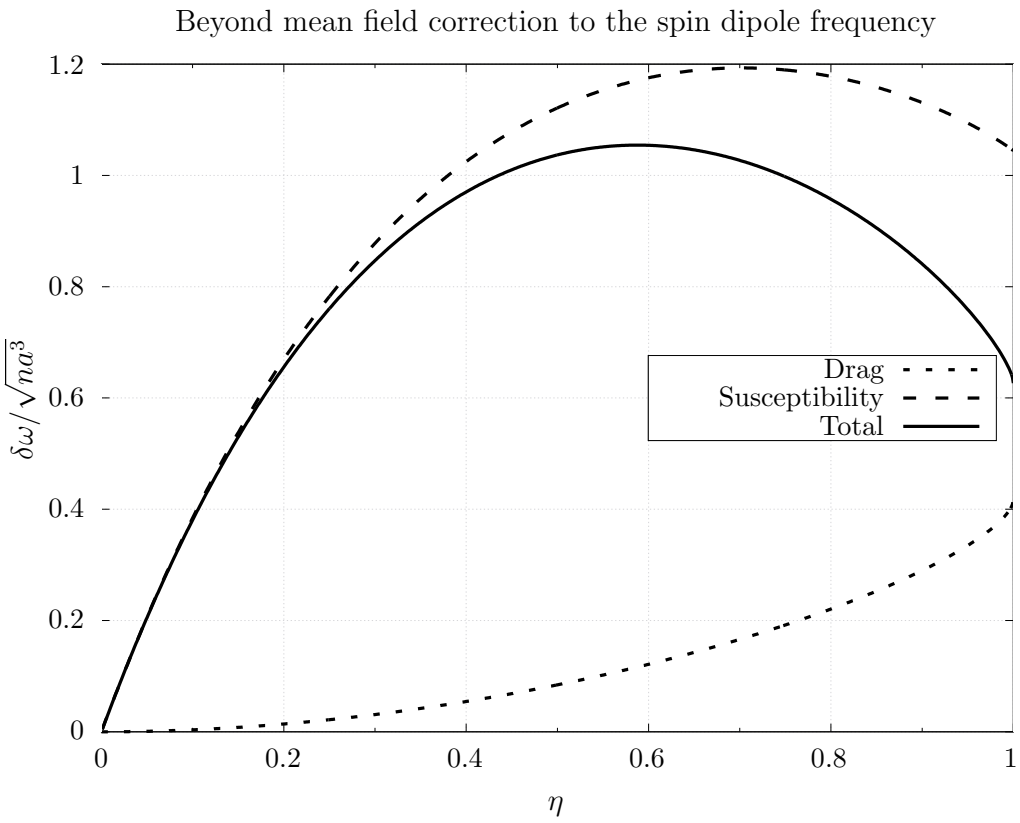

FIGURE 4.5: Beyond mean field correction to the spin dipole frequency (full line) as a function of the interspecies interactions $\eta = |g_{AB}|/g$. We limited the analysis to values of η smaller than 1 to avoid the regimes of phase separation and collapse. Although the overall correction is smaller than in the case of the spin speed of sound, here the effect of the drag (dashed) is comparable with that of the susceptibility (dotted).

would also amplify three body losses Stenger et al. (1999). We also expect that attractive interspecies interactions ($g_{AB} < 0$) would enhance the effect as they increases density fluctuations, a feature that is not captured by the Bogoliubov approximation (see Eq. (4.45)).

4.6 Measuring the drag via a quick perturbation

Collective excitations induced by a static perturbation (where $\omega = 0$) are governed both by the drag, through the moment $M_{1,s}$ or M_{1,D_s}, and the susceptibility of the system, through the moment $M_{-1,s}$ or M_{-1,D_s}. As we showed in Fig. (4.3) and Fig. (4.5) the two effects are of comparable magnitude, so it is convenient to devise an experiment where only the drag effect plays a role. In addition, while it would be desirable to study the effect in strongly interacting mixtures, three body losses will significantly abbreviate the stability of such systems.

In order to overcome both these limitations we consider the linear response of a trapped gas to a perturbation that is suddenly turned on.

We start by considering the the frequency response $\chi_{D_A,D_B}(\omega)$ of the operator $\hat{D}_B = \int d^3\mathbf{r}\, x\, \hat{n}_B(\mathbf{r})$ to a perturbation $\hat{D}_A = \int d^3\mathbf{r}\, x\, \hat{n}_A(\mathbf{r})$, which is given by:

$$\chi_{D_A,D_B}(\omega) = \frac{2}{V}\sum_{n\neq 0}\frac{\langle n|\hat{D}_A|0\rangle\,\langle 0|\hat{D}_B|n\rangle}{\omega^2+(E_0-E_n)^2}\,(E_0-E_n)\,. \tag{4.63}$$

The response function satisfies the following expansion at high frequencies Pitaevskii and Stringari (2016):

$$\begin{aligned}\chi_{D_A,D_B}(\omega) &= -\frac{1}{\omega^2 V}\left\langle\left[\hat{D}_B,\left[\hat{H}_{eff},\hat{D}_A\right]\right]\right\rangle + O\left(\frac{1}{\omega^3}\right) = \\ &= -\frac{1}{\omega^2 V}\int d^3\mathbf{r}\,\frac{\rho_{AB}(\mathbf{r})}{m^2} + O\left(\frac{1}{\omega^3}\right),\end{aligned} \tag{4.64}$$

where in the last equality we made use of Eq. (4.58). We thus see that the response function at high frequencies is directly proportional to the drag. This describes a situation where the probe $\hat{D}_A$ is quickly turned on and the observable $\hat{D}_B$ is measured shortly after, as we will clarify in what follows.

Consider a time dependent perturbation of the form:

$$\hat{V}(t) = \lambda \hat{D}_A\,\theta(t)\,, \tag{4.65}$$

where $\theta(t)$ is the Heaviside step function and λ is a small parameter. The variation of the average of D_B to first order in λ at time t is given by:

$$\langle\delta D_B\rangle(t) = \lambda V\int_{-\infty}^{\infty} dt'\chi_{D_A,D_B}(t-t')\theta(t')\,. \tag{4.66}$$

Using the Fourier transform of the theta function $\tilde{\theta}(\omega) = \frac{1}{i\omega} + \pi\delta(\omega)$ and after some manipulation we arrive at

$$\langle\delta D_B\rangle(t) = -\frac{\lambda V}{2\pi}\int d\omega\,\frac{e^{-i\omega t}-1}{i\omega}\chi_{D_A,D_B}(\omega)\,, \tag{4.67}$$

where we made use of the useful identities $\pi\chi_{D_A,D_B}(0) = i\int d\omega\,\chi_{D_A,D_B}(\omega)/\omega$ and $\int d\omega\,\chi_{D_A,D_B}(\omega) = 0$. While this integral is in principle over all frequencies ω, the response function $\chi_{D_A,D_B}(\omega)$ will have a cutoff in frequency $\overline{\omega}$ above which it vanishes. We thus expand this expression for short times, i.e. times t such that $t \ll 1/\overline{\omega}$:

$$\langle\delta D_B\rangle(t) = -i\frac{\lambda V}{4\pi}\int_{-\infty}^{\infty} d\omega\,\omega t^2\chi_{D_A,D_B}(\omega)\,. \tag{4.68}$$

Since the real part of the response function is an even function of ω we can express the response in terms of the imaginary part of the response function $\chi''_{D_A,D_B}(\omega)$ which at zero temperature satisfies the sum rule Pitaevskii and Stringari (2016):

$$\int_{-\infty}^{\infty} d\omega\, \omega\, \chi''_{D_A,D_B}(\omega) = \frac{\pi}{V} \left\langle \left[\hat{D}_A, \left[\hat{H}_{eff}, \hat{D}_B\right]\right]\right\rangle . \tag{4.69}$$

Using this equality in Eq. (4.68) and making use of Eq. (4.58) we finally obtain the desired equation in terms of the double commutator:

$$\begin{aligned} \langle \delta D_B \rangle (t) &= \frac{\lambda}{4} t^2 \left\langle \left[\hat{D}_A, \left[\hat{H}_{eff}, \hat{D}_B\right]\right]\right\rangle = \\ &= \frac{\lambda t^2}{4} \int d^3\mathbf{r}\, \frac{\rho_{AB}(\mathbf{r})}{m^2} . \end{aligned} \tag{4.70}$$

This calculation outlines a useful experimental procedure to measure the drag coefficient. A superfluid mixture subject to a dipole moment $\hat{D}_A$ that is suddenly turned on will have the other component increase ballistically its dipole moment $\hat{D}_B$ for short times, with a coefficient proportional to the drag coefficient ρ_{AB}. This experimental procedure would allow to measure the drag directly, without the need to independently measure the susceptibility of the system (as in secs. 4.5.1 and 4.5.2). Importantly, the short time scales involved significantly reduce the amount of three body losses. This makes the procedure applicable to strongly interacting systems where the effect is more sizeable.

4.7 Conclusions

In this chapter we analysed the Andreev-Bashkin effect in a two species superfluid within linear response theory. In analogy with the single component case the superfluid densities can be expressed in terms of transverse current-current response functions. A striking result that has no analogy with the single component case is that, while the overall response of the superfluid to a transverse vector field vanishes at zero temperature, such a field will give rise nonzero response even at vanishing temperature when acting only on one component. In this sense, the drag behaves as a sort of normal component, inducing a current response in reaction to a transverse probe.

The presence of a finite drag density arises from multiparticle excited states, which are shown to give an additional contribution to the first moment of the spin structure factor $S_s(\mathbf{q},\omega)$. This result is also in contrast with the case of single component superfluids, where single particle excitations are the only low-lying excited states at zero temperature. Since the moments of $S_s(\mathbf{q},\omega)$ are constrained by a sum rule, the fact that the drag is nonzero means that the single quasiparticle contribution is

changed (see e.g. Eq. (4.35)). Using current-current response functions we evaluate the collisionless drag in a two component weakly interacting Bose gas within the Bogoliubov approximation. This allows us to easily recover the results obtained via energy vacuum calculations Fil and Shevchenko (2005) and give a more direct interpretation of the drag as spin-density phonon mixing. We show how typical measurable quantities as the spin speed of sound and the spin dipole mode frequency are affected by the presence of the drag. While the beyond mean field change in the susceptibility dominates the correction to the spin speed of sound, in the case of the spin dipole frequency the correction due to the presence of the drag can be of the same order of magnitude as that coming from the susceptibility.

We show that the drag can be directly measured in an experiment where a dipole moment is quickly induced on one component. This induces at short times an increasing dipole moment in the other component which is proportional to the drag density.

Our analysis can be replicated to compute the drag and its effect on observables in strongly interacting systems. This is particularly relevant for new cold atoms systems as Bose-Bose mixtures on optical lattices Catani et al. (2008); Gadway et al. (2010); Fukuhara et al. (2013), superfluid Bose-Fermi mixtures Ferrier-Barbut et al. (2014) and in the foreseeable future superfluid Fermi-Fermi mixtures and the short-lived strongly interacting Bose mixtures (as an extension of the recently realized strongly interacting Bose gas Eigen et al. (2017); Eismann et al. (2016)).

A clear conclusion of our study is that weakly interacting Bose gases are not the ideal system in order to measure a sizeable effect. In fact, the drag coefficient in this regime is much smaller than the superfluid density and its effect on observables quantities such as the spin speed of sound or the spin dipole mode frequency is negligible. Thus, provided that the experimental procedure we outlined are not in principle limited to weakly interacting gases, it is natural to ask **in which systems should the drag be more sizeable and measurable?**
In the next chapter we address this question by reporting the study on a superfluid mixture in one dimensional Hubbard lattice.

5

Collisionless drag in a 1D ring lattice

The work contained in this chapter lead to the publication of the paper in Contessi et al. (2021). The numerical analysis were done by Daniele Contessi. I worked on the direction of the study, the analytical calculations, and the interpretations of the results alongside the other authors.

5.1 Introduction: why a 1D ring lattice?

As shown in the previous chapter the drag coefficient is much smaller than the total density in weakly interacting Bose mixtures and, as such, not easily observable in these systems. The magnitude of the drag can be enhanced in principle by increasing the size of quantum fluctuations beyond the mean field equation of state by, for example, increasing the strength of the interactions. This route is made only partially viable by three body losses which are enhanced by strong interactions Stenger et al. (1999), reducing very much the life time of the gas.

A different option comes from systems with low dimensionality which have been recently proposed (Nespolo et al. (2017); Parisi et al. (2018)) as candidates to observe the effect. One striking advantage of low dimensional systems is that the rate of 3-body collisions should be smaller compared to three dimensional systems, thus allowing to reach strongly interacting regimes where the effect should be more sizeable. In particular, in Nespolo et al. (2017) it has been shown that approaching the molecular phase in a double-layer dipolar gas system the drag can become increasingly large. In Parisi et al. (2018), one dimensional mixtures close to the Tonks-Girardeau regime have been shown to exhibit a large drag when approaching the phase separation transition.

Another option is to consider Hubbard-like models where the cold-atoms are constrained in optical lattices. Aside from reducing three-body losses, introducing a discrete lattice enriches the phase diagram of the system of making it possible to study the drag in phases which are not generally accessible for continuous, low dimensional systems Kuklov et al. (2004). Of particular interest for the fate of a sizeable drag is the paired superfluid phase where the two species undergo Bose-Einstein condensation in pairs, much like in the case of Fermions in the BCS superfluid state Kagan and Efremov (2002). An analysis of the AB effect in a two-component single-band two-dimensional Bose-Hubbard model can be found in Sellin and Babaev (2018), where the effect of the proximity to the Mott insulating phase is discussed in detail.

In the present work we focus on the AB drag in a two-component Bose-Hubbard model on a one dimensional ring. Aside from all the advantages outlined above, the presence of the lattice allows us to have a finite range of parameters with attractive interspecies interaction where the two-superfluid state is stable and the drag can be strongly enhanced Nespolo et al. (2017); Parisi et al. (2018). The ring geometry is particularly well suited for studying supercurrents, both theoretically and experimentally.

5.1.1 Outline

We study the Andreev-Bashkin collisionless drag for a two-component one dimensional Bose-Hubbard model on a ring at zero temperature. Using Tensor Network numerical simulations, we compute the superfluid densities (and in particular the drag density) for a variety of regimes depending on the lattice filling and the interactions, both intraspecies and interspecies. We will then focus on the regimes with attractive interactions, where pairing correlations are expected to produce a more sizeable effect. In particular, we will focus on the range of parameters which approaches the transition to pair superfluidity. We will discuss the importance of the drag in the Luttinger liquid theory, particularly its effect on the Luttinger parameter K_S, as a consequence of the sum rule analysis of chapter 4. The Luttinger paramater can also be computed from the long range behaviour of the correlation functions, , independently from any assumption on the drag. This will serve to test the consistency of our results.

The chapter is structured as follows. Sec. 5.2 describes the Bose-Hubbard Hamiltonian for the two component mixtures and the basic formulas that we use to compute the drag. Sec. 5.2.3 shows the computation of the drag for half filling of the lattice, in order to compare it with existing prediction, especially in the attractive intraspecies interaction regime, which will set up the following section. In sec. 5.2.4 we focus on the transition to pair superfluidity and compute the drag in this promising regime.

Finally, in sec. 5.3 we discuss the importance of the drag in determining the Luttinger liquid parameter K_S.

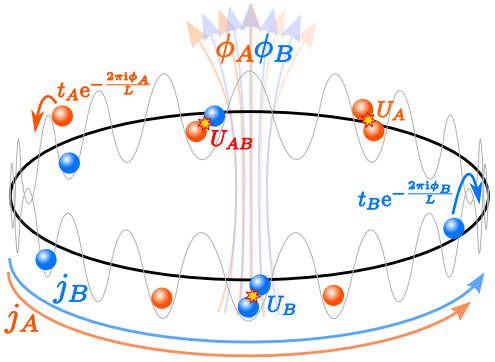

FIGURE 5.1: Sketch of the 2-component Bose-Hubbard ring with hopping parameters $\tilde{t}_\alpha = t_\alpha e^{-i2\pi\phi_\alpha/L}$, intra-species interactions U_α and inter-species interactions U_{AB}. The two fluxes ϕ_α pierce the ring and give rise to the superfluid currents j_α.

5.2 Model and setup

5.2.1 Model: Bose-Hubbard Hamiltonian on a ring

We consider the model for a gas of $N = N_A + N_B$ atoms of two different species in a ring lattice of L sites. The model is described by the Bose-Hubbard Hamiltonian, $\hat{H} = H_A + H_B + H_{AB}$:

$$H_\alpha = \sum_{j=1}^{L}\left[-\left(\tilde{t}_\alpha b^\dagger_{j+1,\alpha} b_{j,\alpha} + \text{h.c.}\right) + \frac{U_\alpha}{2} n_{j,\alpha}(n_{j,\alpha}-1)\right],$$
$$H_{AB} = U_{AB}\sum_{j=1}^{L} n_{j,A} n_{j,B}\,, \tag{5.1}$$

where $b^\dagger_{j,\alpha}$ and $(b_{j,\alpha})$ are the bosonic creation annihilation operator respectively and $n_{j,\alpha} = b^\dagger_{j,\alpha} b_{j,\alpha}$ is the number operator at site j for the species $\alpha = A, B$. The single species Hamiltonian H_α accounts for the hopping between neighboring sites, with $\tilde{t}_\alpha = t_\alpha e^{-i2\pi\phi_\alpha/L}$, and for the on-site repulsion characterised by the parameter $U_\alpha > 0$. The fluxes ϕ_α piercing the ring are introduced in order to compute the superfluid currents and densities (see Appendix, sec. C.2).

We limit ourselves to a zero temperature, $\mathbb{Z}_2$ symmetric mixture $t_\alpha = t$, $U_\alpha = U$ and filling $\nu_\alpha \equiv N_\alpha/L = \nu/2$, in terms of the number of atoms N_α. The phase diagram of the 1D model is very rich and has not yet been determined with the same accuracy as in higher dimensions Kuklov and Svistunov (2003); Kuklov et al. (2004): to our knowledge the most complete analysis can be found in Hu et al. (2009).

For the purpose of the present study we are interested in only two of the possible phases: the two-superfluid phase and the pair-superfluid phase. The two-superfluid phase is characterised by each components A and B being superfluid, as in the previous chapter 4. The low energy spectrum consists of two gapless linear modes corresponding to a density (in-phase) and a spin (out-of-phase) mode. In the PSF phase, the two components are paired, similarly to the case of Cooper pairing in the Bardeen-Cooper-Schrieffer theory for fermionic systems Kagan and Efremov (2002). As a consequence of this pairing the spin-channel acquires a gap which corresponds to the pairing energy of the two bosons. One of our goals here is to determine the superfluid densities in the two superfluid phase while approaching the pair superfluid phase, where the collisionless drag should saturate to its maximum value Sellin and Babaev (2018).

We resort to a Matrix Product States (MPS) ansatz to deal with the full many-body problem. The model (5.1) is not exactly solvable and our numerical treatment is an almost unbiased approach to it.

5.2.2 Setup: computing the superfluid densities

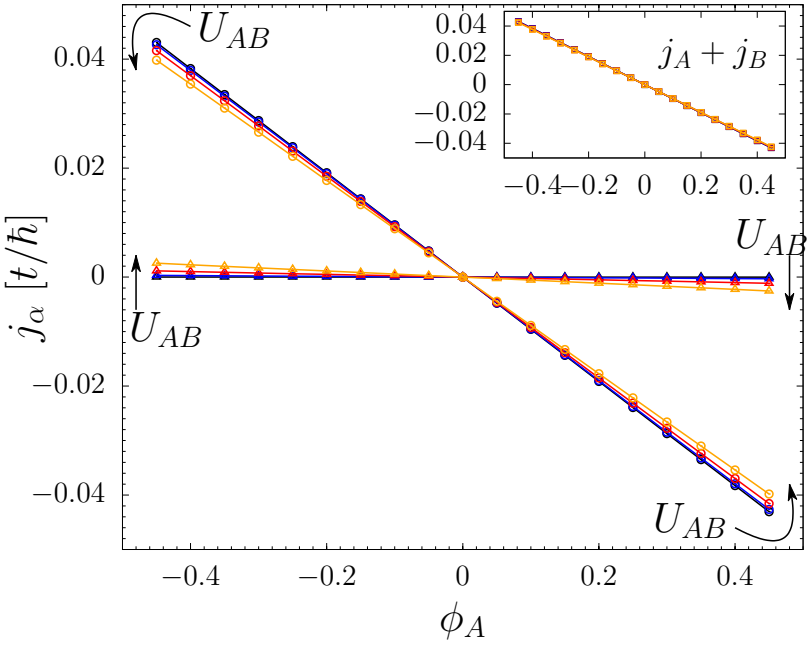

FIGURE 5.2: The superfluid currents j_A and j_B in presence of ϕ_A only for a $L = 32$ system. The four sets of curves (from dark to light color) correspond to $U_{AB}/U = 0.0, 0.25, 0.5, 0.75$, with $U/t = 2$ at half-filling. The drag density $n_{AB}^{(s)}$ is proportional to the slope of j_B in the limit of $\phi_A \to 0$. The inset demonstrates the global momentum conservation because of the constant value of the total current for all values of U_{AB}.

As shown in the appendix C, Sec. C.2, the superfluid densities can be computed as derivatives of the energy with respect to the magnetic fluxes piercing the ring. Using

Eq. (C.17) it follows for the superfluid number densities $n^{(s)}_{\alpha\beta} = \rho_{\alpha\beta}/m^*$ as:

$$n^{(s)}_{\alpha\beta} = \lim_{\phi_\alpha,\phi_\beta\to 0} \frac{Lm^*}{2\pi\hbar}\frac{\partial j_\alpha}{\partial\phi_\beta} = \lim_{\phi_\alpha,\phi_\beta\to 0} \frac{Lm^*}{(2\pi\hbar)^2}\frac{\partial^2 E}{\partial\phi_\alpha\partial\phi_\beta}\,. \tag{5.2}$$

In Fig. (5.2) we illustrate the effect of the AB drag on the currents: in presence of ϕ_A only, the current j_B is constantly zero in absence of inter-species interaction, $U_{AB} = 0$, while it increases monotonically as U_{AB} increases. The drag density $n^{(s)}_{AB}$ is proportional to the slope of the j_B curve in the limit of $\phi_A \to 0$. The plot highlights the smallness of the drag effect at a generic point in parameter space – here the filling is $\nu = 0.5$ with $U/t = 2$ and $L = 32$. For completeness in the inset of Fig. (5.2) we report the total (or density) current in order to show that the result $j_A + j_B = 2\pi\nu\phi_A/L$ is independent from the interaction.

5.2.3 Superfluid drag at half-filling

As disclosed in the introduction to this chapter approaching the superfluid phase we expect a strong enhancement of the drag. However, even in regimes quite distant from the paired superfluid phase we expect that the pairing correlations for attractive interspecies interactions ($U_{AB} < 0$) will be enhanced compared to the case of repulsive interactions ($U_{AB} > 0$), which should result in a more sizeable drag. Intuitively, if we interpret the Andreev-Bashkin effect as the result of a cloud of species B dressing the excitations of species A an attractive interspecies interaction will induce stronger fluctuations in the density of the species B, thus increasing the dressing effect. The density fluctuations that are responsible for this enhancement will diverge at a critical point, causing the so-called collapse transition, which results in the superfluid shrinking and then expelling atoms, and eventually destroying superfluidity Roberts et al. (2001).

In order to test this idea we report in Fig. (5.3) the drag density $n^{(s)}_{AB} = n^{(s)}_{BA}$ as a function of the inter-species interaction U_{AB}/U for half total filling $\nu = 0.5$ and $U/t = 2$. In this regime, as expected from previous analysis Hu et al. (2009), the mixture is always in the two superfluid phase, until it undergoes either phase separation (for $U_{AB} > 0$) or collapse (for $U_{AB} < 0$). In our case, the collapse occurs beyond the black dashed line in the shaded region.

For comparison the Bogoliubov prediction for the entrainment is also reported. Using the method developed in the Appendix C, Sec. C.2, the Bogoliubov approach leads to the simple expression for the drag:

$$n^{(s)}_{AB} \simeq \frac{t}{4L}\sum_k \frac{(\Omega_{d,k} - \Omega_{s,k})^2}{(\Omega_{d,k} + \Omega_{s,k})\Omega_{s,k}\Omega_{d,k}} \sin^2(k)^2, \tag{5.3}$$

with $\Omega_{d(s),k} = \sqrt{\epsilon(k)(\epsilon(k) + U\nu \pm U_{AB}\nu)}$ the excitation energies of the density (spin) channel and $\epsilon(k) = 4t\sin^2(k/2)$ the single particle dispersion relation. The sum in (5.3) is done on the wave vectors in the 1st Brillouin Zone $k = 2\pi/L \cdot n$ with $n = 0, ..., (L-1)$.

The Bogoliubov approach turns out to be valid only for very small interspecies interaction. [1]. More importantly while Eq. (5.3) predicts a symmetric behaviour for $U_{AB} \to -U_{AB}$, the data display an evident asymmetry between the two regimes. In particular, the attractive mixture experiences a much steeper growth of the drag with increasing $|U_{AB}|$ compared to the repulsive mixture. This substantial difference can be ascribed to pairing correlations which are not captured by the Bogoliubov approach.

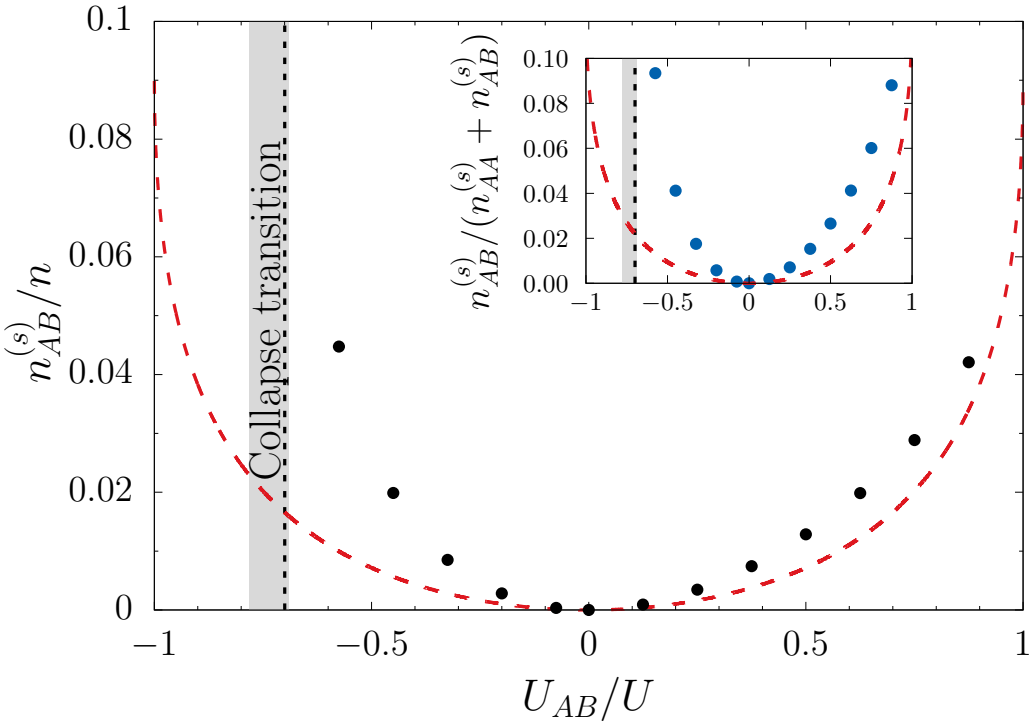

FIGURE 5.3: Superfluid drag in terms of the total density (main panel) and of the total superfluid density (inset), for for half total filling $\nu = 0.5$ and $U/t = 2$. The red dashed line is the analytic prediction via Bogoliubov approximation, Eq. (5.3). The pairing correlations in the attractive regime are responsible for the asymmetry between the attractive regime ($U_{AB} < 0$) and the repulsive regime ($U_{AB} > 0$).

5.2.4 Superfluid drag approaching the paired superfluid phase

We can now move to a regime where the system approaches the transition from the two superfluid to the paired superfluid phase, where the drag will reach its

[1] The same occurs in a continuous one dimensional Bose mixture with repulsive interactions Parisi et al. (2018), where the Monte-Carlo results are compared with the continuous version of Eq. (5.3), i.e., by replacing in Eq. 5.3: $t \to \hbar^2/2m$ and $\sin(k)/k \to 1$.

maximum. Indeed, in this case the current of one component will necessarily result in an equal amount of current of the other component, which implies the following condition at the transition:

$$n_{AB}^{(s)} = n_{AA}^{(s)} . \tag{5.4}$$

The drag $n_{AB}^{(s)}$ at the transition becomes a quarter of the total superfluid density $n^{(s)} = n_{AA}^{(s)} + n_{BB}^{(s)} + 2n_{AB}^{(s)}$, hence saturating to its maximum possible value. At this point, however, it cannot be interpreted as a drag coefficient anymore, since we are dealing with a single superfluid of pairs and not with two superfluids dragging each other. Before the saturation, the magnitude of the drag rapidly increases making the approaching to the pair superfluid phase transition a very suitable region for its measurement. This has already been proven to be the case for Quantum Monte-Carlo simulations in the 2D case Sellin and Babaev (2018).

The results for different system's sizes are reported in Fig. (5.4), where $U/t = 10$ and unit filling $\nu = 1$ are chosen such that the system can undergo the transition (see Hu et al. (2009)). In the inset we report the behaviour of the normalized drag as a function of L^{-1} for different values of the interaction, in order to study the thermodynamic limit. We estimate that the two superfluid to paired superfluid transition should occur in the thermodynamic limit for $U_{AB}/U \in [-0.25, -0.2]$ (shaded region in the main panel). In such a limit – since the transition belongs to the Berezinskii-Kosterlitz-Thouless universality class Hu et al. (2009) – the saturation should happen as a sudden jump of the spin-superfluid density, $n_{AA}^{(s)} - n_{AB}^{(s)}$, from a finite value to zero. We stress, however, that mesoscopic samples like the ones accessible in cold-atomic setups will display no jump, but rather a sizeable value of $n_{AB}^{(s)}$, thus making the AB collisionless drag finally observable.

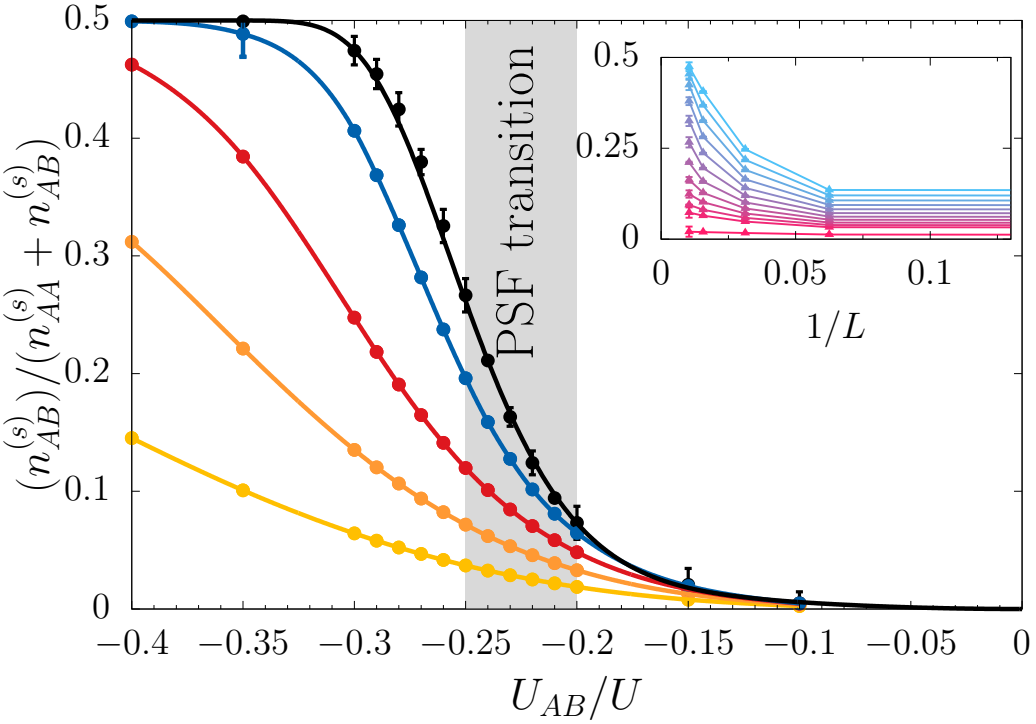

FIGURE 5.4: Drag (normalized with respect to the total superfluid density) for different system's sizes, as a function of U_{AB} for a system with $U = 10t$ and $\nu = 1$. From bottom to top (from light to dark shades) $L = 8, 16, 32, 64, 96$. Points are data, lines are artistic guide-to-the-eyes. The thermodynamic limit should exhibit a saturation to $(n_{AB}^{(s)})/(n_{AA}^{(s)}+n_{AB}^{(s)}) = 0.5$ in the paired superfluid region. In the inset, the same points of the main plot are represented as a function of the inverse of the system's size L^{-1} for different values of $-0.30 \leq U_{AB}/U \leq -0.15$ from top to bottom.

5.3 Collisionless Drag and Luttinger liquid parameters

In the superfluid phase, the elementary excitations of the Bose-Hubbard Hamiltonian for a single component can be described by the so-called Luttinger liquid theory Giamarchi (2004). This description consists in recasting the Bose-Hubbard Hamiltonian in terms of the canonically conjugated operators $\hat{\phi}$ and $\hat{\theta}$ representing respectively the phase and the density of the superfluid. These operators are related to the creation operators $\hat{b}_j^\dagger$ by the following equation:

$$\hat{b}_j^\dagger = \sqrt{\hat{\theta}} e^{i\hat{\phi}}\,. \tag{5.5}$$

The Hamiltonian at low energies can be shown to take the form:

$$\hat{H} = \frac{1}{2\pi}\int \left[cK(\partial_x\hat{\phi})^2 + \frac{c}{K}(\partial_x\hat{\theta})^2\right] \mathrm{d}x, \tag{5.6}$$

where c and K are the so-called Luttinger parameter which will depend on the interactions. The Luttinger parameter c has the meaning of the speed of sound as it is

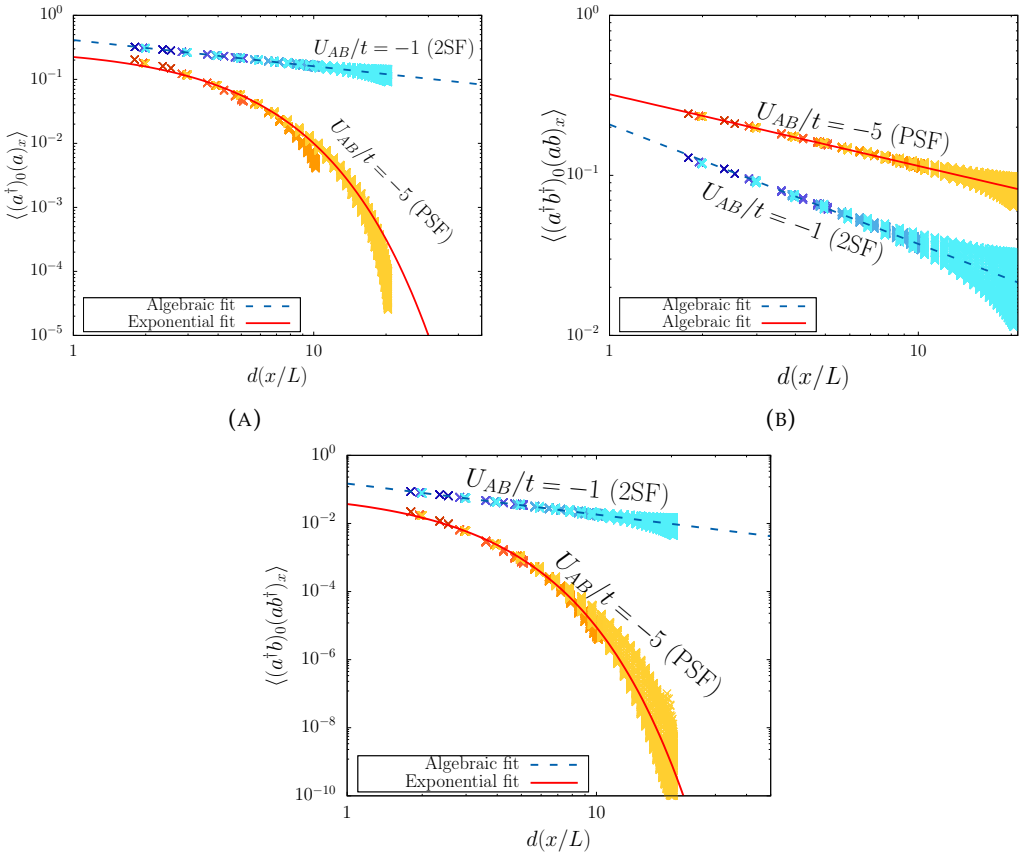

FIGURE 5.5: The correlation functions of Eq. (5.11) (the (a) panel is G_α, (b) is R_D and (c) is R_S) as function of the distance for a unitary total filling system $\nu = 1$, $t = 1$ and $U = 10$. The orange points are taken for the system in the paired superfluidity phase while the blue ones concern the two superfluid phase and we represent with a color gradient from dark to light different system's sizes from $L = 8$ to $L = 64$. The dashed lines are exponential and algebraic fits depending on the expected behaviour of the functions for $U_{AB}/U = -0.1$ and the solid one for $U_{AB}/U = -0.5$.

the proportionality coefficient in the linear dispersion relation of the elementary excitations. The Luttinger parameter K is uniquely determined by the speed of sound and the compressibility.

In the case of a two component mixture, the result is similar. By applying the Luttinger description to each of the two species one obtains, in the two superfluid phase, the Hamiltonian of two coupled Luttinger liquids Giamarchi (2004). We call θ_A (θ_B) and ϕ_A (ϕ_B) the density and phase of species A (B).

The coupled Luttinger Hamiltonian can be diagonalised by introducing the density (D) and spin/polarisation (S) channels:

$$H_\mu = \frac{1}{2\pi} \int \left[c_\mu K_\mu (\partial_x \phi_\mu)^2 + \frac{c_\mu}{K_\mu} (\partial_x \theta_\mu)^2 \right] \mathrm{d}x, \tag{5.7}$$

where $\phi_{D(S)} = (\phi_A \pm \phi_B)/\sqrt{2}$ and $\theta_{D(S)} = (\theta_A \pm \theta_B)/\sqrt{2}$ are the bosonic fields related to the fluctuations of the phase and the amplitude of the total density (spin) of the two coupled superfluids. We dropped the "hat" symbol on the operators for simplicity. The speeds of sound $c_{D(S)}$, and $K_{D(S)}$ are the Luttinger parameters. There's an additional non-linear coupling between the densities of the two Luttinger liquids which can be perturbatively accounted for by a term proportional to $U_{AB}\cos(2\sqrt{2}\theta_S)$. This term is irrelevant in the two superfluid phase and relevant in the paired superfluid phase. Similarly to the one component case, the Luttinger parameters K_S and K_D are uniquely determined by the speed of the spin and density sound and the respective susceptibilities, namely, for the paramater K_S Giamarchi (2004):

$$K_S = \pi\hbar\chi c_s/2, \tag{5.8}$$

where $\chi = \left[\partial^2 e/\partial(\nu_A - \nu_B)^2\right]^{-1}$ is the spin susceptibility with $e = E/L$ the energy density. The same goes for the density channel with the compressibility $\chi_D = \left[\partial^2 e/\partial(\nu_A + \nu_B)^2\right]^{-1}$ rather than the susceptibility.

On the other hand as we showed in chapter 4 the relation between the spin speed of sound and the superfluid density depends on the drag, as a result of the modification in the energy weighted sum rule for the spin channel. The sum rule formalism implies the following relation between the spin-speed of sound and the superfluid densities

$$c_S^2 = 2\frac{n_{AA}^{(s)} - n_{AB}^{(s)}}{m^*\chi}. \tag{5.9}$$

By direct comparison of Eqs. (5.8) and (5.9), the following also holds:

$$K_S = \sqrt{\frac{\pi^2\hbar^2\left(n_{AA}^{(s)} - n_{AB}^{(s)}\right)\chi}{2m^*}}. \tag{5.10}$$

The drag thus appears in the constitutive relations of the Luttinger parameters. This important fact, is often overlooked in literature Hu et al. (2009); Mathey et al. (2009); Orignac et al. (2017); Citro et al. (2018); Kleine et al. (2008a,b); Citro et al. (2018) where only the diagonal superfluid density $n_{AA}^{(s)}$ appears. Its inclusion is crucial in obtaining consistent results in the perturbative approach of Luttinger liquids. In particular, the msot dramatic effect is at the pair superfluidity transition where comparison with Eq. (5.4) implies that K_S must vanish.

In order to test the consistency of Eq. (5.10) we compare the prediction on K_S obtained by computing the speed of sound c_S and the susceptibility χ and the prediction that we can obtain independently from the correlation functions of the model. Indeed, as long as the Hamiltonian Eq. (5.7) holds, an algebraic decay governed by the Luttinger parameters characterises the correlation functions (also known as quasi-long-range

order) Giamarchi (2004):

$$\begin{aligned} G_\alpha(x) &= \langle b^\dagger_{i+x,\alpha} b_{i,\alpha} \rangle \propto |d|^{-\frac{1}{4K_D}-\frac{1}{4K_S}}, \\ R_D(x) &= \langle b^\dagger_{i+x,A} b^\dagger_{i+x,B} b_{i,B} b_{i,A} \rangle \propto |d|^{-\frac{1}{K_D}}, \\ R_S(x) &= \langle b^\dagger_{i+x,A} b_{i+x,B} b^\dagger_{i,B} b_{i,A} \rangle \propto |d|^{-\frac{1}{K_S}}. \end{aligned} \tag{5.11}$$

Here we expressed the algebraic decay in terms of the natural measure of the distances between sites on a ring geometry, i.e., the *chord* function Cazalilla et al. (2011):

$$d(x/L) = \frac{L}{\pi} \sin\left(\frac{\pi x}{L}\right), \tag{5.12}$$

where L is the number of sites and $x \in \mathbb{N}$ the linear distance between the sites. For very large rings the expression further simplifies according to the substitution $d \to x$. The relations in (5.11) can be easily checked by using the leading term in the long-wavelength field representation $b_{j,\alpha} \propto \exp(i\phi_\alpha)$ Haldane (1981).

The single-body correlations, G_α, have a mixed density/spin character, consistently with the fact that the imaginary part of their nearest-neighbor value gives back the species current j_α. The correlation functions R_D and R_S correspond instead to two-body correlations: R_D concerns the superfluid character of pairs of $A-B$ particles and therefore the density channel, while R_S relates to anticorrelated pairs and therefore the spin channel Hu et al. (2009); Sellin and Babaev (2018).

Away from commensurate filling ν, which could possibly lead to a Mott insulator phase, the density channel is always superfluid, i.e., R_D scales algebraically. A change in R_S and G_α from algebraic to exponential decay – or equivalently a drop of K_S to 0 – happens instead when entering the paired superfluid phase, due to the opening of a gap in the spin channel. The intuitive idea is that in the pair superfluid phase the density channel stays superfluid as its excitations correspond to excitations of the system as a whole. On the contrary, the spin channel loses it superfluid character as out-of-phase spin excitations are suppressed by the pairing. This is illustrated in Fig. (5.5), where the correlations measured for different system sizes ($L = 8, 16, 32, 64, 96$) are reported for two sample parameter values deep in the two superfluid (blue) and paired superfluid (orange) phases. The region where the correlation functions R_S and G_α show exponential decay is in agreement with the region predicted from the drag saturation (Fig. (5.4)).

Thanks to the Luttinger parameter K_S appearing as an exponent in the algebraic decay of the correlation functions we can compare the prediction given by the Luttinger liquid theory and the drag effect (Eq. (5.10)) and the long-range behaviour of the correlation functions (Eq. (5.11)). We do so in Fig. (5.6), where we show that the two estimates give consistent results.

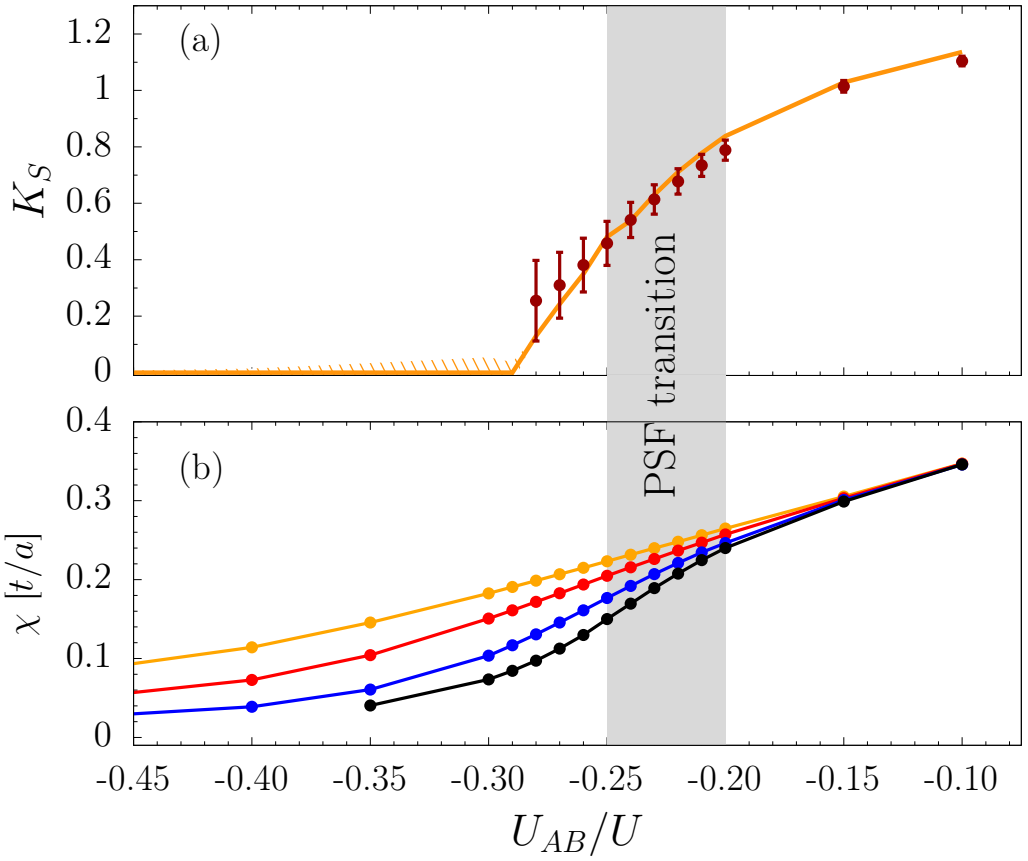

FIGURE 5.6: In (a) Luttinger parameter K_S for the spin channel, as obtained from the hydrodynamic relation in Eq. (5.10) (solid line with error shadow) and from the correlation functions, Eq. (5.11) (points with error bars). Points are reported until the algebraic fit makes sense: the shaded region indicates where deviations become sizeable. In the paired superfluid the parameter K_S must go to zero. (b) displays the behaviour of the susceptibility as function of the interaction, as estimated from various system sizes (color code as in Fig. (5.4) except for $L = 8$ that is omitted).

For the sake of comparison with mesoscopic experiments accessible with ultra-cold gases in optical lattices, we report in Fig. (5.6) (b) also the estimated spin susceptibility for different system's sizes.

5.4 Conclusions

In conclusion, we provide a numerical estimation of the AB superfluid drag via a Tensor Network approach for a 1D Bose mixture on a ring lattice. The regime for attractive interspecies interaction seems to be the most promising to increase the value of the drag, thanks to the pairing correlations. In particular, the most dramatical enhancement of the effect occurs when approaching the transition to the pair superfluid phase, where the drag becomes comparable in magnitude with the total

superfluid density. Dealing with a mesoscopic system avoids the inconvenience of a sudden jump of the drag at the transition and would allow for a range of parameters where the effect is observables.

State of the art experiments in ultracold atoms are able to measure the spin speed of sound Shin et al. (2006) and the spin susceptibility Fava et al. (2018) with great accuracy for weakly interacting Bose gases. A measurement of these quantities in a one dimensional mixture of cold atoms in an optical lattice would allow to finally observe the effect. Hyperfine states mixtures of $^{(39)41}$K atoms, or ^{41}K-^{87}Rb mixtures (see for example Semeghini et al. (2018); Tanzi et al. (2018); Cabrera et al. (2018); D'Errico et al. (2019)), whose inter-species interaction can be tuned by exploiting Feshbach resonances, could be promising platform to carry the experiment. The typical number of atoms in these setups is comparable to the ones used in our simulation, thus overcoming the issue of the jump of the drag at the transition.

A second important result of this chapter regards the fundamental implications that the presence of the drag has on the Luttinger liquid approach to the two species Bose-Hubbard Hamiltonian. In particular we show that the inclusion of the Andreev-Bashkin effect in the Luttinger liquid description provides a reliable expression for the Luttinger parameters of the spin-channel.

6

Conclusions

In this thesis I have presented our results on ultracold atoms theory. We explored the behaviour of ultracold systems in various regimes: from a noninteracting gas to a strongly correlated mixture, in the homogeneous case and in the case of an optical lattice. Results were obtained both via analytical methods and numerical simulations.

In chapter 2 the localisation-delocalisation transition of periodically driven non interacting Aubry-André model is studied. It is showed that within this model one can reproduce a phase diagram that has the same features as the corresponding interacting model. We find that the critical frequency and amplitude of the periodic driving for delocalisation can be predicted from an intuitive physical picture, which interprets them as the values for which the driving sweeps adiabatically through the critical disorder strength of the undriven model. Moreover, we show that the transition is analogue to the Anderson localisation of the undriven model, in the sense that the phase diagram is determined by the Inverse Participation Ratio of the Floquet eigenstates. Our results raise the question on whether the inclusion of interactions can conduce to phase diagrams of isolated systems that are qualitatively different from the single particle ones, and what physical observables can reveal such differences.

In chapter 3 I have presented our work on a light impurity interacting with N heavy, non interacting fermions. We approach the question of the existence of arbitrarily large clusters through a simplified model based on the zero-range approximation and the Born-Oppenheimer. We assume that the impurity in the hypothetical $N+1$ cluster behaves as a Fermi polaron. Our results seem to indicate that there is no stable cluster for large N, as it will fission into smaller and smaller subclusters. Although our model is simplified it seems to reasonably account for the physics of the problem. Moreover, it begs the question of whether modeling the impurity as polaron in the cluster can lead to sufficiently acccurate predictions. Future works could focus on improving the model, for example discarding the zero-range approximation and using a model potential.

In chapters 4 and 5 we obtained a number of results for the Andreev-Bashkin effect in superfluid mixture. In particular, in chapter 4 we develop a microscopic theory of the drag based on linear response theory which predicts the drag to be proportional to the transverse current-current response function. From this definition we are able to further identify the drag as the multiparticle excitations contribution to the spin sum rule. We find that this implies a reduced frequency of the spin phonon and spin dipole excitations. However we show that in a weakly interacting Bose mixture the contribution of the drag to these frequencies is typically much smaller than the correction coming from the beyond mean field susceptibility. We propose then an experimental procedure where a quickly initiated dipole moment produces at short times a ballistic motion of the mixture that is entirely governed by the drag, independently from the susceptibility. Moreover, it is applicable to strongly interacting systems where the limitations of weakly interacting gases could be overcome.

In chapter 5 we focus on such strongly correlated system, by considering a one dimensional Bose-Hubbard model for a mixture of superfluids. By means of Tensor Network analysis we compute the magnitude of the drag in avariety of regimes of the intra- and interparticle interactions. When the latter is attractive we find a strong enhancement of the drag coefficient, particularly when approaching the transition from the two superfluids to the paired superfluidity phase. Lastly, we compute the Luttinger parameters for the Luttinger liquid theory of the model, showing that the drag modifies the constitutive relations between the spin Luttinger parameter K_S and the spin susceptibility, as a result of its effect on the spin speed of sound. We compute the correlation functions of the model both to study their behaviour at the transition to paired superfluidity and to compute the Luttinger spin parameter indipendently, testing the consistency of our equations.

Appendix A

Scattering length and zero range approximation

We give here a quick overview of the scattering theory that is mostly relevant for ultracold atomic systems. The analysis will be narrowed down to explain the meaning of the scattering length in a typical cold atoms setting and the approximations that lead to it. The presentation given here is mostly based on the books Leggett et al. (2006) and Pethick and Smith (2008).

A.1 The dilute limit and the low energy limit for short range interactions

Cold atoms interact with a potential $V(\mathbf{r})$ that is in general a complicated function of the separation $\mathbf{r}$ between the two atoms. However, in order to describe the scattering processes that take place in a cold quantum gas, the long-distance ($\mathbf{r} \to \infty$) behaviour of such potential is sufficient Leggett (1998). The potential at long distances is well described by the van der Waals interaction, which is a central potential of the form $-C_6/r^6$. The parameter C_6 defines a natural length scale that sets the range of the interaction:

$$r_0 = \left(2\mu C_6/\hbar^2\right)^{1/4}, \tag{A.1}$$

where μ is the reduced mass of the two interacting atoms. The length scale r_0 is called the range of the potential. Beyond the length scale r_0 the relative motion of two atoms interacting is essentially free. We mention that the interatomic potential need not to be of the van der Waals type in order for it to have a well defined range r_0. The actual requirement is that it is short ranged, i.e. that it decays faster than $1/r^3$.

It turns out that in most cold atoms experiments the range of the potential is much smaller than the typical interparticle distance. In fact, while the typical range of the potential is of the order $50 - 100$Å the interparticle distance is usually bigger than 1000Å. This defines the regime in which we are interested, called the **dilute limit**, where the density n of the atoms satisfies:

$$nr_0^3 \ll 1\,, \tag{A.2}$$

In words, the average interparticle distance is much bigger than the range of the potential.

Another condition that defines the dilute limit is a consequence of cold atoms experiments being performed in the *degenerate regime*. In this regime the thermal de Broglie wavelength $\lambda_T = \sqrt{2\pi\hbar^2/mk_BT}$ is also much bigger than the tipical interparticle distance. Since k_BT represents the typical energy of the states that have an appreciable probability of being occupied, this implies that all such states will have a wavevector satisfying:

$$kr_0 \ll 1 \tag{A.3}$$

Eq. (A.3) goes in the literature under the name of **low energy limit**.

We shall assume in what follows, as is customary, that both these limits are realised.

A.2 Low energy scattering and effective range expansion

In the region of space outside the range of the spherical potential, i.e. when the relative distance between two atoms r is much bigger than the range of the potential r_0, the wavefunction describing the relative motion of the two particles is essentially that of a free particles. The wavefunction at long distances from the range of the potential can be separated into an incoming plane wave and an outgoing spherical wave:

$$\psi(\mathbf{r}) = e^{i\mathbf{k}\cdot\mathbf{r}} + f(\theta)\frac{e^{ikr}}{r} \tag{A.4}$$

where k is the relative momentum of the scattering particles and r is their relative distance, while θ is the polar angle at which the incoming particle is deflected.

The function $f(\theta)$ can be expanded in partial waves, where each partial wave corresponds to an outgoing wave of momentum l:

$$f(\theta) = \sum_{l=0}^{\infty} (2l+1)\, P_l(\cos(\theta)) f_l \tag{A.5}$$

The partial wave expansion is extremely valuable to describe scattering at low energies (i.e. $kr_0 \ll 1$), where only the s-wave ($l = 0$) scattering amplitude needs to be considered as higher partial waves are suppressed by powers of k^2. The coefficients f_l can be expressed in terms of phase shifts δ_l which represent by how much each partial wave is phase shifted by the interaction:

$$f_l = (k \cot(\delta_l) - ik)^{-1} . \tag{A.6}$$

In absence of interactions, the phase shifts are all $\delta_l = 0$ and so is the scattering amplitude. In the opposite case, the strongest dephasing happens for $\delta_l = \pi/2$ when the modulus of the scattering amplitude takes its maximum value and the interaction is said to be resonant in that partial wave. This limit is called the unitary limit, as its the maximum for the modulus of the scattering amplitude that is allowed by the unitarity of time evolution.

The s-wave scattering amplitude satisfies in the dilute, low energy regime, the so-called effective range expansion which allows to describe scattering at low energies by means of few parameters:

$$f_{l=0}(k)^{-1} + ik = -\frac{1}{a} + (r_{\text{eff}}/2)^2 k + ... \tag{A.7}$$

where a and r_{eff} are called *scattering length* and *effective range* respectively. For most interactions the parameters are of the same order of magnitude of the range of the interactions r_0, and **the first term in the effective range expansion is sufficient at low energies**.

The unitary limit (or resonant interactions) is reached when $a \to \infty$, while for $a = 0$ the system is noninteracting and the interaction potential will produce no phase shift.

The effective range expansion is a crucial result for low energy scattering: combined with Eqs. (A.4) and (A.5) it implies that the asymptotic wavefunction describing the relative motion of two scattering particles is determined by few parameters **regardless of the details of the interaction potential**. In the limit where only the first term in Eq. (A.7) is retained, the wavefunction in Eq. (A.4) in the range $r_0 \ll r \ll k^{-1}$ takes the very simple form:

$$\psi(r) \propto \left(\frac{1}{a} - \frac{1}{r}\right) . \tag{A.8}$$

Thus the scattering length is the position outside the range of the potential at which the wavefunction has a node, and as such it quantifies the "strength" of the scattering process. When $a > 0$ the potential can be said to have pushed away the wavefunction with respect to the non interacting case, while when $a < 0$ the wavefunction has been pulled in. This is why it is often customary to call a potential with positive scattering length repulsive and a potential with negative scattering length attractive. However, one must keep in mind that this refers only to an effective description valid at low

energies and not to the underlying potential. Indeed while a purely repulsive potential can only have a positive scattering length, an attractive potential can have both a positive and a negative scattering length.

The scattering length can be tuned in ultracold atoms experiments by means of a magnetic field, exploiting an effect that goes under the name of Feshbach resonance Feshbach (1962) (see e.g. Chin et al. (2010) for a review on the topic). The system can then be controlled and interactions can be set to be in the weakly interacting limit, i.e. when $na^3 \ll 1$, or in the strongly interacting one, i.e. $na^3 \gg 1$.

A.2.1 The zero range approximation

The effective range expansion shows that the scattering of particles at low energies behaves the same regardless of the underlying potential, and is instead determined only by the scattering length. Therefore we may choose scattering potentials that make our analysis as simple as possible. An exemplary choice could be a square well potential with range r_0 with the boundary condition that the wave function and its derivative are continuous at $r = r_0$.

However, we might also take this approach to the extreme and consider a zero range potential. This is called the *zero range approximation* and it consists in taking the solution we obtain outside the range of the potential and extrapolating it inside it, but forcing it to satisfy Eq. (A.8) as boundary condition at vanishing separation r. This procedure thus effectively replaces the potential with a boundary condition which depends on its scattering length Petrov (2013).

All in all, the Schrodinger equation for the relative motion of two particles interacting with a potential $V(r)$ is mapped into the Schrodinger equation of two free particles, with their wavefunction satsifying the boundary condition:

$$\frac{(r\psi(r))'}{r\psi(r)}\Big|_{r=0} = -\frac{1}{a} \tag{A.9}$$

This boundary condition is called **Bethe-Peierls boundary condition**. It is used in chapter 3 to solve the Schrodinger equation of the impurity interacting with the heavy fermions.

Appendix B

Experimental realization of the periodically modulated quasicrystal

In this appendix we will briefly illustrate how the many-body experiment for the periodically driven Aubry-André model was realized in Bordia et al. (2017).

The first section will explain how the optical lattice is generated. The second section will illustrate the steps that were taken in order to realize the experiment.

The first section is a summary of what contained in Pitaevskii and Stringari (2016), while the experimental procedure is taken from Bordia et al. (2017). They are presented here for the convenience of the reader.

B.1 Realization of the optical lattice

In order to generate the lattice structure for the experiment, the interaction of atoms with the electric field of a laser is exploited. This interaction can be treated in the dipole approximation, as long as the wavelength of the laser is chosen to be much larger than the typical atomic size. In this approximation the interaction energy $V(\mathbf{r}, t)$can be written:

$$V(\mathbf{r}, t) = -\mathbf{d} \cdot \mathbf{E}(\mathbf{r}, t)\,, \tag{B.1}$$

where $\mathbf{d}$ is the electric dipole operator for a single atom and $\mathbf{E}(\mathbf{r}, t)$ is the plane wave electric potential produced by the laser, namely:

$$\mathbf{E}(\mathbf{r}, t) = \mathbf{E}(\mathbf{r})e^{-i\omega t} + c.c \tag{B.2}$$

This interaction induces an oscillating dipole polarization in the atoms, proportional to the electric field:

$$\langle \mathbf{d} \rangle = \alpha(\omega)\big(\mathbf{E}(\mathbf{r})e^{-i\omega t} + c.c\big) \tag{B.3}$$

The coefficient $\alpha(\omega)$ is called dynamic polarizability, as it quantifies the susceptibility of the dipole moment to a time dependent electric field that is polarising it.

The polarization causes a change in energy of the system (called Stark Shift) which can be calculated from second-order perturbation theory. This change in energy can be regarded as an effective potential which is felt by each atom and reads:

$$U(\mathbf{r}) = -\frac{1}{2}\alpha(\omega)\langle \mathbf{E}^2(\mathbf{r},t)\rangle_t \tag{B.4}$$

where by $\langle\cdot\rangle_t$ we indicate a time average.

The potential of Eq. (B.4) is valid under three assumptions: that perturbation theory is applicable, that the time variations of the laser field are much faster than the typical frequencies of atomic motion (justifying the time averaging) and that $\alpha(\omega)$ is real. The latter is valid if ω is not too close to resonances between atomic energy levels.

The trapping of atoms in an optical lattice can obtained thanks to this effect by superimposing two counter propagating laser beams in a certain direction (say x), producing a standing wave of the form:

$$E(r,t) = E\cos(kx)e^{-i\omega t} + c.c. \tag{B.5}$$

and the effective potential becomes:

$$U(\mathbf{r}) = -\alpha(\omega)E^2\cos^2(kx) \tag{B.6}$$

Which corresponds to a periodic potential with spatial periodicity $\lambda = 4\pi/k$.

The sign of the polarizability is determined by the sign of the detuning $\delta = \omega - \omega_R$, where ω_R is the frequency of the atomic resonance closest to ω. This allows to decide the sign of the potential, which will discriminate wether the atoms will be forced to move towards region of high or low field.

In particular the potential will be attractive when ω is smaller than the frequency of the closer resonance, and repulsive in the opposite case.

Optical traps are an useful alternative to magnetic traps. For example they are not limited to specific magnetic states and so allow for the investigation of coexisting multi-spin components. Moreover they allow to independently add a magnetic field whose purpose is to tune the scattering length to a given value, by means of a Feschbach resonance (see Pitaevskii and Stringari (2016)).

B.2 Experimental Sequence

The experiment in Bordia et al. (2017) is realized with a Fermi gas of ^{40}K(Potassium 40).

The ^{40}K is sympathetically cooled (see Pitaevskii and Stringari (2016)) with the bosonic ^{87}Rb (Rubidium 87). Then the trapping potential is lowered to allow the gravitational force to remove the bosonic gas, leaving only the Potassium 40. The Fermi gas of ^{40}K consists of an equal mixture of its two spin states, the lowest total angular momentum states $|F, m_F\rangle = |9/2, -9/2\rangle$ and $|F, m_F\rangle = |9/2, -7/2\rangle$. After the sympathetic cooling the gas is cooled further by evaporation to the temperature $T = 0.15T_F$, where T_F is the Fermi temperature.

The gas is then loaded into a three dimensional optical lattice whose lattice potential is extremely deep. More precisely, the depth of the confining potentials is set at $40E_r^{(i)}$ for all the directions, where $E_r^{(i)} = h^2/(2m\lambda_i^2)$ is the recoil energy of the lattice with wavelength λ_i. This allows to have a negligible tunneling while setting up the experiment. The wavelength in the x direction is set at $\lambda_x^{(l)} = 1064$nm and $\lambda_{y,z} = 738.2$nm in the other two directions. In order to avoid double occupancies of single sites the interaction is made strong ($U \approx 140a_0$) and repulsive by means of a Feschbach resonance.

Over the long lattice with wavelength $\lambda_x^{(l)}$ a shorter superlattice of wavelength $\lambda_x^{(s)} = 532nm = \lambda_x^{(l)}/2$ is superimposed. The result is the density wave pattern along the x direction, described in chapter 2. The short lattice sets the lattice spacing, while the long lattice imprints the density wave pattern. The interaction strength U is now set at the desired value with a Feschbach resonance.

At this point the "long" lattice with wavelength $\lambda_x^{(l)}$ is suppressed and the disordered potential is generated by superimposing along the x direction a laser of wavelength $\lambda_d = 738nm$. Then the "short" lattice along the x direction is lowered to an intensity $8E_r^{(s)}$ so that tunneling is restored and the dynamics is initiated, while the disorder lattice is modulated by modulating its amplitude. The lattice depth along the y and z directions is kept at $40E_r^{y,z}$ in order to make the system effectively one-dimensional.

As a last step the system is frozen by ramping up the depth of the long and the short lattice to $20E_r^{(s)}$ and $20E_r^{(l)}$ respectively, so that the tunelling is suppressed. Simultaneously the disordered potential (and its modulation) are switched off.

The number of atoms in the even and odd sites (and so the imbalance) are calculated by a bandmapping procedure in time-of-flight imaging (Schreiber et al. (2015)).

A brief diagram of the full experiment is showed in B.1.

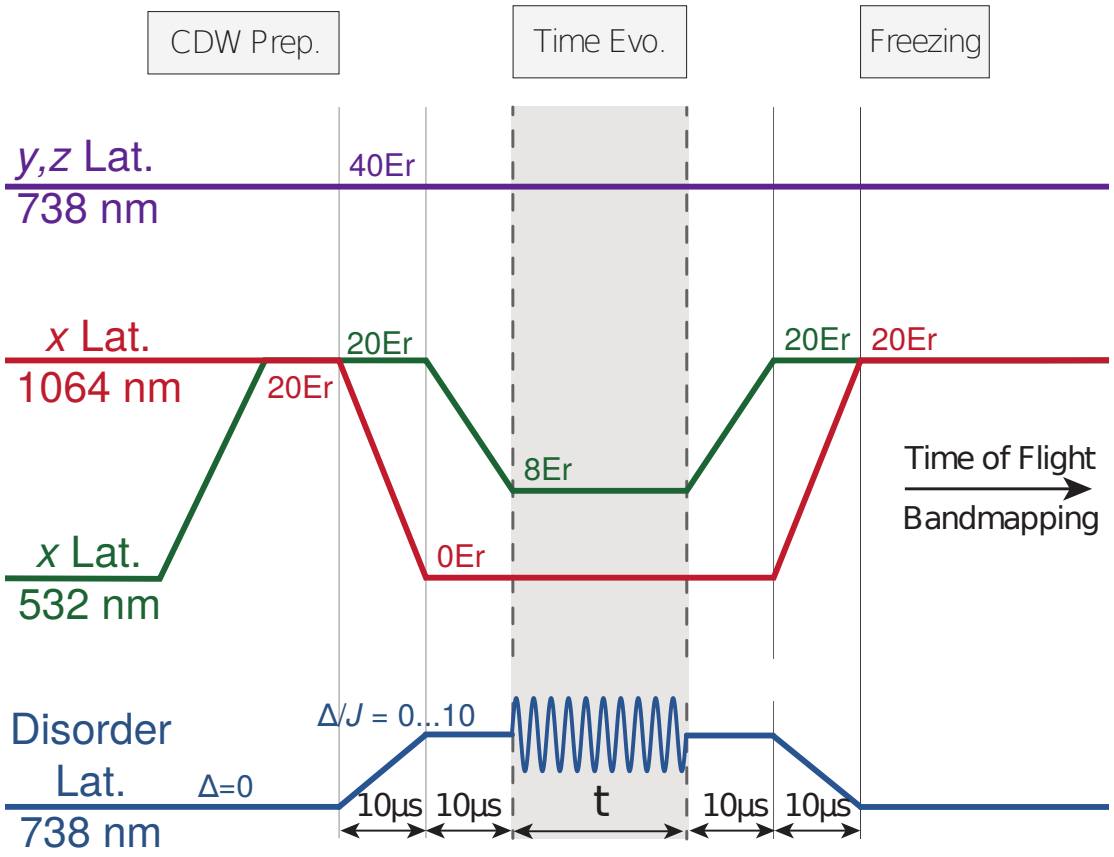

FIGURE B.1: Experimental sequence for the measurement of the imbalance in the driven Aubry-Andrè model, taken from Bordia et al. (2017). The horizontal axis is not to scale.

Appendix C

2-component Bose-Hubbard model

In this appendix we derive the drag in a 2-component Bose-Hubbard model following two routes. One is the linear response formalism of chapter 4, the other allows to compute the superfluid densities as derivatives of the energy.

C.1 Linear response on a lattice

In particular we derive the equations for the superfluid and normal stiffnesses in a system lacking Galilean invariance, where one loses the normalization condition of Eq. (4.4). The drag in the weakly interacting case is not enhanced in the Bose-Hubbard model compared to the continuum case Linder and Sudbø (2009). The introduction of the lattice can be interesting to reach regimes where the correlations are strong but the condensate is still stable with respect to three-body losses Fukuhara et al. (2013).

We consider a weakly interacting Bose-Bose mixture of N bosons in a cubic lattice of volume L^3 with periodic boundary conditions, in the thermodynamic limit. We call l the lattice spacing and I the total the number of sites. The tunneling coefficient t is the same for both species. We recall the form of the Bose-Hubbard Hamiltonian describing the system:

$$\hat{H} = \hat{H}_A + \hat{H}_B + \hat{H}_{AB}\,, \tag{C.1}$$

with

$$\begin{aligned} H_\alpha &= \sum_{j=1}^{L} \left[-\left(\tilde{t}_\alpha b^\dagger_{j+1,\alpha} b_{j,\alpha} + \text{h.c.} \right) + \frac{U_\alpha}{2} n_{j,\alpha}(n_{j,\alpha} - 1) \right], \\ H_{AB} &= U_{AB} \sum_{j=1}^{L} n_{j,A} n_{j,B}\,, \end{aligned} \tag{C.2}$$

where $b^\dagger_{j,\alpha}$ and $b_{j,\alpha}$ are the bosonic creation annihilation operator respectively and $n_{j,\alpha} = b^\dagger_{j,\alpha} b_{j,\alpha}$ is the number operator at site j for the species $\alpha = A, B$.

From the tunneling coefficient t we can define the usual effective mass as $m^* \equiv \hbar^2/(2tl^2)$. The current density operator at a given site $\mathbf{r}$ on the cubic lattice is defined as:

$$\hat{\mathbf{j}}_\alpha(\mathbf{r}) = -i\frac{t\,l}{\hbar L^3}\sum_{\mathbf{u}}(\hat{b}^\dagger_{\mathbf{r},\alpha}\hat{b}_{\mathbf{r}+\mathbf{u},\alpha} - h.c.)\mathbf{u}\,, \tag{C.3}$$

where $\mathbf{u}$ is a lattice vector of unit length. The linear response treatment of the three-fluid hydrodynamics in the case of a lattice is very similar to that of subsec. 4.3.1. The difference is in the transformation law of the current operator and of the Hamiltonian in presence of a vector potential $\mathbf{A}(\mathbf{r})$. The transformation for the current, corresponding to Eq. (4.11) in the continuous model:

$$\hat{\mathbf{j}}_\alpha(\mathbf{r}) \to \hat{\mathbf{j}}_\alpha(\mathbf{r}) - \sum_{\mathbf{u}}\frac{e_\alpha}{m_\alpha}\frac{\hat{K}_{u,\alpha}(\mathbf{r})}{2t}A_u(\mathbf{r})\,\mathbf{u}\,, \tag{C.4}$$

where $\hat{K}_{u,\alpha}(\mathbf{r})$ is the kinetic energy density operator for a species α along $\mathbf{u}$ directed links, namely

$$\hat{K}_{u,\alpha}(\mathbf{r}) = -\frac{t}{L^3}(\hat{b}^\dagger_{\mathbf{r},\alpha}\hat{b}_{\mathbf{r}+\mathbf{u},\alpha} + h.c.)\,. \tag{C.5}$$

For a system with discrete translational invariance we have that $\langle\hat{K}_{u,\alpha}(\mathbf{r})\rangle = K_{u,\alpha}$. The Hamiltonian gets transformed to (compare with Eq. (4.12)):

$$\begin{aligned}\hat{H} \to \hat{H} - \sum_{\alpha=A,B}\sum_{\mathbf{r}}\frac{e_\alpha}{m_\alpha}\hat{\mathbf{j}}_\alpha(\mathbf{r})\cdot\mathbf{A}(\mathbf{r}) + \\ + \sum_{\alpha=A,B}\sum_{\mathbf{r},u}\frac{e_\alpha^2}{2m_\alpha}\frac{\hat{K}_{u,\alpha}(\mathbf{r})}{2t}A^2(\mathbf{r})\,.\end{aligned} \tag{C.6}$$

Applying linear response theory as in subsec. 4.3.1 we obtain:

$$-m^{*2}\lim_{\mathbf{q}\to 0}\chi^T_{\mathbf{j}_A,\mathbf{j}_B}(\mathbf{q}) = \rho_{AB}\,, \tag{C.7}$$

$$m^*\left(-\frac{1}{2t}\langle\hat{K}_{u,\alpha}\rangle - m^*\lim_{\mathbf{q}\to 0}\chi^T_{\mathbf{j}_\alpha,\mathbf{j}_\alpha}(\mathbf{q})\right) = \rho_{\alpha\alpha}\,, \tag{C.8}$$

$$m^{*2}\sum_{\alpha,\beta=A,B}\lim_{\mathbf{q}\to 0}\chi^T_{\mathbf{j}_\alpha,\mathbf{j}_\beta}(\mathbf{q}) = \rho_n\,. \tag{C.9}$$

Eqs. (C.7), (C.8) and (C.9) are the discrete space analogous to Eqs. (4.18), (4.19) and (4.20) of Sec. 4.3. The only difference is the operator $\hat{K}_\alpha/2t$ in place of the density of particles, as a result of the different transformation rule of the current $\hat{\mathbf{j}}(\mathbf{r})$ and the Hamiltonian $\hat{H}$ under a vector potential in presence of a lattice, Eqs. (C.4) and (C.6).

We can compute the drag in the Bogoliubov approximation as we did in the translational invariant system to obtain Eq. (4.44):

$$\rho_{AB} = \frac{\hbar^2}{8L^3} \sum_{\mathbf{k}} \frac{(\Omega_{d,\mathbf{k}} - \Omega_{s,\mathbf{k}})^2 k_x^2}{(\Omega_{d,\mathbf{k}} + \Omega_{s,\mathbf{k}})\Omega_{s,\mathbf{k}}\Omega_{d,\mathbf{k}}} \left(\frac{\sin(k_x l)}{k_x l} \right)^2 , \tag{C.10}$$

where $\Omega_{d,\mathbf{k}}$ and $\Omega_{s,\mathbf{k}}$ are the excitation energies of the density and spin degrees of freedom respectively, namely:

$$\Omega_{d(s),\mathbf{k}} = \sqrt{\epsilon(\mathbf{k})(\epsilon(\mathbf{k}) + Uf \pm U_{AB} f)} , \tag{C.11}$$

with $\epsilon(\mathbf{k}) = 4t \sum_{i=x,y,z} \sin^2(k_i l/2)$ and $\nu = N/I$ is the total filling fraction. In the limit $l \to 0$, Eq. (C.10) coincides with the result for the homogeneous system, Eq. (4.44). The sum runs on the wavevectors of the first Brillouin zone- This result was already obtained in Linder and Sudbø (2009) through a different method that is analogous in lattice systems to the one used in Fil and Shevchenko (2005).

In chapter 5 the Bogoliubov result for the drag has been compared with a microscopic calculation for a one-dimensional system. Interestingly Eq. (C.10) turns out to give a reasonable estimate of the drag even in this case provided $U_{AB} > 0$.

C.2 Alternative derivation: drag coefficient as a derivative of the energy

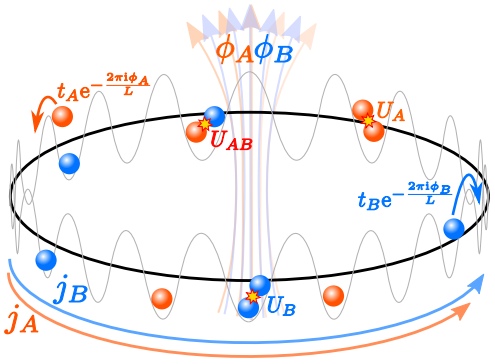

FIGURE C.1: Sketch of the 2-component Bose-Hubbard ring with hopping parameters $\tilde{t}_\alpha = t_\alpha e^{-i2\pi\phi_\alpha/L}$, intra-species interactions U_α and inter-species interactions U_{AB}. The two fluxes ϕ_α pierce the ring and give rise to the superfluid currents j_α.

For simplicity we will consider a 1-dimensional ring geometry as we will use this derivation in chapter 5. Moreover, we take the lattice spacing l to be 1 in this case, as we're not interested in taking the continuum limit.

We subject the 1 dimensional ring to a vector potential $\mathbf{A}_\alpha(\mathbf{r}) = A_\alpha\,\hat{\theta}$, where θ is the radial unit vector. This corresponds to a magnetic flux ϕ_α piercing perpendicularly the plane of the ring:

$$\phi_\alpha = \frac{e}{2\pi\hbar}\oint \mathbf{A}_\alpha(\mathbf{r})\cdot d\mathbf{l} = \frac{e}{2\pi\hbar}LA_\alpha \tag{C.12}$$

This magnetic flux modifies the hopping parameter t by a phase factor, according to the Peierls substitution:

$$t \to \tilde{t}_\alpha = t\,e^{-i2\pi\phi_\alpha/L} \tag{C.13}$$

We can now calculate the total superfluid currents in the ring induced by the vector potential using the continuity equation:

$$\frac{\partial\langle n_\alpha\rangle}{\partial t} = \frac{1}{i\hbar}\langle[n_\alpha, H]\rangle = \frac{2\tilde{t}_\alpha}{\hbar}\left(Im\,\langle\hat{b}^\dagger_{i+1,\alpha}\hat{b}_{i,\alpha}\rangle - Im\,\langle\hat{b}^\dagger_{i,\alpha}\hat{b}_{i-1,\alpha}\rangle\right), \tag{C.14}$$

which yields:

$$J_\alpha = \frac{2\tilde{t}_\alpha}{\hbar}Im\,\langle\hat{b}^\dagger_{i+1,\alpha}\hat{b}_{i,\alpha}\rangle = \frac{1}{2\pi\hbar}\langle\frac{\partial H}{\partial\phi_\alpha}\rangle = \frac{1}{2\pi\hbar}\frac{\partial E}{\partial\phi_\alpha}, \tag{C.15}$$

where in the last line we made use of the Hellmann-Feynman theorem.

The superfluid velocities of each species α read, according to Eq. 4.9:

$$v^{(s)}_\alpha = \frac{eA_\alpha}{m^*} = \frac{\hbar}{m^*}\frac{2\pi\phi_\alpha}{L}. \tag{C.16}$$

Using now the Andreev-Bashkin equation we can derive the expression for the superfluid densities $\rho_{\alpha\beta}$:

$$\rho_{\alpha\beta} = \lim_{\phi_\alpha,\phi_\beta\to 0}\frac{Lm^{*2}}{2\pi\hbar}\frac{\partial j_\alpha}{\partial\phi_\beta} = \lim_{\phi_\alpha,\phi_\beta\to 0}\frac{Lm^{*2}}{(2\pi\hbar)^2}\frac{\partial^2 E}{\partial\phi_\alpha\partial\phi_\beta}. \tag{C.17}$$

The relation between this expression and the linear response one is made apparent by considering the magnetic fluxes ϕ_α as small perturbations and expanding the Hamiltonian up to second order in the fluxes:

$$H \to H + \sum_\alpha\left(\frac{2\pi\phi_\alpha}{L}\hat{J}_\alpha - \frac{1}{2}\left(\frac{2\pi\phi_\alpha}{L}\right)^2\hat{K}_\alpha\right) \tag{C.18}$$

Thus, applying second order perturbation theory, the energy variation $\Delta E_{\phi_\alpha} = E_{\phi_\alpha} - E_0$ gets two contributions:

$$\Delta E_1 = -\left(\frac{2\pi\phi_\alpha}{L}\right)^2\left(-\frac{1}{2}\langle\psi_0|\hat{K}_\alpha|\psi_0\rangle\right) \tag{C.19}$$

and

$$\Delta E_2 = -\left(\frac{2\pi}{L}\right)^2 \phi_\alpha \phi_\beta \left(-\frac{\langle \psi_\nu | \hat{J}_\alpha | \psi_0 \rangle \langle \psi_0 | \hat{J}_\beta | \psi_\nu \rangle}{E_\nu - E_0} + c.c. \right) \tag{C.20}$$

And taking the derivatives with respect to the fluxes we get back Eqs. (C.7), (C.8) and (C.9).

Appendix D

Thermodynamic quantities for the weakly interacting Bose-Bose mixture

In this appendix we will derive quantities which were used in 4, sec 4.3.2. We consider the case of a homogeneous weakly interacting Bose-Bose mixture. The energy of a Bose-Bose mixture in the mean field approximation is just given by:

$$\frac{E_{MF}}{V} = \frac{1}{2} g_{AA} n_A^2 + \frac{1}{2} g_{BB} n_B^2 + g_{AB} n_A n_B \,. \tag{D.1}$$

The lowest order beyond mean field correction to this energy, known as the Lee-Huang-Yang term, can be found in Petrov (2013) and reads for equal masses $m_A = m_B = m$ and intraspecies coupling $g_{AA} = g_{BB} = g$:

$$E_{LHY}/V = \frac{8}{15\pi^2} m^{3/2} \left(g n_A\right)^{5/2} f\left(1, \frac{g_{AB}^2}{g^2}, \frac{n_B}{n_A}\right) \tag{D.2}$$

with $f(1,x,y) = \sum_{\pm} \left(1 + y \pm \sqrt{(1-y)^2 + 4xy}\right)^{5/2} / 4\sqrt{2}$, a dimensionless function.

From equation (D.2) we can obtain the chemical potential $\mu_\alpha = \frac{\partial E}{\partial N_\alpha}$ of each species α. In the $\mathbb{Z}_2$ symmetric case where $\mu_A = \mu_B = \mu$ we get:

$$\mu = \left(g + g_{AB}\right) n \left(1 + \frac{2}{3}\sqrt{n a^3} B(\eta)\right) \tag{D.3}$$

where $\eta = \frac{|g_{AB}|}{g}$ and:

$$B(\eta) = \frac{8}{\sqrt{\pi}(1+\eta)} \left((1+\eta)^{5/2} + (1-\eta)^{5/2}\right) . \tag{D.4}$$

We can also derive the magnetic susceptibility $\chi_s = \frac{\partial^2(E/V)}{\partial(n_A - n_B)^2}$, which reads:

$$\chi_s^{-1} = g\frac{1-\eta}{2}\left[1 + \sqrt{na^3}C(\eta)\right] \tag{D.5}$$

where we defined the function

$$C(\eta) = \frac{16}{3\sqrt{\pi}}\frac{1+\eta}{\eta}\left((1+\eta)^{3/2} - (1-\eta)^{3/2})\right) . \tag{D.6}$$

These formulas have been used for the calculation of the beyond mean field correction to the spin speed of sound in section 4.5.1.

For the case of the spin dipole oscillations we need instead to consider the trapped case. In presence of harmonic trapping the chemical potential μ and the susceptibility become position-dependent through the equilibrium density profile $n(\mathbf{r})$. At mean field level the latter reads:

$$n(\mathbf{r}) = \frac{2\mu_{TF}}{(g + g_{AB})}\left(1 - \frac{r^2}{R_{TF}^2}\right) \tag{D.7}$$

where $R_{TF} = \sqrt{\frac{2\mu_{TF}}{m\omega_0^2}}$ is the Thomas-Fermi radius and μ_{TF} the Thomas-Fermi chemical potential. Imposing that the integrated density gives the total number of particles we find:

$$R_{TF} = \left(\frac{15N\,(g + g_{AB})}{8\pi m\omega_0^2}\right)^{1/5} , \tag{D.8}$$

from which we can derive the chemical potential as a function of the total number of particles, the trapping potential and the interactions.

The inclusion of beyond mean fields effects results in a correction in the value of μ_{TF} and of the Thomas-Fermi radius R_{TF}. The chemical potential at first order in the gas parameter $\sqrt{n(0)a^3}$ reads:

$$\mu_{TF}^1 = \mu_{TF}\left(1 + \frac{\pi}{16}\sqrt{n(0)a^3}B(\eta)\right) \tag{D.9}$$

and as a consequence:

$$R_{TF}^1 = R_{TF}\left(1 + \frac{\pi}{32}\sqrt{n(0)a^3}B(\eta)\right) . \tag{D.10}$$

References

Dmitry A Abanin, Wojciech De Roeck, and François Huveneers. Theory of many-body localization in periodically driven systems. *Annals of Physics*, 372:1–11, 2016.

Monika Aidelsburger, Marcos Atala, Sylvain Nascimbène, Stefan Trotzky, Y-A Chen, and Immanuel Bloch. Experimental realization of strong effective magnetic fields in an optical lattice. *Physical review letters*, 107(25):255301, 2011.

P. W. Anderson. Absence of diffusion in certain random lattices. *Phys. Rev.*, 109: 1492–1505, Mar 1958. . URL http://link.aps.org/doi/10.1103/PhysRev.109.1492.

A.F. Andreev and E.P. Bashkin. Three-velocity hydrodynamics of superfluid solutions. *Sov. Phys.-JETP*, 42:164–167, Sep 1975. URL http://jetp.ac.ru/cgi-bin/e/index/e/42/1/p164?a=list.

Neil W Ashcroft, N David Mermin, et al. Solid state physics, 1976.

Serge Aubry and Gilles André. Analyticity breaking and anderson localization in incommensurate lattices. *Ann. Israel Phys. Soc*, 3(133):18, 1980.

Artur Avila and Svetlana Jitomirskaya. The ten martini problem. *Annals of Mathematics*, pages 303–342, 2009.

J. Bardeen, G. Baym, and D. Pines. Effective interaction of he^3 atoms in dilute solutions of he^3 in he^4 at low temperatures. *Phys. Rev.*, 156:207–221, Apr 1967. . URL https://link.aps.org/doi/10.1103/PhysRev.156.207.

Gordon Baym. *The Microscopic Description of Superfluidity*, pages 121–156. Springer US, Boston, MA, 1968. ISBN 978-1-4899-6435-9. . URL https://doi.org/10.1007/978-1-4899-6435-9_3.

B. Bazak and D. S. Petrov. Five-body efimov effect and universal pentamer in fermionic mixtures. *Phys. Rev. Lett.*, 118:083002, Feb 2017. . URL https://link.aps.org/doi/10.1103/PhysRevLett.118.083002.

D. Blume. Universal four-body states in heavy-light mixtures with a positive scattering length. *Phys. Rev. Lett.*, 109:230404, Dec 2012. . URL https://link.aps.org/doi/10.1103/PhysRevLett.109.230404.

Pranjal Bordia, Henrik Luschen, Ulrich Schneider, Michael Knap, and Immanuel Bloch. Periodically driving a many-body localized quantum system. *Nat Phys*, advance online publication, Jan 2017. ISSN 1745-2481. URL http://dx.doi.org/10.1038/nphys4020. Article.

C. R. Cabrera, L. Tanzi, J. Sanz, B. Naylor, P. Thomas, P. Cheiney, and L. Tarruell. Quantum liquid droplets in a mixture of bose-einstein condensates. *Science*, 359 (6373):301–304, 2018. ISSN 0036-8075. . URL https://science.sciencemag.org/content/359/6373/301.

J. Catani, L. De Sarlo, G. Barontini, F. Minardi, and M. Inguscio. Degenerate bose-bose mixture in a three-dimensional optical lattice. *Phys. Rev. A*, 77:011603, Jan 2008. . URL https://link.aps.org/doi/10.1103/PhysRevA.77.011603.

M. A. Cazalilla, R. Citro, T. Giamarchi, E. Orignac, and M. Rigol. One dimensional bosons: From condensed matter systems to ultracold gases. *Reviews of Modern Physics*, 83(4):1405–1466, 2011. ISSN 00346861. .

Cheng Chin, Rudolf Grimm, Paul Julienne, and Eite Tiesinga. Feshbach resonances in ultracold gases. *Rev. Mod. Phys.*, 82:1225–1286, Apr 2010. . URL https://link.aps.org/doi/10.1103/RevModPhys.82.1225.

R. Citro, S. De Palo, M. Di Dio, and E. Orignac. Quantum phase transitions of a two-leg bosonic ladder in an artificial gauge field. *Phys. Rev. B*, 97:174523, May 2018. . URL https://link.aps.org/doi/10.1103/PhysRevB.97.174523.

R. Combescot, A. Recati, C. Lobo, and F. Chevy. Normal state of highly polarized fermi gases: Simple many-body approaches. *Phys. Rev. Lett.*, 98:180402, May 2007. . URL https://link.aps.org/doi/10.1103/PhysRevLett.98.180402.

Daniele Contessi, Donato Romito, Matteo Rizzi, and Alessio Recati. Collisionless drag for a one-dimensional two-component bose-hubbard model. *Phys. Rev. Research*, 3: L022017, May 2021. . URL https://link.aps.org/doi/10.1103/PhysRevResearch.3.L022017.

Jean Dalibard, Fabrice Gerbier, Gediminas Juzeliūnas, and Patrik Öhberg. Colloquium: Artificial gauge potentials for neutral atoms. *Rev. Mod. Phys.*, 83: 1523–1543, Nov 2011. . URL https://link.aps.org/doi/10.1103/RevModPhys.83.1523.

C. D'Errico, A. Burchianti, M. Prevedelli, L. Salasnich, F. Ancilotto, M. Modugno, F. Minardi, and C. Fort. Observation of quantum droplets in a heteronuclear

bosonic mixture. *Phys. Rev. Research*, 1:033155, Dec 2019. . URL https://link.aps.org/doi/10.1103/PhysRevResearch.1.033155.

J. M. Deutsch. Quantum statistical mechanics in a closed system. *Phys. Rev. A*, 43: 2046–2049, Feb 1991. . URL https://link.aps.org/doi/10.1103/PhysRevA.43.2046.

Klaus Drese and Martin Holthaus. Exploring a metal-insulator transition with ultracold atoms in standing light waves? *Phys. Rev. Lett.*, 78:2932–2935, Apr 1997. . URL https://link.aps.org/doi/10.1103/PhysRevLett.78.2932.

D. H. Dunlap and V. M. Kenkre. Dynamic localization of a charged particle moving under the influence of an electric field. *Phys. Rev. B*, 34:3625–3633, Sep 1986. . URL http://link.aps.org/doi/10.1103/PhysRevB.34.3625.

A. Eckardt and M. Holthaus. Ac-induced superfluidity. *EPL (Europhysics Letters)*, 80 (5):50004, 2007. URL http://stacks.iop.org/0295-5075/80/i=5/a=50004.

André Eckardt, Christoph Weiss, and Martin Holthaus. Superfluid-insulator transition in a periodically driven optical lattice. *Phys. Rev. Lett.*, 95:260404, Dec 2005. . URL http://link.aps.org/doi/10.1103/PhysRevLett.95.260404.

André Eckardt, Martin Holthaus, Hans Lignier, Alessandro Zenesini, Donatella Ciampini, Oliver Morsch, and Ennio Arimondo. Exploring dynamic localization with a bose-einstein condensate. *Phys. Rev. A*, 79:013611, Jan 2009. . URL http://link.aps.org/doi/10.1103/PhysRevA.79.013611.

Christoph Eigen, Jake A. P. Glidden, Raphael Lopes, Nir Navon, Zoran Hadzibabic, and Robert P. Smith. Universal scaling laws in the dynamics of a homogeneous unitary bose gas. *Phys. Rev. Lett.*, 119:250404, Dec 2017. . URL https://link.aps.org/doi/10.1103/PhysRevLett.119.250404.

Ulrich Eismann, Lev Khaykovich, Sébastien Laurent, Igor Ferrier-Barbut, Benno S. Rem, Andrew T. Grier, Marion Delehaye, Frédéric Chevy, Christophe Salomon, Li-Chung Ha, and Cheng Chin. Universal loss dynamics in a unitary bose gas. *Phys. Rev. X*, 6:021025, May 2016. . URL https://link.aps.org/doi/10.1103/PhysRevX.6.021025.

Ferdinand Evers and Alexander D. Mirlin. Anderson transitions. *Rev. Mod. Phys.*, 80: 1355–1417, Oct 2008. . URL http://link.aps.org/doi/10.1103/RevModPhys.80.1355.

Eleonora Fava, Tom Bienaimé, Carmelo Mordini, Giacomo Colzi, Chunlei Qu, Sandro Stringari, Giacomo Lamporesi, and Gabriele Ferrari. Observation of spin superfluidity in a bose gas mixture. *Phys. Rev. Lett.*, 120:170401, Apr 2018. . URL https://link.aps.org/doi/10.1103/PhysRevLett.120.170401.

I. Ferrier-Barbut, M. Delehaye, S. Laurent, A. T. Grier, M. Pierce, B. S. Rem, F. Chevy, and C. Salomon. A mixture of bose and fermi superfluids. *Science*, 345(6200): 1035–1038, 2014. ISSN 0036-8075. . URL https://science.sciencemag.org/content/345/6200/1035.

Herman Feshbach. A unified theory of nuclear reactions. ii. *Annals of Physics*, 19(2): 287–313, 1962. ISSN 0003-4916. . URL https://www.sciencedirect.com/science/article/pii/000349166290221X.

D. V. Fil and S. I. Shevchenko. Nondissipative drag of superflow in a two-component bose gas. *Phys. Rev. A*, 72:013616, Jul 2005. . URL https://link.aps.org/doi/10.1103/PhysRevA.72.013616.

Takeshi Fukuhara, Peter Schauß, Manuel Endres, Sebastian Hild, Marc Cheneau, Immanuel Bloch, and Christian Gross. Microscopic observation of magnon bound states and their dynamics. *Nature*, 502(7469):76–79, Oct 2013. ISSN 1476-4687. . URL https://doi.org/10.1038/nature12541.

Bryce Gadway, Daniel Pertot, René Reimann, and Dominik Schneble. Superfluidity of interacting bosonic mixtures in optical lattices. *Phys. Rev. Lett.*, 105:045303, Jul 2010. . URL https://link.aps.org/doi/10.1103/PhysRevLett.105.045303.

Thierry Giamarchi. *Quantum Physics in One Dimension*. Oxford University Press, Oxford, UK, 2004.

N. Goldman and J. Dalibard. Periodically driven quantum systems: Effective hamiltonians and engineered gauge fields. *Phys. Rev. X*, 4:031027, Aug 2014. . URL http://link.aps.org/doi/10.1103/PhysRevX.4.031027.

Sarang Gopalakrishnan, Michael Knap, and Eugene Demler. Regimes of heating and dynamical response in driven many-body localized systems. *Physical Review B*, 94 (9):094201, 2016.

Milena Grifoni and Peter Hänggi. Driven quantum tunneling. *Physics Reports*, 304 (5–6):229 – 354, 1998. ISSN 0370-1573. . URL http://www.sciencedirect.com/science/article/pii/S0370157398000222.

F. D. M. Haldane. Effective harmonic-fluid approach to low-energy properties of one-dimensional quantum fluids. *Phys. Rev. Lett.*, 47:1840–1843, Dec 1981. . URL https://link.aps.org/doi/10.1103/PhysRevLett.47.1840.

Douglas R Hofstadter. Energy levels and wave functions of bloch electrons in rational and irrational magnetic fields. *Physical review B*, 14(6):2239, 1976.

Martin Holthaus. Collapse of minibands in far-infrared irradiated superlattices. *Phys. Rev. Lett.*, 69:351–354, Jul 1992. . URL http://link.aps.org/doi/10.1103/PhysRevLett.69.351.

Anzi Hu, L. Mathey, Ippei Danshita, Eite Tiesinga, Carl J. Williams, and Charles W. Clark. Counterflow and paired superfluidity in one-dimensional Bose mixtures in optical lattices. *Physical Review A - Atomic, Molecular, and Optical Physics*, 80(2):1–13, 2009. ISSN 10502947. .

Svetlana Ya Jitomirskaya. Metal-insulator transition for the almost mathieu operator. *Annals of Mathematics*, 150(3):1159–1175, 1999.

Gregor Jotzu, Michael Messer, Rémi Desbuquois, Martin Lebrat, Thomas Uehlinger, Daniel Greif, and Tilman Esslinger. Experimental realization of the topological haldane model with ultracold fermions. *Nature*, 515(7526):237–240, 2014.

M. Yu. Kagan and D. V. Efremov. Two-particle pairing and phase separation in a two-dimensional bose gas with one or two sorts of bosons. *Phys. Rev. B*, 65:195103, Apr 2002. . URL https://link.aps.org/doi/10.1103/PhysRevB.65.195103.

Volker Karle, Nicolò Defenu, and Tilman Enss. Coupled superfluidity of binary bose mixtures in two dimensions. *Phys. Rev. A*, 99:063627, Jun 2019. . URL https://link.aps.org/doi/10.1103/PhysRevA.99.063627.

O I Kartavtsev and A V Malykh. Low-energy three-body dynamics in binary quantum gases. *Journal of Physics B: Atomic, Molecular and Optical Physics*, 40(7):1429, 2007. URL http://stacks.iop.org/0953-4075/40/i=7/a=011.

I. M. Khalatnikov. Hydrodynamics of solutions of 2 superfluid liquids. *Sov. Phys.-JETP5*, 5(4):542–545, 1957. URL http://jetp.ac.ru/cgi-bin/e/index/e/5/4/p542?a=list.

Joon Hyun Kim, Deokhwa Hong, and Y. Shin. Observation of two sound modes in a binary superfluid gas. *Phys. Rev. A*, 101:061601, Jun 2020. . URL https://link.aps.org/doi/10.1103/PhysRevA.101.061601.

A. Kleine, C. Kollath, I. P. McCulloch, T. Giamarchi, and U. Schollwöck. Spin-charge separation in two-component bose gases. *Phys. Rev. A*, 77:013607, Jan 2008a. . URL https://link.aps.org/doi/10.1103/PhysRevA.77.013607.

A Kleine, C Kollath, I P McCulloch, T Giamarchi, and U Schollwöck. Excitations in two-component bose gases. *New Journal of Physics*, 10(4):045025, apr 2008b. . URL https://doi.org/10.1088/1367-2630/10/4/045025.

A. B. Kuklov and B. V. Svistunov. Counterflow superfluidity of two-species ultracold atoms in a commensurate optical lattice. *Phys. Rev. Lett.*, 90:100401, Mar 2003. . URL https://link.aps.org/doi/10.1103/PhysRevLett.90.100401.

Anatoly Kuklov, Nikolay Prokof'ev, and Boris Svistunov. Commensurate two-component bosons in an optical lattice: Ground state phase diagram. *Phys. Rev.*

Lett., 92:050402, Feb 2004. . URL https://link.aps.org/doi/10.1103/PhysRevLett.92.050402.

L. Landau. Theory of the superfluidity of helium ii. *Phys. Rev.*, 60:356–358, Aug 1941. . URL https://link.aps.org/doi/10.1103/PhysRev.60.356.

Lev Davidovich Landau and Evgenii M Lifshitz. *Course of Theoretical Physics Vol 3 Quantum Mechanics*. Pergamon Press, 1958.

David M Larsen. Binary mixtures of dilute bose gases with repulsive interactions at low temperature. *Annals of Physics*, 24:89–101, 1963. ISSN 0003-4916. . URL https://www.sciencedirect.com/science/article/pii/0003491663900666.

J. M. Lattimer and M. Prakash. The physics of neutron stars. *Science*, 304(5670): 536–542, 2004. ISSN 0036-8075. . URL https://science.sciencemag.org/content/304/5670/536.

A. J. Leggett. Theory of a superfluid fermi liquid. i. general formalism and static properties. *Phys. Rev.*, 140:A1869–A1888, Dec 1965. . URL https://link.aps.org/doi/10.1103/PhysRev.140.A1869.

A. J. Leggett. On the superfluid fraction of an arbitrary many-body system at t=0. *Journal of Statistical Physics*, 93(3):927–941, Nov 1998. ISSN 1572-9613. . URL https://doi.org/10.1023/B:JOSS.0000033170.38619.6c.

Anthony James Leggett et al. *Quantum liquids: Bose condensation and Cooper pairing in condensed-matter systems*. Oxford university press, 2006.

Dov Levine and Paul Joseph Steinhardt. Quasicrystals: a new class of ordered structures. *Physical review letters*, 53(26):2477, 1984.

H. Lignier, C. Sias, D. Ciampini, Y. Singh, A. Zenesini, O. Morsch, and E. Arimondo. Dynamical control of matter-wave tunneling in periodic potentials. *Phys. Rev. Lett.*, 99:220403, Nov 2007. . URL http://link.aps.org/doi/10.1103/PhysRevLett.99.220403.

Jacob Linder and Asle Sudbø. Calculation of drag and superfluid velocity from the microscopic parameters and excitation energies of a two-component bose-einstein condensate in an optical lattice. *Phys. Rev. A*, 79:063610, Jun 2009. . URL https://link.aps.org/doi/10.1103/PhysRevA.79.063610.

F. London. On the problem of the molecular theory of superconductivity. *Phys. Rev.*, 74:562–573, Sep 1948. . URL https://link.aps.org/doi/10.1103/PhysRev.74.562.

Enrique Maciá. On the nature of electronic wave functions in one-dimensional self-similar and quasiperiodic systems. *ISRN Condensed Matter Physics*, 2014, 2014.

J.A. Maruhn, P.G. Reinhard, and E. Suraud. *Simple Models of Many-Fermion Systems*. Springer Berlin Heidelberg, 2010. ISBN 9783642038396. URL https://books.google.it/books?id=AaZAAAAAQBAJ.

Vieri Mastropietro. Dense gaps in the interacting aubry-andré model. *Phys. Rev. B*, 93: 245154, Jun 2016. . URL https://link.aps.org/doi/10.1103/PhysRevB.93.245154.

L. Mathey, Ippei Danshita, and Charles W. Clark. Creating a supersolid in one-dimensional bose mixtures. *Phys. Rev. A*, 79:011602, Jan 2009. . URL https://link.aps.org/doi/10.1103/PhysRevA.79.011602.

Daniel C. Mattis. The few-body problem on a lattice. *Rev. Mod. Phys.*, 58:361–379, Apr 1986. . URL https://link.aps.org/doi/10.1103/RevModPhys.58.361.

Pascal Naidon and Shimpei Endo. Efimov physics: a review. *Reports on Progress in Physics*, 80(5):056001, 2017. URL http://stacks.iop.org/0034-4885/80/i=5/a=056001.

Jacopo Nespolo, Grigori E Astrakharchik, and Alessio Recati. Andreev–bashkin effect in superfluid cold gases mixtures. *New Journal of Physics*, 19(12):125005, 2017. URL http://stacks.iop.org/1367-2630/19/i=12/a=125005.

P. Nozieres and D. Pines. *Theory Of Quantum Liquids*. Advanced Books Classics. Avalon Publishing, 1999. ISBN 9780813346533. URL https://books.google.it/books?id=q3wCwaV-gmUC.

E. Orignac, R. Citro, M. Di Dio, and S. De Palo. Vortex lattice melting in a boson ladder in an artificial gauge field. *Phys. Rev. B*, 96:014518, Jul 2017. . URL https://link.aps.org/doi/10.1103/PhysRevB.96.014518.

Miki Ota and Stefano Giorgini. Thermodynamics of dilute bose gases: Beyond mean-field theory for binary mixtures of bose-einstein condensates. *Phys. Rev. A*, 102:063303, Dec 2020. . URL https://link.aps.org/doi/10.1103/PhysRevA.102.063303.

L. Parisi, G. E. Astrakharchik, and S. Giorgini. Spin dynamics and andreev-bashkin effect in mixtures of one-dimensional bose gases. *Phys. Rev. Lett.*, 121:025302, Jul 2018. . URL https://link.aps.org/doi/10.1103/PhysRevLett.121.025302.

C. J. Pethick and H. Smith. *Bose–Einstein Condensation in Dilute Gases*. Cambridge University Press, 2 edition, 2008. .

Dmitry Petrov. Personal communication, 2021.

D.S. Petrov. The few-atom problem. *Proceedings of the Les Houches Summer Schools*, Session 94, 2013.

L.P. Pitaevskii and S. Stringari. *Bose-Einstein Condensation and Superfluidity*. International series of monographs on physics. Oxford University Press, 2016. ISBN 9780198758884. URL https://books.google.it/books?id=_y4ZswEACAAJ.

S. Ray, A. Ghosh, and S. Sinha. Drive-induced delocalization in the aubry-andré model. *Phys. Rev. E*, 97:010101, Jan 2018. . URL https://link.aps.org/doi/10.1103/PhysRevE.97.010101.

Alessio Recati and Sandro Stringari. Spin fluctuations, susceptibility, and the dipole oscillation of a nearly ferromagnetic fermi gas. *Phys. Rev. Lett.*, 106:080402, Feb 2011. . URL https://link.aps.org/doi/10.1103/PhysRevLett.106.080402.

Jorge Rehn, Achilleas Lazarides, Frank Pollmann, and Roderich Moessner. How periodic driving heats a disordered quantum spin chain. *Physical Review B*, 94(2): 020201, 2016.

Giacomo Roati, Chiara D'Errico, Leonardo Fallani, Marco Fattori, Chiara Fort, Matteo Zaccanti, Giovanni Modugno, Michele Modugno, and Massimo Inguscio. Anderson localization of a non-interacting bose–einstein condensate. *Nature*, 453(7197): 895–898, 2008.

J. L. Roberts, N. R. Claussen, S. L. Cornish, E. A. Donley, E. A. Cornell, and C. E. Wieman. Controlled collapse of a bose-einstein condensate. *Phys. Rev. Lett.*, 86: 4211–4214, May 2001. . URL https://link.aps.org/doi/10.1103/PhysRevLett.86.4211.

Donato Romito. Periodic modulation of a quasicrystal. Master's thesis, Università degli Studi di Trento, 2017.

Donato Romito, Carlos Lobo, and Alessio Recati. Localisation transition in the driven aubry-andré model. *The European Physical Journal D*, 72(8):135, Aug 2018. ISSN 1434-6079. . URL https://doi.org/10.1140/epjd/e2018-90081-3.

Donato Romito, Carlos Lobo, and Alessio Recati. Linear response study of collisionless spin drag. *Phys. Rev. Research*, 3:023196, Jun 2021. . URL https://link.aps.org/doi/10.1103/PhysRevResearch.3.023196.

Hideo Sambe. Steady states and quasienergies of a quantum-mechanical system in an oscillating field. *Phys. Rev. A*, 7:2203–2213, Jun 1973. . URL http://link.aps.org/doi/10.1103/PhysRevA.7.2203.

A Sartori, J Marino, S Stringari, and A Recati. Spin-dipole oscillation and relaxation of coherently coupled bose–einstein condensates. *New Journal of Physics*, 17(9):093036, sep 2015. .

Michael Schreiber, Sean S. Hodgman, Pranjal Bordia, Henrik P. Lüschen, Mark H. Fischer, Ronen Vosk, Ehud Altman, Ulrich Schneider, and Immanuel Bloch.

Observation of many-body localization of interacting fermions in a quasirandom optical lattice. *Science*, 349(6250):842–845, 2015. ISSN 0036-8075. . URL https://science.sciencemag.org/content/349/6250/842.

J.R. Schrieffer. *Theory Of Superconductivity*. Advanced Books Classics. Avalon Publishing, 1999. ISBN 9780738201207. URL https://books.google.it/books?id=let7wRir74MC.

Karl Sellin and Egor Babaev. Superfluid drag in the two-component bose-hubbard model. *Phys. Rev. B*, 97:094517, Mar 2018. . URL https://link.aps.org/doi/10.1103/PhysRevB.97.094517.

G. Semeghini, G. Ferioli, L. Masi, C. Mazzinghi, L. Wolswijk, F. Minardi, M. Modugno, G. Modugno, M. Inguscio, and M. Fattori. Self-bound quantum droplets of atomic mixtures in free space. *Phys. Rev. Lett.*, 120:235301, Jun 2018. . URL https://link.aps.org/doi/10.1103/PhysRevLett.120.235301.

Dan Shechtman, Ilan Blech, Denis Gratias, and John W Cahn. Metallic phase with long-range orientational order and no translational symmetry. *Physical review letters*, 53(20):1951, 1984.

Y. Shin, M. W. Zwierlein, C. H. Schunck, A. Schirotzek, and W. Ketterle. Observation of phase separation in a strongly interacting imbalanced fermi gas. *Phys. Rev. Lett.*, 97:030401, Jul 2006. . URL https://link.aps.org/doi/10.1103/PhysRevLett.97.030401.

Jon H. Shirley. Solution of the schrödinger equation with a hamiltonian periodic in time. *Phys. Rev.*, 138:B979–B987, May 1965. . URL https://link.aps.org/doi/10.1103/PhysRev.138.B979.

Aritra Sinha, Marek M. Rams, and Jacek Dziarmaga. Kibble-zurek mechanism with a single particle: Dynamics of the localization-delocalization transition in the aubry-andré model. *Phys. Rev. B*, 99:094203, Mar 2019. . URL https://link.aps.org/doi/10.1103/PhysRevB.99.094203.

J. Stenger, S. Inouye, M. R. Andrews, H.-J. Miesner, D. M. Stamper-Kurn, and W. Ketterle. Strongly enhanced inelastic collisions in a bose-einstein condensate near feshbach resonances. *Phys. Rev. Lett.*, 82:2422–2425, Mar 1999. . URL https://link.aps.org/doi/10.1103/PhysRevLett.82.2422.

S. Stringari. Collective excitations of a trapped bose-condensed gas. *Phys. Rev. Lett.*, 77:2360–2363, Sep 1996. . URL https://link.aps.org/doi/10.1103/PhysRevLett.77.2360.

J. Struck, C. Ölschläger, M. Weinberg, P. Hauke, J. Simonet, A. Eckardt, M. Lewenstein, K. Sengstock, and P. Windpassinger. Tunable gauge potential for neutral and

spinless particles in driven optical lattices. *Phys. Rev. Lett.*, 108:225304, May 2012. . URL http://link.aps.org/doi/10.1103/PhysRevLett.108.225304.

L. Tanzi, C. R. Cabrera, J. Sanz, P. Cheiney, M. Tomza, and L. Tarruell. Feshbach resonances in potassium bose-bose mixtures. *Phys. Rev. A*, 98:062712, Dec 2018. . URL https://link.aps.org/doi/10.1103/PhysRevA.98.062712.

Paolo Tommasini, E. J. V. de Passos, A. F. R. de Toledo Piza, M. S. Hussein, and E. Timmermans. Bogoliubov theory for mutually coherent condensates. *Phys. Rev. A*, 67:023606, Feb 2003. . URL https://link.aps.org/doi/10.1103/PhysRevA.67.023606.

K Winkler, G Thalhammer, F Lang, R Grimm, J Hecker Denschlag, AJ Daley, A Kantian, HP Büchler, and P Zoller. Repulsively bound atom pairs in an optical lattice. *Nature*, 441(7095):853, 2006.

J. Zak. Finite translations in time and energy. *Phys. Rev. Lett.*, 71:2623–2625, Oct 1993. . URL http://link.aps.org/doi/10.1103/PhysRevLett.71.2623.

Alessandro Zenesini, Hans Lignier, Donatella Ciampini, Oliver Morsch, and Ennio Arimondo. Coherent control of dressed matter waves. *Phys. Rev. Lett.*, 102:100403, Mar 2009. . URL http://link.aps.org/doi/10.1103/PhysRevLett.102.100403.